Electrocatalysis for selective oxidation of biomass-derived compounds

by

David J. Chadderdon

A dissertation submitted to the graduate faculty

in partial fulfillment of the requirements for the degree of

DOCTOR OF PHILOSOPHY

Major: Chemical Engineering

Program of Study Committee:
Wenzhen Li, Major Professor
Brent H. Shanks
Jean-Philippe Tessonnier
Matthew G. Panthani
Robbyn K. Anand

The student author, whose presentation of the scholarship herein was approved by the program of study committee, is solely responsible for the content of this dissertation. The Graduate College will ensure this dissertation is globally accessible and will not permit alterations after a degree is conferred.

Iowa State University

Ames, Iowa

2018

TABLE OF CONTENTS

ACKNOWLEDGMENTS

I am very grateful to my major professor, Wenzhen Li, and my committee members, Prof. Brent Shanks, Prof. Jean-Philippe Tessonnier, Prof. Robbyn Anand, and Prof. Matthew Panthani for their guidance and support throughout the course of my doctoral research. I would also like to thank the faculty and staff of the Department of Chemical & Biological Engineering for their assistance and support.

I was fortunate to have excellent collaborators including Prof. Matthew Panthani of Iowa State University, Prof. Michael Janik of Pennsylvania State University, and Dr. Karren L. More of Oakridge National Laboratory. I am grateful to my many coworkers at Iowa State University including Dr. Xiaotong Chadderdon, Dr. Yang Qiu, Dr. Neeva Benipal, and Dr. Ji Qi, and at Michigan Technological University including Dr. Le Xin, Dr. Zhiyong Zhang and Phani Krishna. I must also acknowledge the wonderful undergraduate researchers I have advised over the years, without whom I could not have completed this work, including Dexter Clark, Zachary McGraw, Ivy Wu, Andy Fogerty, and Joshua Otto.

I am thankful for my funding sources including the U.S. National Science Foundation (NSF CBET-1159448 and CBET-1501124), the Iowa State University Startup Fund, and the Bailey Research Career Development Award. This work was supported by the U.S. Department of Energy (DOE), Office of Science, Basic Energy Sciences, Materials Science and Engineering Division at the Ames Laboratory under contract number DE-AC02-07CH11358. Ames Laboratory is operated for the DOE by Iowa State University. The document number assigned to this dissertation is IS-T 3237.

ABSTRACT

Producing chemicals from biomass feedstocks is a potential route for reducing our dependence on unsustainable petroleum resources. However, unlike petrochemicals, biomass-derived chemicals are highly oxygenated, and there is a need to develop new processes to efficiently upgrade them to useful chemicals and products. One approach is to perform the desired transformations using electrochemistry. Electrochemical reactions are usually conducted at mild temperatures, which is advantageous for the conversion of thermally-unstable bioderived compounds. Additionally, electroanalytical methods can reveal mechanistic information about the complex processes occurring at electrode/electrolyte interfaces. Electrochemical cells are uniquely capable of integrating sustainable chemical production and renewable energy conversion. Alcohol-fed fuel cells can convert chemical energy to electricity, and may also generate value-added chemical products. Electrolytic cells can utilize renewable energy directly by employing sunlight-absorbing semiconductor photoelectrodes, or indirectly by using renewable electricity to drive non-spontaneous reactions. Electrochemistry may play key roles in our future chemical and energy landscapes, yet fundamental and applied research is needed to develop these technologies.

In this work, the electrochemical oxidation of biomass-derived compounds to valuable chemicals was explored. Specifically, this research focused on overcoming challenges related to catalyst activity and product selectivity for the electrocatalytic oxidation of bioderived polyols and polyfunctional molecules. Selective oxidation of vicinal diols under electrochemical conditions was studied using 1,2-propanediol (PDO) as a model compound. Potential-dependent pathways and selectivity trends were elucidated for PDO oxidation with

carbon-supported Pt and Au nanoparticle electrocatalysts in anion-exchange membrane fuel cells. Electrochemical conversion of a polyfunctional substrate, namely 5-hydroxymethylfurfural (HMF), was studied in electrolytic flow cells. HMF was selectively oxidized to 2,5-furandicarboxylic acid (FDCA), an important precursor for biobased polymers, using carbon-supported palladium and gold bimetallic nanoparticle electrocatalysts. Tuning anode potential and catalyst composition were critical for achieving high selectivity to FDCA. Efficient photoelectrochemical oxidation of HMF to FDCA was demonstrated using a homogeneous electrocatalyst, 2,2,6,6-tetramethylpiperidine-1-oxyl (TEMPO), together with a heterostructured photoanode. Modifying bismuth vanadate semiconductor films with electrodeposited cobalt phosphate simultaneously enhanced TEMPO oxidation photocurrent and suppressed the undesired oxygen evolution reaction.

CHAPTER 1

GENERAL INTRODUCTION

1.1 Global Energy Trends and Climate Change

The global energy demand is largely met by the combustion of fossil resources such as liquid petroleum fuels, coal, and natural gas. This demand is projected to reach over 800 quadrillion BTUs annually by 2040.[1] There is significant scientific consensus that human behavior contributes to climate change, particularly through the release of carbon dioxide (CO_2) from the combustion of fossil fuels.[2-3] These changes have disastrous effects such as melting ice sheets, rising sea levels, acidifying oceans, and increasing frequency of extreme weather events.[3-4] Moreover, fossil fuels are a finite resource.[5] Accordingly, it is inevitable that there will be a major shift in the global energy supply to low-carbon, renewable energy sources (**Figure 1.1a**). Biofuels such as biodiesel, bioethanol, and biomethane derived from renewable oils, biomass, and organic wastes, are expected to have an increased role as alternative transportation fuels.[6] Additionally, renewable electricity from hydroelectric, biomass, geothermal, solar, and wind sources is projected to meet over 25% of the U.S. electricity demand by 2030 (**Figure 1.1b**), dependent on future energy policies.[7] Much of that increase will likely be from wind and solar, which together accounted for over 98% of the additional capacity added to U.S. renewable electricity generation in 2017.

The growing contribution of variable power sources like wind and solar introduces new challenges, due to fluctuations in their generation capacity on an hourly or daily basis. Conventional power sources are necessary to provide baseline power generation during periods of low renewable electricity production, but may be unable to accommodate rapidly fluctuating

loads.[8] This can lead to overgeneration and curtailed renewable energy, which increase costs and reduce the overall environmental benefit. Common strategies to alleviate curtailment include: application of large-scale energy storage, expansion of transmission zones, improvements in load forecasting, and increased automation.[8-9] An alternative approach is to use the low-cost, overgenerated renewable electricity to drive electrochemical reactions as a means to store or convert the energy into fuels or chemicals. Electrochemical energy conversion is expected to be a key component of the future energy landscape, as a safe, clean, and sustainable alternative to the current fossil-based energy system.[10] Examples of promising electrochemical technologies for storage or utilization of renewable electricity include sustainable hydrogen production from water electrolysis, CO_2 fixation and conversion to chemicals and fuels, electrosynthesis of fine chemicals, and energy storage in redox flow batteries.

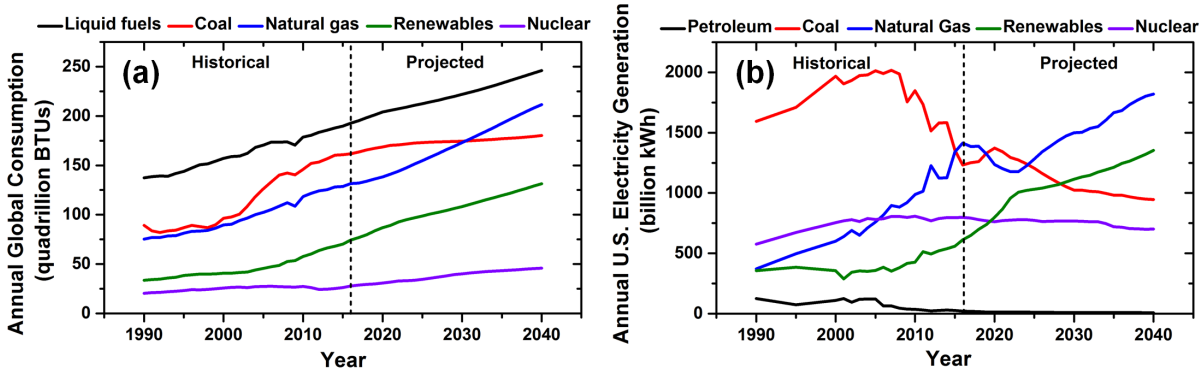

Figure 1.1. Historical and projected (a) annual global energy consumption and (b) annual U.S. electricity generation by source. Data from US Energy Information Administration.[7]

1.2. Biomass to Chemicals

Since the industrial revolution of the early 19th century, our society has heavily relied on inexpensive carbon-based chemicals derived from fossil sources. As such, nearly 4% of

worldwide oil consumption is attributed to the production of chemicals and plastics.[11] However, fossil resources are an inherently unsustainable carbon source on the timescale of human activity, because they require millions of years to be regenerated. As an alternative, biomass is a large-scale and renewable source of organic carbon. In particular, lignocellulosic biomass is the most abundant source of biomass, and is widely available from non-food sources such as wood, straw, husks, and grass.[12] The manufacturing of industrial chemicals is closely tied to energy production. Therefore, it is expected that as the energy sector shifts to become more dependent on renewable sources, there will also be opportunities to develop biorenewable chemical manufacturing in parallel.[13]

Significant efforts have been spent to integrate the production of chemicals and fuels from raw biomass feedstocks in a so-called 'biorefinery'.[11, 14-15] Analogous to conventional oil refineries, a successful biorefinery will likely follow a platform chemical approach, in which a small collection of chemicals are efficiently produced by chemical or biological transformations and then used for manufacturing of a wide variety of commercial chemicals and products.[13] Unlike petrochemical feeds which characteristically contain very little oxygen, biomass-derived carbohydrates contain excess oxygen functionality (cf. **Figure 1.2**).[14] Accordingly, new catalytic processes must be developed to efficiently convert the highly-functionalized biomass-derived platform molecules to desired products.[16-18] Two main directions for conversion of biomass-derived chemicals are available: (1) removing all oxygen functionalities to more closely resemble petrochemical feedstocks or (2) selectively tuning the existing oxygen groups to obtain the desired functionalities.[11] Complete removal of oxygen content is energy-intensive and typically requires large amounts of molecular hydrogen, which is mainly obtained from unsustainable fossil sources.[19] This approach is necessary for

production of biofuels, for which low oxygen content is required to give high energy density and good mixing compatibility with current liquid fuels.[11] However, applications for chemical production require less deoxygenation. Instead, the existing oxygen functionalities may be treated as valuable assets that can be efficiently tuned through chemical reactions, such as selective oxidation.

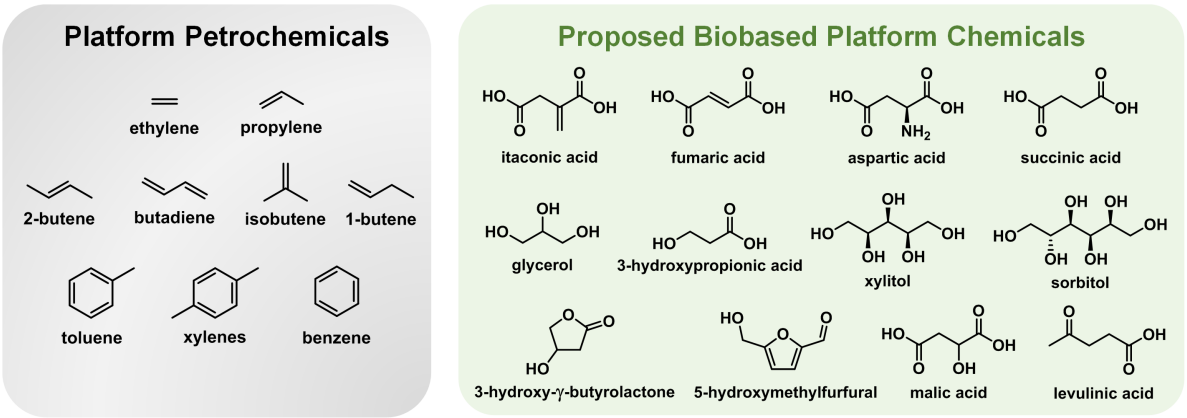

Figure 1.2. Platform chemicals derived from petroleum or biomass.

A prime example of chemical production by the selective oxidation of bioderived chemicals is the conversion of 5-hydroxymethylfurfural (HMF) to 2,5-furandicarboxylic acid (FDCA).[20] HMF is readily available from the acid-catalyzed dehydration of hexoses, and is considered to be a promising feedstock for bioderived products.[21-23] Selective oxidation of the alcohol and aldehyde side-groups of HMF yields FDCA, a versatile building block for biobased polymers. For example, Avantium Technologies BV (Netherlands) has developed a process to produce polyethylene 2,5-furandicarboxylate (PEF) from FDCA and ethylene glycol that has reached pilot-scale operation.[24] The valorization of glycerol through selective oxidation has also received great attention.[25-29] Glycerol is major coproduct of the transesterification process used for biodiesel production, and comprises approximately 10% of

the product stream.[30] U.S. annual biodiesel production climbed steadily over the last decade to about 1.6 billion gallons in 2017.[31] It is desirable to find processes to upgrade renewable glycerol to more valuable chemicals, thereby further improving the feasibility of biodiesel production and reducing our reliance on petroleum sources. Because it has three hydroxyl groups, glycerol can be oxidized to a variety of value-added products, such as dihydroxyacetone, glyceric acid, tartronic acid, and mesoxalic acid; however, it can be challenging to achieve high product selectivity.[32]

1.3. Electrochemistry: Integrating Chemical and Energy Conversions

Electrochemistry is the study of processes occurring at the interface between electron conductors (i.e. electrodes) and ionic conductors (i.e. electrolytes).[33] The driving force for an electrochemical reaction is the difference in electrochemical potential between the electrode and the electroactive species in solution. This driving force can be measured or controlled relative to another electrode with a known potential, named a reference electrode, through external circuitry and equipment (i.e. potentiostat). Quantitative measurement of the current-potential (*i*-*E*) relationship can be made using a three-electrode electrochemical cell, composed of working, reference, and counter electrodes.

Electrochemistry is uniquely capable of integrating the sustainable production of chemicals with renewable energy conversion. Electrochemical syntheses are flexible, with the benefit that reaction activation barriers and product selectivity can be regulated by tuning the electrode potential.[34] As the electrochemical reactions are activated by external potential, rather than thermally, they are generally operable at very mild temperatures and pressures. These conditions make electrochemical methods especially well-suited for conversion of biomass-derived compounds, which are typically thermally unstable.[35] Additionally, electrochemical

methods and analysis give insight into processes occurring at electrode/electrolyte interfaces that would be otherwise unavailable without complex in situ spectroscopic techniques.[36] Electrochemistry also gives rise to fuel cells, which transform chemical energy to electricity and can also coproduce valuable chemicals.[37-39] Moreover, electrochemical cells can utilize renewable energy resources directly through the use of sunlight-harnessing semiconductor electrodes in photoelectrochemical cells, or indirectly using renewable to drive non-spontaneous reactions. Electrocatalysis may play a key role in moving our chemical and energy landscapes towards a sustainable future, yet more fundamental and applied research is needed to develop these new technologies.

1.3.1 Brief overview of electrochemistry theory

The standard cell potential (E^0_{cell}) of an electrochemical reaction is calculated from the change in Gibbs free energy of reaction at standard conditions (ΔG^0_{rxn}), the number of electrons transferred (n), and the Faraday constant (F = 96485.3 C mol^{-1}), by **Equation 1.1**.

$$E^0_{cell} = -\frac{\Delta G^0_{rxn}}{nF} \tag{1.1}$$

The standard electrode potentials for the anode (E^0_a) and cathode (E^0_c) are related to standard cell potential by **Equation 1.2**.

$$E^0_{cell} = E^0_c - E^0_a \tag{1.2}$$

The Nernst relationship describes the equilibrium electrode potential (E_{eq}) at non-standard conditions, shown for an anodic half-reaction in **Equation 1.3**:

$$E_{eq} = E^0 + \frac{RT}{nF}\ln\frac{a_{ox}}{a_{red}} \tag{1.3}$$

in which a_{ox} and a_{red} are the activities of the oxidized and reduced species of the half-reaction, respectively. The actual electrode potential during an electrochemical operation (E) may vary

from E_{eq} due to overpotentials (η) resulting from charge transfer resistance, mass transfer resistance, or resistances associated with a proceeding reaction, as shown in **Equation 1.4**.

$$\eta = E - E_{eq} \tag{1.4}$$

The relationship between kinetic activation overpotentials (η_{ct}) and reaction rate, or current density (j), is often described by the Butler-Volmer equation. So-called "Tafel" behavior is observed for moderate overpotentials, at which j increases exponentially with η_{ct}. Mass transfer overpotentials occur when concentrations at the electrode surface deviate from in the bulk solution. Mass transfer to an electrode is governed by the Nernst-Planck equation, which accounts for migration, diffusion, and convention transport modes.[40] The actual cell voltage (E_{cell}) depends on the cell current (i_{cell}), anode potential (E_a), cathode potential (E_c), and ohmic losses associated with the ionic and electrical conductors that complete the charge circuit, as shown by **Equation 1.5**:

$$E_{cell} = E_c - E_a - |i_{cell}|\left(R_{contact} + R_{electrolyte}\right) \tag{1.5}$$

in which $R_{contact}$ is the electrical contact resistance and $R_{electrolyte}$ is the ionic resistance of the liquid electrolyte solution or solid electrolyte membrane.

1.3.2. Introduction to electrochemical devices

An electrochemical half-reaction cannot proceed without a corresponding counter half-reaction to balance ionic and electronic charges generated or consumed. In experimental research, it is common to use a three-electrode configuration to facilitate direct study of the electrode of interest. Meanwhile, the counter reaction is basically neglected. However in real applications, both electrodes must be considered in order to evaluate the overall energetics and economic viability of the process. Therefore, a common theme throughout this work is to consider the electrochemical reactor as a whole, in terms of the required electrical power input

for electrolytic cells or power generation for fuel cells. Three electrochemical devices for conducting selective alcohol oxidation are introduced in **Figure 1.3**. Conventional electrolytic cells use external electricity input to drive electrochemical reactions. In many electrolytic cells, desired products are only generated at one electrode of interest, while the other serves as an arbitrary counter electrode. However, paired electrolytic cells utilize both the anode and cathode for production of valuable chemicals or fuels through selective oxidation and reduction reactions, respectively. Photoelectrolytic cells are a subtype of electrolytic cell in which at least one electrode is a light-absorbing semiconductor (i.e. photoelectrode). Direct alcohol fuel cells integrate alcohol oxidation at the anode with the thermodynamically-favorable oxygen reduction reaction at the cathode to operate without external electrical energy input, and instead they can generate electricity along with valuable alcohol oxidation products.

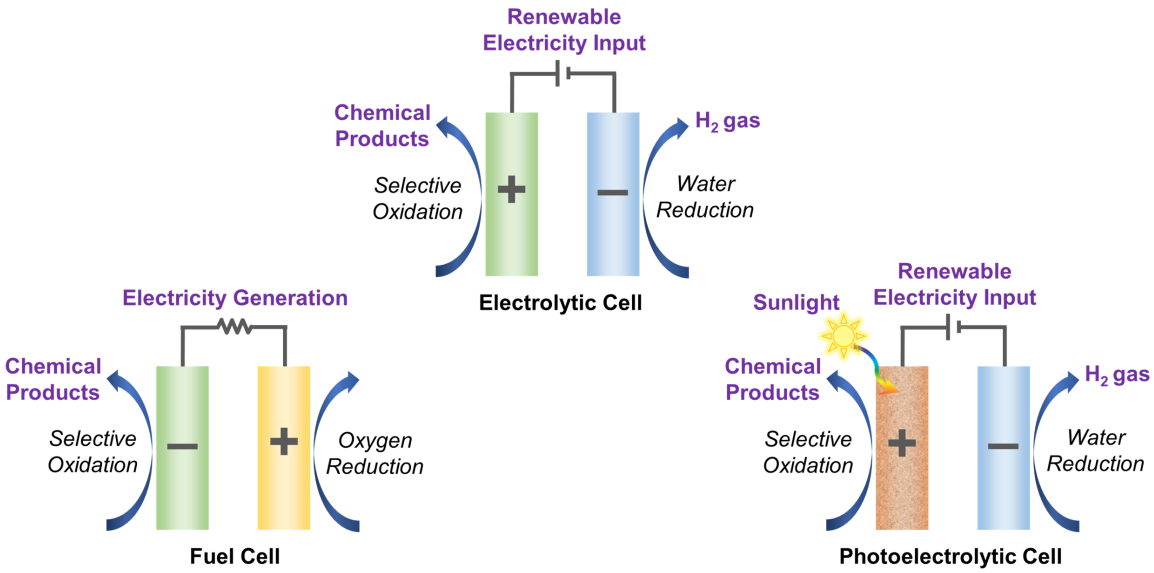

Figure 1.3. Three configurations of electrochemical devices for selective alcohol oxidation.

1.3.3. Electrolytic Cells

Electrolytic cells are electrochemical reactors that require external electrical energy input. The E^0_{cell} of an electrolytic cell is negative by definition, corresponding to a positive ΔG^0_{rxn} for the overall reaction. External voltage is applied to make the cell voltage positive and drive the reactions. The required voltage depends on the thermodynamics and kinetics of the anode and cathode reactions, as well as electrical contact resistances and internal ionic resistances. Large-scale industrial applications of electrolytic cells include the chlor-alkali process for production of chlorine gas and sodium hydroxide, aluminum smelting, perfluorination of hydrocarbons, metal winning and refining, and electroorganic synthesis of adiponitrile.[41] Electrosynthesis has an inherent advantage in terms of sustainability compared to conventional organic synthesis because the electrons used as reagents are clean and inexpensive, and the reactions may be driven by renewable electricity.[42-43] The cost for transferring one mole of electrons is less than ¢1, assuming the average U.S. industrial electricity cost of ¢6.4 per kWh and an operating voltage of 5 V.[44] There is significant interest in developing new technologies related to electrochemical water splitting for sustainable production of H_2, electroreduction of CO_2 to fuels and chemicals, and electrochemical conversion of bioderived chemicals (e.g. alcohols). Generally, the widespread commercialization of electrosynthetic approaches is limited by economic factors, which may be alleviated in the future with development of new catalysts, electrolyte materials, and by the application of electrochemical engineering concepts.

Paired electrolytic cells are a subtype of electrolytic cell that utilize both the anode and cathode for generating valuable products. Electrochemical half-reactions must always occur in pairs. In most electrolytic reactors, desired products are only generated at one electrode of interest, while a sacrificial reaction occurs at the counter electrode to maintain

electroneutrality.[45] However, there are economic and environmental advantages to devising electrochemical schemes in which both electrodes participate in desired reactions. Paired electrolysis may satisfy several aspects of green chemistry by improving atom economy, preventing waste, and reducing energy demands.[42] In 'parallel' paired electrolytic processes, two different starting materials are used, and each reacts at one of the electrodes to generate products.[46] This approach is used commercially for the production of phthalide and 4-(t-butyl)benzaldehyde dimethyl acetal from methyl phthalate and 4-(t-butyl)toluene, respectively.[47] There have also been many parallel electrolytic processes proposed for sustainable production of chemicals and fuels from abundant resources such as biomass, water, and CO_2. For example, CO_2 can be reduced to ethylene, methane, or methanol at a cathode together with simultaneous alcohol oxidation to carboxylic acids at an anode.[48] Also, anodic electrosynthesis paired with water reduction can achieve coproduction of valuable oxidation products and H_2 gas, a clean energy carrier, in a single electrochemical cell.[49-52] A 'divergent' paired electrolytic process involves a single starting material that is oxidized at the anode and reduced at the cathode to generate two different products. An important example is the conversion of glucose to gluconate and sorbitol in a single cell, which is used on an industrial scale.[53] Electrochemical water splitting may be considered a divergent paired electrolytic reaction, as water is the reactant for both H_2 and O_2 generation, although the O_2 produced has limited commercial value.

1.3.4. Photoelectrolytic cells

Photoelectrochemistry is the study of semiconductor/electrolyte interfaces. A photoelectrolytic cell is a subtype of electrolytic cell in which at least one of the electrodes is a semiconductor material. As an extension of the electrochemical approaches outlined so far,

photoelectrochemistry may play an important role in sustainable energy and chemical systems – by which energy from sunlight is directly utilized to partially drive electrochemical reactions. An enormous amount of power is available from the sun over a wide range of wavelengths (i.e. energy), as shown in **Figure 1.4.** By harnessing solar energy to produce photogenerated charges, the electrical energy demand for photoelectrochemical cells is substantially lower than corresponding electrochemical cells.[54-55] The combination of using renewable biomass-derived feedstocks, renewable electricity, and sunlight is potentially one of the most sustainable approaches for chemical production.

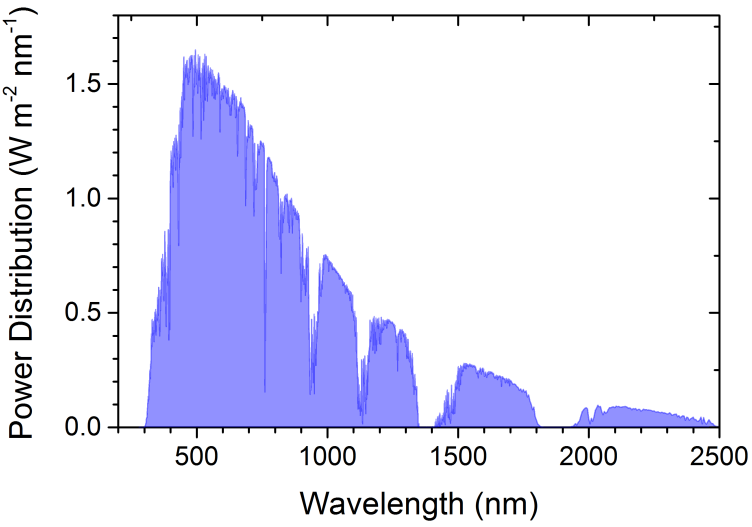

Figure 1.4. Terrestrial solar irradiance spectra (ASTM G173-03 reference).[56]

The electronic properties of a semiconductor are described in terms of the band model, in which there is an energy gap, or band gap, between the valence band (VB) and conduction band (CB). In semiconductors, the VB is almost completely filled while the CB is nearly vacant.[40] Conduction is possible when electrons from the VB are excited to the CB, leaving behind holes in the VB. Both electrons and holes are mobile, and can therefore conduct charge. An intrinsic semiconductor is a material in which the electron and hole densities are equal. A

material doped with donor atoms is called an n-type semiconductor, in which CB electrons are the majority charge carrier. On the other hand, a material doped with acceptor atoms is called a p-type semiconductor, in which the VB holes are the majority charge carriers. The utilization of electron-hole pairs requires spatial separation of the charges, which is induced by the presence of an electric field. Such fields are formed when a semiconductor is put in contact with a redox-active electrolyte, due to equilibrating charge transfer at the semiconductor/electrolyte junction.[40] Charge separation is also enhanced by the application of an external potential to the photoelectrode, usually through a conductive back contact.

For an n-type semiconductor in contact with a redox-active electrolyte, holes migrate toward the semiconductor/electrolyte junction and electrons move toward the electrical contact. The holes have an effective oxidation potential equal to the energy of the VB edge. Therefore, n-type semiconductors promote oxidation reactions at the semiconductor/electrolyte interface and serve as photoanodes. Many of the photoanode materials under investigation are metal oxides, owing to their general chemical stability under oxidizing conditions.[57] A major application for n-type photoelectrochemical materials is as photoanodes for solar water splitting cells. The seminal work by Fujishima and Honda in 1972 demonstrated the photoelectrochemical splitting of water into H_2 and O_2 for the first time, by utilizing an irradiated TiO_2 photoanode and Pt cathode.[58] More recently, there has been inspiration to simultaneously produce H_2 and valuable chemicals by photoelectrochemical alcohol reforming.[49, 59] An efficient photoelectrode should facilitate light absorption, charge separation, charge transport, and electrochemical reactions. Also, photoelectrodes should preferably be composed of Earth-abundant, low-cost, and stable materials. There is motivation to develop heterostructured photoelectrodes composed of multiple materials to meet these

requirements.[60] Other strategies to enhance photoelectrode performance including doping or compositional tuning,[61-66] nanostructuring,[67-68] incorporating heterojunctions,[69-72] and surface modifications,[73-75] have also been widely explored.

1.3.5 Fuel cells

Fuel cells are electrochemical devices in which chemical energy is converted to electricity. The principles of fuel cells are fundamentally similar to batteries, with the key difference that fuel cells operate as open-systems in which electroactive species flow into and out of the device, whereas in conventional batteries the electroactive species are contained within the cell. This attribute gives fuel cells the added flexibility of having separated energy capacity (i.e. in reactant tanks) and power generation (i.e. in the cell). Intrinsically, fuel cells are more efficient than internal combustion engines, which are subject to Carnot efficiency limitations. Fuel cells are a promising energy conversion technology with potential applications including transportation, distributed power generation, backup power generation, and portable power generation. The principles of fuel cell technology were first reported in 1839 by Sir William Grove.[76] Many types of fuel cells have been developed since then, which vary by the type of fuel they consume, the type of electrolyte or membrane employed, and the temperatures at which they operate (**Table 1.1**).[77] The modern revolution of fuel cells was spurred by the introduction of solid polymer electrolytes, developed for the Gemini space mission by Grubb and Niedrach at General Electric.[78-79] The membrane was made of sulfonated polystyrene and had significant advantages over previous designs, such as enabling a more compact design and light-weight construction; however, it was limited by durability issues.[80] Modern solid electrolyte membranes are based on ion exchange polymers and fall into two classes: proton-exchange membranes (PEM) and anion-exchange membranes (AEM).

Table 1.1. Classification and properties of different fuel cells

	Abbreviation	Electrolyte	Temperature (° C)	Fuels	Reference
Alkaline fuel cell	AFC	Aqueous potassium hydroxide	65–220	H_2	81
Polymer electrolyte membrane fuel cell	PEMFC	Polymer membrane	60–140	H_2, alcohols	77
Phosphoric acid fuel cell	PAFC	Phosphoric acid	150–200	H_2	81
Molten carbonate fuel cell	MCFC	Alkali carbonates	600–700	H_2, CO	82
Solid oxide fuel cell	SOFC	Yttria-stabilized zirconia	600–1000	H_2, CO	76, 83

PEM-based fuel cells have received the most attention due to the success of H_2/O_2 fuel cells for automotive and stationary power generation. The most common PEM is Nafion®, a perfluorosulfonic acid ionomer developed by DuPont in 1966, owing to its high conductivity and acceptable thermal and mechanical stabilities.[84] PEM fuel cell performance relies on high loading of platinum-group metals (PGMs), as a result of the generally sluggish electrochemical kinetics in acidic media, especially at the cathode for the oxygen reduction reaction (ORR). The requirement of PGM catalysts limits the widespread application of PEM-based fuel cells due to their high cost and low abundance. Another major disadvantage of PEM-based fuel cells is the limitation of fuel types available, because the PGM catalysts are intolerant to intermediate byproducts (e.g. CO) generated from oxidation of organic fuels, and suffer from potential losses from organic fuel crossover to the cathode.[85] Furthermore, H_2 is not an ideal fuel as it is currently generated by the steam reforming of natural gas, which relies on fossil-

based resources and releases large amounts of greenhouse gases.[19] Additionally, difficulties with H_2 purification, storage and infrastructure issues have inhibited use of PEM fuel cells for transportation applications.[86]

AEM fuel cells (AEMFCs) have many potential advantages over their PEM counterparts. The relevant electrode reactions (e.g. ORR) have generally faster kinetics at high pH in comparison to acidic conditions,[87-88] resulting in higher operating cell voltages and power output. Material corrosion is also minimized in alkaline conditions. The enhanced kinetics and improved material stability in alkaline conditions enable the use of inexpensive ORR catalysts such as non-PGM metals (e.g. Ag) and carbon-based materials.[89-91] These cathode materials are also advantageous in terms of their higher tolerance to poisoning compared to Pt-based catalysts, and also their relative inactivity for oxidations – thereby reducing mixed-potentials losses at the cathode.[92] Furthermore, the direction of ion flow through an AEM is from cathode to anode, eliminating the electroosmotic transport of organic fuels from anode to cathode present in PEM fuel cells, and further reducing crossover issues.[92] Nonetheless, there are many challenges related to the performance, durability, and cost of AEMFCs.

Progress in AEMFC development has motivated extensive research in direct alcohol fuel cells (DAFCs).[93] Early DAFC work focused on small alcohol fuels (e.g. methanol and ethanol) due to their high volumetric energy densities and ease of storage.[92] Alternatively, the selective oxidation of larger alcohols at the fuel cell anode may offer the potential economic advantage of coproducing electricity and chemical products simultaneously.[37-39, 94-96] For example, bioderived polyols (e.g. ethylene glycol, glycerol) have been investigated as potential fuels because of their high energy densities and wide range of useful oxidation products.[38, 97]

1.4 Selective Oxidation of Alcohols and Aldehydes

The selective oxidation of alcohols is a fundamental chemical transformation of key importance in both the industrial and academic realms. Partial oxidation of primary or secondary alcohols yields aldehydes or ketones, respectively, as shown in **Figure 1.5**. Aldehydes may be further oxidized to carboxylic acids following formation of a geminal diol, through reversible hydration.[98] Vicinal diols may also undergo oxidative glycol cleavage, i.e. C–C bond breaking.[99]

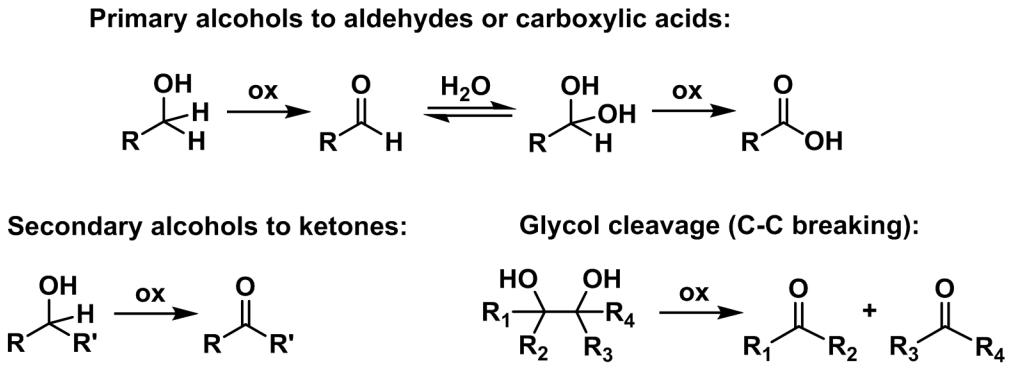

Figure 1.5. Partial oxidation of primary alcohols, secondary alcohols, and vicinal diols.

The total oxidation of alcohols to carbon dioxide is desired in DAFCs, in order to maximize the fuel utilization efficiency, but is undesired for chemical production. Selective oxidation of biomass-derived feedstocks such as polyalcohols (polyols), furanics, and sugars is a potentially environmentally-friendly and sustainable route for chemical production, but has many challenges. Given the range of possible oxidation reactions, it can be difficult to selectively target one product. This is especially true for the conversion of polyfunctional substrates with the existence of multiple alcohol groups or other functional groups that are prone to oxidation. Biomass-derived chemicals are generally complex, multifunctional molecules with high boiling points, and poor thermal stability.[100] As such, mild conditions as used in low

temperature, liquid-phase conversions are generally most suitable. However, conventional liquid-phase oxidation processes, especially those used for fine chemical production, consume stoichiometric amounts of high-oxidation-state transition metals such as potassium permanganate and hexavalent chromium compounds.[101-102] Such reagents have toxicity issues, result in low atom utilization efficiencies, and generate large amounts of inorganic waste. These antiquated methods are not only expensive, but are also not compatible with the principles of green chemistry. As a result, there is a growing need to develop alternative processes that are more efficient and clean.

1.4.1. Homogeneous metal-based catalysts

Catalysis is one of the pillars of green chemistry, with benefits including lower energy requirements, decreased need for additional processing and separation, and less use of toxic materials.[103-104] Extensive research has been done to develop new environmentally-acceptable processes for catalytic alcohol oxidation, particularly based on 'clean' oxidants like oxygen or hydrogen peroxide. Homogeneous catalysts are typically metal complexes based on Cu, Ru, Pd, Au, or V, in the same phase as the reactants.[105] These systems have the major advantage that all active sites are accessible to the reagents. Furthermore, the catalysts usually only contain a single type of active site, which can be tuned by manipulating the complexing ligands to achieve excellent chemoselectivity.[105] However, the use of homogeneous oxidation catalysts in industry has been hindered by energy demands and complications associated with catalyst separation and recovery from the final products. Additionally, problems with corrosion and plating from the catalysts on reaction vessel walls can arise. A hybrid class of catalyst known as 'heterogenized' homogeneous catalysts can be prepared by immobilizing homogeneous catalysts onto support materials, through adsorbing, tethering, or entrapping methods.[106] While

these approaches can alleviate some issues with catalyst separation and recovery, the hybrids typically suffer from leaching, and their stability is a major problem.

1.4.2. Heterogeneous catalysts

Stoichiometric and homogeneous catalytic oxidations are being replaced in industry by heterogeneous catalytic methods using molecular oxygen as the oxidant.[107] As a result of the shift from petroleum-based chemicals to biomass-derived alternatives, there has also been significant academic work focused on selective oxidation of methanol, ethanol, glycerol, and C2–C6 alcohols using heterogeneous catalysis.[36] Heterogeneous catalysts are more practical than homogeneous catalysts in terms of scale-up and process intensification, and can be easily separated from reaction mixtures.[108] The majority of industrial catalysts are metal nanoparticles dispersed on high surface area support materials such as metal oxides (e.g., Al_2O_3, SiO_2, ZrO_2, MgO, and TiO_2) or carbons.[109] Supported PGMs are one of the most commonly used classes of heterogeneous catalysts for alcohol oxidation, because of their ability to activate alcohols and O_2 under relatively mild conditions and produce carbonyls or carboxylic acids with good yields. Pt and Pd are often modified with a promoters such as Pb or Bi, which can enhance oxidation rates or lead to remarkable changes in product selectivity.[110-111] Au is also a good oxidation catalyst, but is only active at high pH. Au catalysts have significant advantages over PGMs, such as being substrate specific, stable against leaching, and resistant to over-oxidation from O_2.[112] Bimetallic or multimetallic catalysts are also widely used for alcohol oxidation, as a result of their advantageous structural or electronic properties compared to monometallic catalysts.[113-117] Unlike homogeneous catalysis, heterogeneous catalysis involves interfacial reactions and processes. Therefore, understanding the nature of catalytically-active sites requires knowledge of solid-state chemistry, physical

chemistry, and of the phenomena occurring across a wide range of spatial and temporal scales. As such, much of the previous progress made in heterogeneous catalyst development has been made by trail-and-error, rather than by rational design of active sites.[118] Recently, advances in the fields of *ab initio* thermochemistry computation, microkinetic modeling, atomic-level characterization, and *in situ* spectroscopy have led to better understanding of catalyst activity, stability and structure-function relations – at least for relatively simple reactions.[119]

A major technical limitation is catalyst deactivation. The blockage of active sites by formation of strongly-bound adsorbates is common during alcohol oxidation, especially for PGM catalysts. These adsorbed species are often formed by undesired side reactions of carbonyl intermediates or products, via aldol condensation, oligomerization, or decomposition to CO or carbonaceous species.[107] Also, it is important to carefully regulate the O_2 supply, because excess O_2 can oxidize the active sites to metal oxides, which are much less active for alcohol oxidation than metallic sites.[120] While the blockage of active sites by adsorbates or oxides is usually reversible, the irreversible loss of active sites can occur through particle sintering or metal dissolution.[121] These irreversible losses are exacerbated by acidic or alkaline conditions and highly oxidizing environments, which are required for facilitating alcohol oxidation. Leaching of the active species not only results in loss of activity, but can also promote undesired side reactions in solution.[122]

1.4.3. Electrocatalysts

The development of electrocatalysts for alcohol oxidation has been largely centered around anode catalysts for oxidation of methanol, ethanol, glycerol, and C2–C6 alcohols in fuel cells.[123] In this section, the term “electrocatalyst” refers to a heterogeneous catalyst that modifies the rate of a redox process occurring at an electrode surface.[40, 124] This term is also

sometimes used to describe electrochemically-active molecular catalysts (e.g. TEMPO). Electrocatalytic reactions involve an electrified electrode/electrolyte interface. Nonetheless, there are many parallels between conventional heterogeneous catalysis and electrocatalysis. Most aspects of conventional catalysis are relevant for electrocatalysis, such as the identification of active sites, identifying intermediates and reaction mechanisms, and studying competitive adsorption phenomena, metal-support interactions, and particle size effects. The materials used in catalysis and electrocatalysis are also similar; they both often involve supported metal nanoparticles. Many of the metals that are most active for conventional catalysis (e.g., Pt, Pd, and Au) are also very active electrocatalysts. Unlike conventional catalysts that are dispersed in the reaction mixture as powders, electrocatalysts are anchored to a conductive substrate for current collection. In this way, catalyst recovery requires no additional separation steps.

1.4.4. Mechanisms of catalytic alcohol oxidation on metal catalysts

The accepted mechanism for catalytic alcohol oxidation occurs through three steps: (1) formation of an adsorbed alkoxide, (2) β-hydride elimination to produce a carbonyl and metal hydride, and (3) oxidation of the metal hydride to regenerate the metal site or metal-hydroxide.[112, 125-126] Further oxidation of the carbonyl (i.e. aldehyde) proceeds by the same mechanism as alcohol oxidation, after formation of a geminal diol through reversible hydration in solution, or on the metal surface via the reaction with surface-bound hydroxides. Formation of the adsorbed alkoxide intermediate requires an initial deprotonation of the alcohol, which may occur in solution or on the metal surface. Both routes are facilitated by hydroxides. The deprotonation in solution depends on the solution pH and is enhanced in alkaline conditions, whereas deprotonation on the metal surface is facilitated by surface-bound hydroxides. β-

hydride elimination occurs on the metal surface, and also may be facilitated by surface-bound hydroxide. Clearly, high pH conditions facilitate several steps of the alcohol oxidation mechanism, and as a result catalytic alcohol oxidations are usually performed in either alkaline or weakly acidic conditions.[127] This is especially important for Au catalysts, which are very active at high pH but have little or no activity for alcohol oxidation in acidic conditions.[112, 126, 128] The third step is oxidation of the metal hydride to regenerate the metal site or metal-hydroxide, which likely proceeds by reductive decomposition of associatively adsorbed O_2, as evidenced by the formation of peroxides during oxidations.[129] Catalytic oxidation does not proceed without O_2; however, isotopic labelling studies revealed that oxygen from O_2 is not directly incorporated into oxidation products.[128] Therefore, the proposed role of O_2 is to remove electrons from the metal surface, oxidize metal hydride bonds, and regenerate hydroxides, thus closing the catalytic cycle.

The most defining differences between catalytic and electrocatalytic alcohol oxidation mechanisms are related to the regeneration of active surface intermediates and the removal of electrons (**Figure 1.6**). In aerobic catalysis, O_2 serves as an electron scavenger; O_2 is reduced to peroxides and hydroxides, thus sustaining electroneutrality. Furthermore, O_2 reduction regenerates active sites by oxidizing the metal hydride bonds. Wieckowski and Neurock elegantly described this as a "local, short-circuited, electrochemical cell".[36] In such a system, O_2 provides the chemical potential required to drive oxidation reactions. In electrocatalysis, the electrochemical potential drives the reaction and facilitates the adsorption of reaction species and hydroxides. Removal of electrons from the metal surface is achieved with an external circuit, and the rate of electron transfer can be directly measured or controlled.

Electroneutrality is achieved by the electrocatalytic oxygen reduction reaction (ORR) at the cathode, which consumes electrons and regenerates hydroxide.

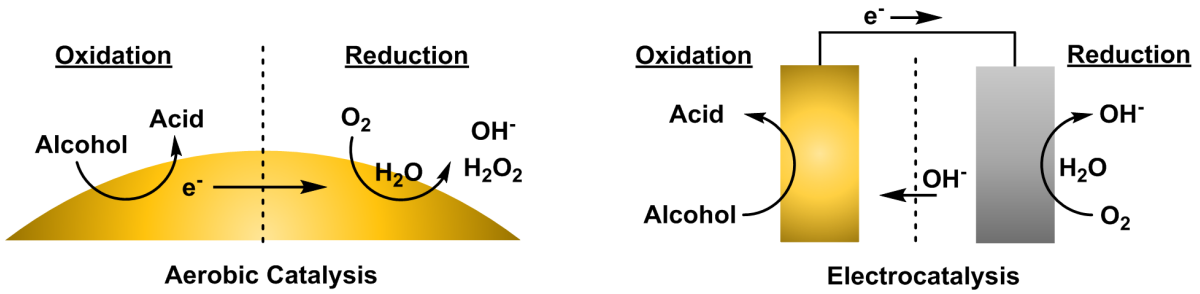

Figure 1.6. Schematic comparison of aerobic catalysis and electrocatalysis for alcohol oxidation. Reaction stoichiometry is not indicated. Adapted from Ide and Davis.[128]

1.4.5. TEMPO-based organocatalysts

Organic nitroxyls are widely used as catalysts for oxidation of primary and secondary alcohols.[130] The most widely used class are based on 2,2,6,6-tetramethylpiperidine-1-oxyl (TEMPO). TEMPO is usually employed as a homogeneous catalyst, and as such suffers from the drawbacks previously mentioned. Nevertheless, conventional oxidation methods are being replaced by TEMPO-catalyzed routes, especially for manufacturing of fine chemicals and pharmaceuticals, because of their remarkable selectivity, low-cost, and metal-free nature.[98, 131] TEMPO is a stable radical and is not active for alcohol oxidation by itself. However, the one-electron oxidation of TEMPO yields an oxoammonium cation (i.e. $TEMPO^+$) which is a relatively strong oxidant. $TEMPO^+$ can also be produced by the acid-catalyzed disproportionation of TEMPO (**Figure 1.7**). However, alcohol oxidation rates are typically much lower in acidic conditions, so the reactions are usually performed with mildly basic conditions.[132]

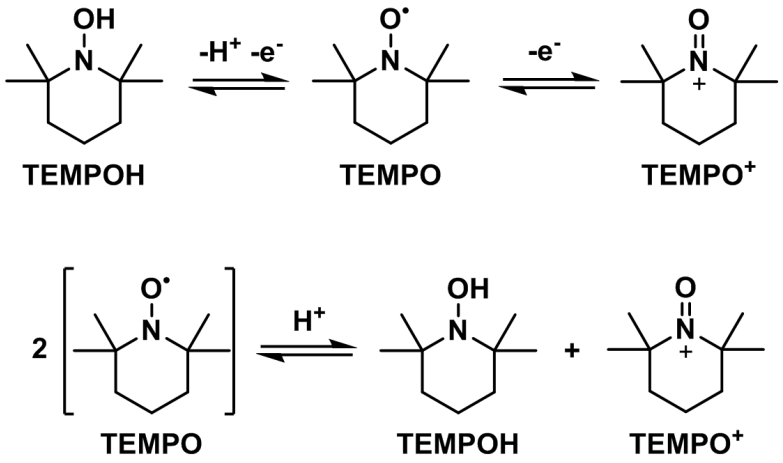

Figure 1.7. TEMPO is oxidized by a one-electron transfer to the oxoammonium cation ($TEMPO^+$) or reduced to hydroxylamine (i.e. TEMPOH). In acidic media, the disproportionation of TEMPO generates TEMPOH and $TEMPO^+$. In basic media, the comproportionation of TEMPOH and $TEMPO^+$ yields TEMPO. [133]

It has been proposed that alcohol oxidation by $TEMPO^+$ in basic conditions begins with deprotonation of the alcohol to form an alkoxide, followed by nucleophilic attack on the nitrogen atom of the oxoammonium ion. Finally, intermolecular proton transfer yields the TEMPO hydroxylamine (i.e. TEMPOH) and the aldehyde (**Figure 1.8**).[134-135] Aldehydes may be further oxidized in a similar manner only after they are hydrated in solution to generate the geminal diol (cf. **Figure 1.5**).[136] Accordingly, aldehydes are the major product of primary alcohol oxidation by TEMPO in non-aqueous conditions, whereas both aldehyde and carboxyl groups may be formed in aqueous conditions. TEMPO and its derivatives are sterically hindered nitroxyls. As such, they are remarkably selective for primary alcohol oxidation in the presence of unprotected secondary alcohols under basic conditions. On the other hand, less hindered bicyclic nitroxyls such as 9-azabicyclo[3.3.1]nonane-N-oxyl (ABNO) or 2-azaadamantane-N-oxyl (AZADO) are suitable for oxidation of either primary and secondary alcohols.[137-138]

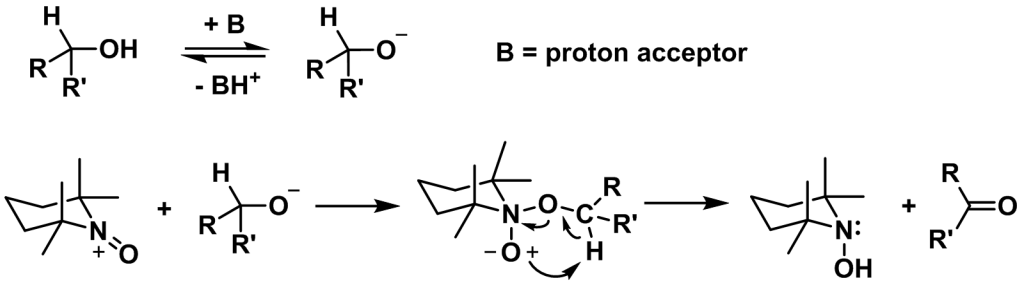

Figure 1.8. Proposed mechanism of alcohol oxidation by the oxoammonium cation of TEMPO in basic solution.

As previously noted, an oxidant is required to generate the reactive oxoammonium cation from TEMPO and to establish the catalytic cycle. Industrial applications of TEMPO-catalyzed alcohol oxidations traditionally followed the Anelli-Montanari protocol,[139] in which stoichiometric amounts of aqueous hypochlorite serve as the primary oxidant while 4-hydroxy-TEMPO and sodium bromide serve as cocatalysts. However, this protocol suffers from environmental drawbacks, such as the use of hypochlorite as the terminal oxidant which generates one equivalent of sodium chloride waste, and also can lead to undesired chlorinated byproducts.[133] There has been significant interest in aerobic oxidations using TEMPO-based catalysts, however TEMPO is not easily activated directly by molecular O_2. Therefore, aerobic oxidations require the aid of a heterogeneous cocatalyst such as graphene oxide,[140-141] or homogeneous transition metals catalysts often based on Ru or Cu metals.[142-148]

Alternatively, the oxoammonium cation can be generated anodically by the one-electron electrochemical oxidation of TEMPO (**Figure 1.9**), as first demonstrated by Semmelhack et al. in 1983.[149] The hydroxylamine (i.e. TEMPOH) resulting from alcohol oxidation can be reoxidized to TEMPO at the electrode to establish a catalytic cycle.[150-152] Alternatively, TEMPO may be regenerated by the comproportionation of TEMPOH with $TEMPO^+$ in basic media (cf. **Figure 1.7**). Electrochemical oxidation with TEMPO-based nitroxyl catalysts is

convenient and clean, as electrical current replaces the primary oxidant, thus preventing the formation of waste. Moreover, this approach has notable applications for energy conversion, as the energy input required to drive the electrochemical cell may be met with renewable electricity, or partially met using sunlight as recently demonstrated in a photoelectrochemical cell.[49] Lastly, TEMPO or its derivatives may be anchored to electrodes, thereby simplifying product separation and catalyst recovery steps.[153-154]

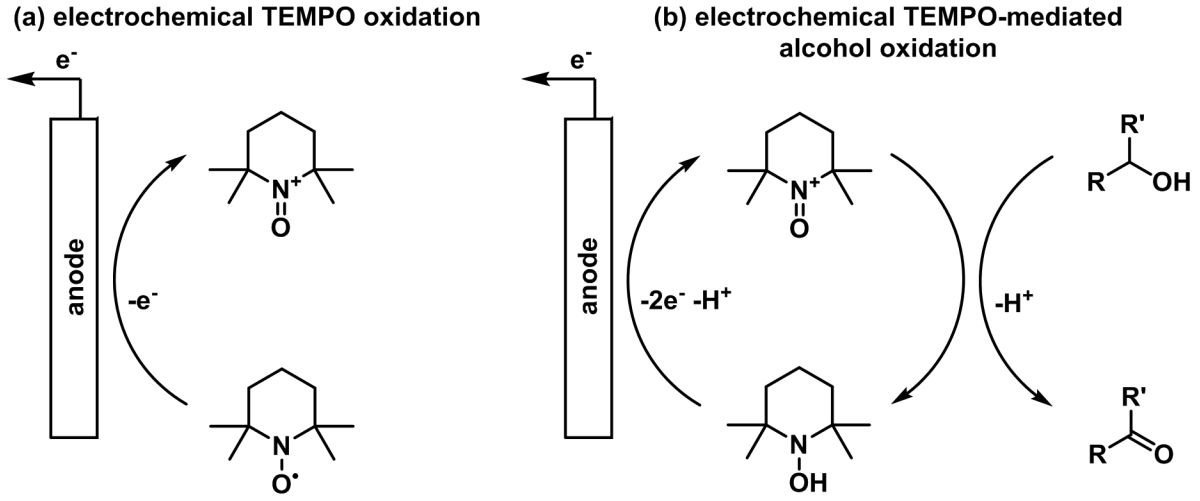

Figure 1.9. Schemes for the (a) electrochemical oxidation of TEMPO and (b) TEMPO-mediated electrochemical alcohol oxidation.

1.5. Current Challenges and Limitations

Many challenges related to electrochemical alcohol oxidations are exacerbated when using biomass-derived feedstocks, which are highly oxygenated and functionalized. Product selectivity can be a serious problem, given the wide range of possible oxidative transformations and the presence of multiple functional groups. It has been demonstrated that product selectivity can greatly depend on reaction conditions, such as electrode potential and electrolyte pH, as well as the nature of the electrocatalyst.[155] Alcohol oxidations with heterogeneous electrocatalysts typically have very large kinetic barriers, especially for bulky

molecules, so expensive precious metal electrocatalysts are usually required to reduce overpotentials and energy demands. Using high pH electrolytes can help alleviate kinetic limitations,[126] but may bring up other issues related to poor stability of reactants, intermediates or products and result in low product selectivity and yield. This is especially true for carbonyl groups, which are prevalent in biomass-derived feedstocks and intermediates, and are susceptible to condensation and polymerization reactions.[35] Additionally, the base-catalyzed Cannizzaro-type disproportionation reactions of aldehydes generate alcohols and carboxyls, and can significantly impact product pathways and selectivity.[156] Therefore, there is a need to better understand how catalysts and reaction conditions affect the reaction pathways and product selectivity for oxidation of biomass-derived molecules in electrochemical cells.

1.6. Research Outline

The overall objective of this research is to further the body of knowledge related to electrocatalysis for selective oxidation of biomass-derived compounds. Specifically, this work focuses on overcoming challenges related to catalyst activity and product selectivity for the electrocatalytic oxidation of bioderived polyols and polyfunctional molecules. The first chapter presents general background information and a literature review of relevant research. The second chapter explores the selective oxidation of 1,2-propanediol on carbon-supported nanoparticle electrocatalysts to gain information about the influences of catalyst material and electrode potential on competing primary and secondary alcohol oxidations. The third chapter extends the work to HMF oxidation with carbon-supported palladium and gold bimetallic nanoparticle electrocatalysts in order to study the competitive oxidation of alcohol and aldehyde groups separated by a heterocyclic ring structure. The dependency of product selectivity on electrode potential, as well as the benefits of bimetallic catalysts compared to

their monometallic counterparts are elucidated. The fourth chapter investigates the use of homogeneous electrocatalysts for selective oxidation of alcohols in photoelectrolytic cells. Specifically, heterostructured photoanodes are developed to facilitate TEMPO-mediated oxidation of HMF to FDCA under very mild conditions. Strategic modifications of semiconductor films using electrodeposition techniques are explored to reduce charge recombination losses, improve energy efficiency, and suppress undesired side reactions

1.7. References

(1) *Monthly Energy Review September 2017*; U.S. Energy Information Administration.

(2) Oreskes, N., The Scientific Consensus on Climate Change. *Science* **2004,** *306* 1686–1688.

(3) Das, S.; Diffenbaugh, N.; Emanuel, K.; Frumkin, H.; Hayhoe, K.; Parmesan, C.; Shepherd, M., What We Know: The Reality, Risks, and Response to Climate Change. *American Association for the Advancement of Science* **2014**.

(4) *Quadrennial Defense Review*. U.S. Department of Defense: 2014.

(5) Höök, M.; Tang, X., Depletion of fossil fuels and anthropogenic climate change—A review. *Energy Policy* **2013,** *52* 797–809.

(6) Guo, M.; Song, W.; Buhain, J., Bioenergy and biofuels: History, status, and perspective. *Renew. Sustainable Energy Rev.* **2015,** *42* 712–725.

(7) *Annual Energy Outlook 2017*. U.S. Energy Information Administration: 2017.

(8) Bird, L.; Cochran, J.; Wang, X. *Wind and Solar Energy Curtailment: Experience and Practices in the United States*; National Renewable Energy Laboratory: 2014.

(9) Denholm, P.; Ela, E.; Kirby, B.; Milligan, M. *The Role of Energy Storage with Renewable Electricity Generation*; 2010.

(10) Gu, S.; Xu, B.; Yan, Y., Electrochemical energy engineering: a new frontier of chemical engineering innovation. *Annu. Rev. Chem. Biomol. Eng.* **2014,** *5* 429–454.

(11) Cherubini, F., The biorefinery concept: Using biomass instead of oil for producing energy and chemicals. *Energy Convers. Manage.* **2010,** *51* 1412–1421.

(12) Isikgor, F. H.; Becer, C. R., Lignocellulosic biomass: a sustainable platform for the production of bio-based chemicals and polymers. *Polym. Chem.* **2015,** *6* 4497–4559.

(13) Nikolau, B. J.; Perera, M. A.; Brachova, L.; Shanks, B., Platform biochemicals for a biorenewable chemical industry. *Plant J.* **2008,** *54* 536–545.

(14) Chheda, J. N.; Huber, G. W.; Dumesic, J. A., Liquid-Phase Catalytic Processing of Biomass-Derived Oxygenated Hydrocarbons to Fuels and Chemicals. *Angew. Chem. Int. Ed.* **2007,** *46* 7164–7183.

(15) Sheldon, R. A., Green and sustainable manufacture of chemicals from biomass: state of the art. *Green Chem.* **2014,** *16* 950−963.

(16) Shanks, B. H., Conversion of Biorenewable Feedstocks: New Challenges in Heterogeneous Catalysis. *Ind. Eng. Chem. Res.* **2010,** *49* 10212–10217.

(17) Shanks, B. H., Across the board: Brent H. Shanks. *ChemSusChem* **2015,** *8* 928–930.

(18) Schwartz, T. J.; O'Neill, B. J.; Shanks, B. H.; Dumesic, J. A., Bridging the Chemical and Biological Catalysis Gap: Challenges and Outlooks for Producing Sustainable Chemicals. *ACS Catal.* **2014,** *4* 2060–2069.

(19) Schüth, F., Hydrogen: Economics and its Role in Biorefining. In *Catalytic Hydrogenation for Biomass Valorization*, Rinaldi, R., Ed. The Royal Society of Chemistry: 2014; pp 1–21.

(20) Gandini, A.; Silvestre, A. J. D.; Neto, C. P.; Sousa, A. F.; Gomes, M., The furan counterpart of poly(ethylene terephthalate): An alternative material based on renewable resources. *J. Polym. Sci. A Polym. Chem.* **2009,** *47* 295–298.

(21) Roman-Leshkov, Y.; Barrett, C. J.; Liu, Z. Y.; Dumesic, J. A., Production of dimethylfuran for liquid fuels from biomass-derived carbohydrates. *Nature* **2007,** *447* 982–985.

(22) Chheda, J. N.; Román-Leshkov, Y.; Dumesic, J. A., Production of 5-hydroxymethylfurfural and furfural by dehydration of biomass-derived mono- and poly-saccharides. *Green Chem.* **2007,** *9* 342–350.

(23) Gallo, J. M. R.; Alonso, D. M.; Mellmer, M. A.; Dumesic, J. A., Production and upgrading of 5-hydroxymethylfurfural using heterogeneous catalysts and biomass-derived solvents. *Green Chem.* **2013,** *15* 85–90.

(24) de Jong, E.; Dam, M. A.; Sipos, L.; Gruter, G. J. M., Furandicarboxylic Acid (FDCA), A Versatile Building Block for a Very Interesting Class of Polyesters. In *Biobased Monomers, Polymers, and Materials*, Smith, P. B.; Gross, R. A., Eds. American Chemical Society: 2012; Vol. 1105, pp 1–13.

(25) Prati, L.; Spontoni, P.; Gaiassi, A., From Renewable to Fine Chemicals Through Selective Oxidation: The Case of Glycerol. *Top. Catal.* **2009,** *52* 288–296.

(26) Katryniok, B.; Kimura, H.; Skrzynska, E.; Girardon, J. S.; Fongarland, P.; Capron, M.; Ducoulombier, R.; Mimura, N.; Paul, S.; Dumeignil, F., Selective catalytic oxidation of glycerol: perspectives for high value chemicals. *Green Chem.* **2011,** *13* 1960–1979.

(27) Simões, M.; Baranton, S.; Coutanceau, C., Electrochemical Valorisation of Glycerol. *ChemSusChem* **2012,** *5* 2106–2124.

(28) Wang, H.; Thia, L.; Li, N.; Ge, X.; Liu, Z.; Wang, X., Pd Nanoparticles on Carbon Nitride–Graphene for the Selective Electro-Oxidation of Glycerol in Alkaline Solution. *ACS Catal.* **2015,** *5* 3174–3180.

(29) Villa, A.; Dimitratos, N.; Chan-Thaw, C. E.; Hammond, C.; Prati, L.; Hutchings, G. J., Glycerol oxidation using gold-containing catalysts. *Acc. Chem. Res.* **2015,** *48* 1403–1412.

(30) Yang, F.; Hanna, M. A.; Sun, R., Value-added uses for crude glycerol–a byproduct of biodiesel production. *Biotechnol. Biofuels* **2012,** *5* 13−22.

(31) *U.S. Energy Information Administration: Monthly Biodiesel Production Report* **2018**.

(32) Pagliaro, M.; Ciriminna, R.; Kimura, H.; Rossi, M.; Della Pina, C., From Glycerol to Value-Added Products. *Angew. Chem. Int. Ed.* **2007,** *46* 4434–4440.

(33) Schmickler, W.; Santos, E., *Interfacial Electrochemistry*. Oxford University Press: Berlin Heidelberg, 1996.

(34) Horányi, G., Heterogeneous catalysis and electrocatalysis. *Catal. Today* **1994,** *19* 285–312

(35) Huber, G. W.; Iborra, S.; Corma, A., Synthesis of Transportation Fuels from Biomass: Chemistry, Catalysts, and Engineering. *Chem. Rev.* **2006,** *106* 4044−4098.

(36) Wieckowski, A.; Neurock, M., Contrast and Synergy between Electrocatalysis and Heterogeneous Catalysis. *Adv. Phys. Chem.* **2011,** *2011* 1–18.

(37) Yuan, X.; Ma, Z.; Bueb, H.; Drillet, J. F.; Hagen, J.; Schmidt, V. M., Cogeneration of electricity and organic chemicals using a polymer electrolyte fuel cell. *Electrochim. Acta* **2005,** *50* 5172–5180.

(38) Simões, M.; Baranton, S.; Coutanceau, C., Electro-oxidation of glycerol at Pd based nano-catalysts for an application in alkaline fuel cells for chemicals and energy cogeneration. *Appl. Catal., B* **2010,** *93* 354–362.

(39) Zhang, Z.; Xin, L.; Li, W., Electrocatalytic oxidation of glycerol on Pt/C in anion-exchange membrane fuel cell: Cogeneration of electricity and valuable chemicals. *Appl. Catal., B* **2012,** *119–120* 40–48.

(40) Bard, A. J.; Faulkner, L. R., *Electrochemical Methods: Fundamentals and Applications*. 2nd ed.; John Wiley & Sons, Inc.: New York, 2001.

(41) Grotheer, M.; Alkire, R.; Varjian, R., Industrial Electrolysis and Electrochemical Engineering. *Electrochem. Soc. Inter.* **2006,** *Spring* 52–54.

(42) Frontana-Uribe, B. A.; Little, R. D.; Ibanez, J. G.; Palma, A.; Vasquez-Medrano, R., Organic electrosynthesis: a promising green methodology in organic chemistry. *Green Chem.* **2010,** *12* 2099–2119.

(43) Aust, N., Organic Electrochemistry, Industrial Aspects. In *Encyclopedia of Applied Electrochemistry*, Kreysa, G.; Ota, K.-i.; Savinell, R. F., Eds. Springer: 2014.

(44) *Electric Power Monthly*. U.S. Energy Information Administration: 2017.

(45) Baizer, M. M.; Hallcher, R. C., Paired Electro-Organic Syntheses I. Cathodic Adipate with Anodic Bimalonate. *J. Electrochem. Soc.* **1976,** *123* 809–813.

(46) Ibanez, J. G.; Frontana-Uribe, B. A.; Vasquez-Medrano, R., Paired Electrochemical Processes: Overview, Systematization, Selection Criteria, Design Strategies, and Projection. *J. Mex. Chem. Soc.* **2016,** *60* 247–260.

(47) Paddon, C. A.; Atobe, M.; Fuchigami, T.; He, P.; Watts, P.; Haswell, S. J.; Pritchard, G. J.; Bull, S. D.; Marken, F., Towards paired and coupled electrode reactions for clean organic microreactor electrosyntheses. *J. Appl. Electrochem.* **2006,** *36* 617−634.

(48) Teamey, K.; Kaczur, J. J.; Cole, E. B.; Majsztrik, P.; Sivasankar, N.; Bocarsly, A. B. Electrochemical reduction of CO_2 with co-oxidation of an alcohol. US 8,845,875 B2, Sep. 30, 2014, 2014.

(49) Cha, H. G.; Choi, K.-S., Combined biomass valorization and hydrogen production in a photoelectrochemical cell. *Nat. Chem.* **2015,** *7* 328–333.

(50) You, B.; Jiang, N.; Liu, X.; Sun, Y., Simultaneous H_2 Generation and Biomass Upgrading in Water by an Efficient Noble-Metal-Free Bifunctional Electrocatalyst. *Angew. Chem. Int. Ed.* **2016,** *55* 9913–9917.

(51) Jiang, N.; You, B.; Boonstra, R.; Terrero Rodriguez, I. M.; Sun, Y., Integrating Electrocatalytic 5-Hydroxymethylfurfural Oxidation and Hydrogen Production via Co–P-Derived Electrocatalysts. *ACS Energy Lett.* **2016,** *1* 386–390.

(52) You, B.; Liu, X.; Jiang, N.; Sun, Y., A General Strategy for Decoupled Hydrogen Production from Water Splitting by Integrating Oxidative Biomass Valorization. *J. Am. Chem. Soc.* **2016,** *138* 13639−13646.

(53) Pintauro, P. N.; Johnson, D. K.; Park, K.; Baizer, M. M.; Nobe, K., The paired electrochemical synthesis of sorbitol and gluconic acid in undivided flow cells. I. *J. Appl. Electrochem.* **1984,** *14* 209–220.

(54) Sun, K.; Park, N.; Sun, Z.; Zhou, J.; Wang, J.; Pang, X.; Shen, S.; Noh, S. Y.; Jing, Y.; Jin, S.; Yu, P. K. L.; Wang, D., Nickel oxide functionalized silicon for efficient photo-oxidation of water. *Energy Environ. Sci.* **2012,** *5* 7872–7877.

(55) Roylance, J. J.; Kim, T. W.; Choi, K.-S., Efficient and Selective Electrochemical and Photoelectrochemical Reduction of 5-Hydroxymethylfurfural to 2,5-Bis(hydroxymethyl)furan using Water as the Hydrogen Source. *ACS Catal.* **2016,** *6* 1840–1847.

(56) Reference Solar Spectral Irradiance: ASTM G-173. http://rredc.nrel.gov/solar/spectra/am1.5/ASTMG173/ASTMG173.html (accessed April 1st, 2017).

(57) Walter, M. G.; Warren, E. L.; McKone, J. R.; Boettcher, S. W.; Mi, Q.; Santori, E. A.; Lewis, N. S., Solar Water Splitting Cells. *Chem. Rev.* **2010,** *110* 6446–6473.

(58) Fujishima, A.; Honda, K., Electrochemical Photolysis of Water at a Semiconductor Electrode. *Nature* **1972,** *238* 37–39.

(59) Lu, X.; Xie, S.; Yang, H.; Tong, Y.; Ji, H., Photoelectrochemical hydrogen production from biomass derivatives and water. *Chem. Soc. Rev.* **2014,** *43* 7581–7593.

(60) van de Krol, R.; Grätzel, M., *Photoelectrochemical Hydrogen Production*. Springer: 2012.

(61) Yao, W.; Iwai, H.; Ye, J., Effects of molybdenum substitution on the photocatalytic behavior of $BiVO_4$. *Dalton Trans.* **2008,** 1426–1430.

(62) Luo, W.; Yang, Z.; Li, Z.; Zhang, J.; Liu, J.; Zhao, Z.; Wang, Z.; Yan, S.; Yu, T.; Zou, Z., Solar hydrogen generation from seawater with a modified $BiVO_4$ photoanode. *Energy Environ. Sci.* **2011,** *4* 4046–4051.

(63) Jeong, H. W.; Jeon, T. H.; Jang, J. S.; Choi, W.; Park, H., Strategic Modification of $BiVO_4$ for Improving Photoelectrochemical Water Oxidation Performance. *J. Phys. Chem. C.* **2013,** *117* 9104−9112.

(64) Jo, W. J.; Jang, J. W.; Kong, K. J.; Kang, H. J.; Kim, J. Y.; Jun, H.; Parmar, K. P.; Lee, J. S., Phosphate doping into monoclinic $BiVO_4$ for enhanced photoelectrochemical water oxidation activity. *Angew. Chem. Int. Ed.* **2012,** *51* 3147−3151.

(65) Berglund, S. P.; Rettie, A. J.; Hoang, S.; Mullins, C. B., Incorporation of Mo and W into nanostructured $BiVO_4$ films for efficient photoelectrochemical water oxidation. *Phys. Chem. Chem. Phys.* **2012,** *14* 7065–7075.

(66) Cho, S. K.; Park, H. S.; Lee, H. C.; Nam, K. M.; Bard, A. J., Metal Doping of $BiVO_4$ by Composite Electrodeposition with Improved Photoelectrochemical Water Oxidation. *J. Phys. Chem. C.* **2013,** *117* 23048−23056.

(67) McDonald, K. J.; Choi, K.-S., A new electrochemical synthesis route for a BiOI electrode and its conversion to a highly efficient porous $BiVO_4$ photoanode for solar water oxidation. *Energy Environ. Sci.* **2012,** *5* 8553–8557.

(68) Liu, X.; Wang, F.; Wang, Q., Nanostructure-based WO_3 photoanodes for photoelectrochemical water splitting. *Phys. Chem. Chem. Phys.* **2012,** *14* 7894–7911.

(69) Chatchai, P.; Murakami, Y.; Kishioka, S.-y.; Nosaka, A. Y.; Nosaka, Y., Efficient photocatalytic activity of water oxidation over $WO_3/BiVO_4$ composite under visible light irradiation. *Electrochim. Acta* **2009,** *54* 1147–1152.

(70) Hong, S. J.; Lee, S.; Jang, J. S.; Lee, J. S., Heterojunction $BiVO_4/WO_3$ electrodes for enhanced photoactivity of water oxidation. *Energy Environ. Sci.* **2011,** *4* 1781–1787.

(71) Cheng, B. Y.; Yang, J. S.; Cho, H. W.; Wu, J. J., Fabrication of an Efficient $BiVO_4$-TiO_2 Heterojunction Photoanode for Photoelectrochemical Water Oxidation. *ACS Appl. Mater. Interfaces* **2016,** *8* 20032−20039.

(72) Su, J.; Guo, L.; Bao, N.; Grimes, C. A., Nanostructured $WO_3/BiVO_4$ heterojunction films for efficient photoelectrochemical water splitting. *Nano Lett.* **2011,** *11* 1928–1933.

(73) Zhong, D. K.; Choi, S.; Gamelin, D. R., Near-complete suppression of surface recombination in solar photoelectrolysis by "Co-Pi" catalyst-modified W:$BiVO_4$. *J. Am. Chem. Soc.* **2011,** *133* 18370–18377.

(74) Ye, H.; Park, H. S.; Bard, A. J., Screening of Electrocatalysts for Photoelectrochemical Water Oxidation on W-Doped $BiVO_4$ Photocatalysts by Scanning Electrochemical Microscopy. *J. Phys. Chem. C* **2011,** *115* 12464–12470.

(75) Jeon, T. H.; Choi, W.; Park, H., Cobalt-phosphate complexes catalyze the photoelectrochemical water oxidation of $BiVO_4$ electrodes. *Phys. Chem. Chem. Phys.* **2011,** *13* 21392–21401.

(76) Minh, N. Q., Ceramic Fuel Cells. *J. Am. Ceram. Soc.* **1993,** *76* 563−588.

(77) Ramani, V., Fuel Cells. *Electrochem. Soc. Inter.* **2006,** *Spring* 41–44.

(78) Grubb, W. T. Fuel Cell. 2,913,511, 1959.

(79) Niedrach, L. W. Fuel cell. US3134697 A, 1964.

(80) Ru-Shi; Zhang, L.; Sun, X.; Liu, H.; Zhang, J., *Electrochemical Technologies for Energy Storage and Conversion*. First ed.; Wiley-VCH: 2012.

(81) Barbir, F., *PEM Fuel Cells: Theory and Practice*. Elsevier Inc.: 2013.

(82) Lee, C.-G., Molten Carbonate Fuel Cells. In *Encyclopedia of Sustainability Science and Technology*, Meyers, R. A., Ed. Springer: 2012.

(83) Park, S.; Vohs, J. M.; Gorte, R. J., Direct oxidation of hydrocarbons in a solid-oxide fuel cell. *Nature* **2000,** *404* 265–267.

(84) Merle, G.; Wessling, M.; Nijmeijer, K., Anion exchange membranes for alkaline fuel cells: A review. *J. Membr. Sci.* **2011,** *377* 1–35.

(85) Schiller, C. A.; Richter, F.; Gülzow, E.; Wagner, N., Relaxation impedance as a model for the deactivation mechanism of fuel cells due to carbon monoxide poisoning. *Phys. Chem. Chem. Phys.* **2001,** *3* 2113–2116.

(86) Moore, R. B.; Raman, V., Hydrogen infrastructure for fuel cell transportation. *Int. J. Hydrogen Energy* **1998,** *23* 617–620.

(87) Wang, Y.; Li, L.; Hu, L.; Zhuang, L.; Lu, J.; Xu, B., A feasibility analysis for alkaline membrane direct methanol fuel cell: thermodynamic disadvantages versus kinetic advantages. *Electrochem. Comm.* **2003,** *5* 662–666.

(88) Antolini, E.; Gonzalez, E. R., Alkaline direct alcohol fuel cells. *J. Power Sources* **2010,** *195* 3431–3450.

(89) Xin, L.; Zhang, Z.; Wang, Z.; Qi, J.; Li, W., Carbon supported Ag nanoparticles as high performance cathode catalyst for H_2/O_2 anion exchange membrane fuel cell. *Front. Chem.* **2013,** *1* 16–20.

(90) Wang, Z.; Xin, L.; Zhao, X.; Qiu, Y.; Zhang, Z.; Baturina, O. A.; Li, W., Carbon supported Ag nanoparticles with different particle size as cathode catalysts for anion exchange membrane direct glycerol fuel cells. *Renew. Energy* **2014,** *62* 556–562.

(91) Qiu, Y.; Huo, J.; Jia, F.; Shanks, B. H.; Li, W., N- and S-doped mesoporous carbon as metal-free cathode catalysts for direct biorenewable alcohol fuel cells. *J. Mater. Chem. A* **2016,** *4* 83–95

(92) Varcoe, J. R.; Slade, R. C. T., Prospects for Alkaline Anion-Exchange Membranes in Low Temperature Fuel Cells. *Fuel cells* **2005,** *5* 187–200.

(93) Kabir, S.; Serov, A., Anodic materials for electrooxidation of alcohols in alkaline media. *Electrochemistry* **2017,** *14* 61–101.

(94) Alcaide, F.; Cabot, P.-L.; Brillas, E., Fuel cells for chemicals and energy cogeneration. *J. Power Sources* **2006,** *153* 47–60.

(95) Qi, J.; Xin, L.; Chadderdon, D. J.; Qiu, Y.; Jiang, Y.; Benipal, N.; Liang, C.; Li, W., Electrocatalytic selective oxidation of glycerol to tartronate on Au/C anode catalysts in anion exchange membrane fuel cells with electricity cogeneration. *Appl. Catal., B* **2014,** *154–155* 360–368.

(96) Chadderdon, D. J.; Xin, L.; Qi, J.; Brady, B.; Miller, J. A.; Sun, K.; Janik, M. J.; Li, W., Selective Oxidation of 1,2-Propanediol in Alkaline Anion-Exchange Membrane Electrocatalytic Flow Reactors: Experimental and DFT Investigations. *ACS Catal.* **2015,** *5* 6926−6936.

(97) Xin, L.; Zhang, Z.; Qi, J.; Chadderdon, D.; Li, W., Electrocatalytic oxidation of ethylene glycol (EG) on supported Pt and Au catalysts in alkaline media: Reaction pathway investigation in three-electrode cell and fuel cell reactors. *Appl. Catal., B* **2012,** *125* 85–94.

(98) Alcohols, Diols, and Thiols. In *Organic Chemistry*, 6th Edition ed.; Carey, F. A., Ed. McGraw-Hill Companies: 2006.

(99) Perlin, A. S., *Glycol-Cleavage Oxidation*. Academic Press: 2006; Vol. 60, p 183–250.

(100) Delidovich, I.; Leonhard, K.; Palkovits, R., Cellulose and hemicellulose valorisation: an integrated challenge of catalysis and reaction engineering. *Energy Environ. Sci.* **2014,** *7* 2803–2830.

(101) Sheldon, R. A.; Dakka, J., Heterogeneous catalytic oxidations in the manufacture of fine chemicals *Catal. Today* **1994,** *19* 215–246

(102) Sheldon, R. A., Catalysis: The Key to Waste Minimization. *J. Chem. Tech. Biotechnol.* **1997,** *68* 381–388.

(103) Anastas, P. T.; Kirchhoff, M. M.; Williamson, T. C., Catalysis as a foundational pillar of green chemistry. *Appl. Catal., A* **2001,** *221* 3–13.

(104) Sheldon, R. A., Fundamentals of green chemistry: efficiency in reaction design. *Chem. Soc. Rev.* **2012,** *41* 1437–1451.

(105) Cardona, F.; Parmeggiani, C., *Transition Metal Catalysis in Aerobic Alcohol Oxidation*. The Royal Society of Chemistry: 2014.

(106) Kirschning, A., *Immobilized Catalysts: Solid Phases, Immobilization and Applications*. Springer: 2004; Vol. 242.

(107) Mallat, T.; Baiker, A., Oxidation of Alcohols with Molecular Oxygen on Solid Catalysts. *Chem. Rev.* **2004,** *104* 3037–3058.

(108) Gavriilidis, A.; Constantinou, A.; Hellgardt, K.; Hii, K. K.; Hutchings, G. J.; Brett, G. L.; Kuhn, S.; Marsden, S. P., Aerobic oxidations in flow: opportunities for the fine chemicals and pharmaceuticals industries. *React. Chem. Eng.* **2016,** *1* 595–612.

(109) Bell, A. T., The Impact of Nanoscience on Heterogeneous Catalysis. *Science* **2003,** *299* 1688–1691.

(110) Kimura, H.; Tsuto, K., Selective oxidation of glycerol on a platinum-bismuth catalyst. *Appl. Catal., A* **1993,** *96* 217–228.

(111) Alardin, F.; Delmon, B.; Ruiz, P.; Devillers, M., Stability of bimetallic Bi–Pd and Pb–Pd carbon-supported catalysts during their use in glyoxal oxidation. *Catal. Today* **2000,** *61* 255–262.

(112) Zope, B. N.; Hibbitts, D. D.; Neurock, M.; Davis, R. J., Reactivity of the Gold/Water Interface. *Science* **2010,** *330* 74–78.

(113) Suntivich, J.; Xu, Z.; Carlton, C. E.; Kim, J.; Han, B.; Lee, S. W.; Bonnet, N.; Marzari, N.; Allard, L. F.; Gasteiger, H. A.; Hamad-Schifferli, K.; Shao-Horn, Y., Surface composition tuning of Au-Pt bimetallic nanoparticles for enhanced carbon monoxide and methanol electro-oxidation. *J. Am. Chem. Soc.* **2013,** *135* 7985−7991.

(114) Griffin, M. B.; Rodriguez, A. A.; Montemore, M. M.; Monnier, J. R.; Williams, C. T.; Medlin, J. W., The selective oxidation of ethylene glycol and 1,2-propanediol on Au, Pd, and Au–Pd bimetallic catalysts. *J. Catal.* **2013,** *307* 111–120.

(115) Hutchings, G. S., Selective oxidation using supported gold bimetallic and trimetallic nanoparticles. *Catal. Today* **2014,** *238* 69–73.

(116) Pizzutilo, E.; Freakley, S. J.; Geiger, S.; Baldizzone, C.; Mingers, A.; Hutchings, G. J.; Mayrhofer, K. J. J.; Cherevko, S., Addressing stability challenges of using bimetallic electrocatalysts: the case of gold–palladium nanoalloys. *Catal. Sci. Technol.* **2017,** *7* 1848–1856

(117) Marx, S.; Baiker, A., Beneficial Interaction of Gold and Palladium in Bimetallic Catalysts for the Selective Oxidation of Benzyl Alcohol. *J. Phys. Chem. C* **2009,** *113* 6191–6201.

(118) Ball, P., Catalysis: facing the future. *Natl. Sci. Rev.* **2015,** *2* 202–204.

(119) Kalz, K. F.; Kraehnert, R.; Dvoyashkin, M.; Dittmeyer, R.; Glaser, R.; Krewer, U.; Reuter, K.; Grunwaldt, J. D., Future Challenges in Heterogeneous Catalysis: Understanding Catalysts under Dynamic Reaction Conditions. *ChemCatChem* **2017,** *9* 17–29.

(120) Van Dam, H. E.; Kieboom, A. P. G.; Van Bekkum, H., Pt/C oxidation catalysts. Part 1. Effect of carrier structure on catalyst deactivation during the oxidation of glucose 1-phosphate into glucuronic acid 1-phosphate. *Appl. Catal.* **1987,** *33* 361–372.

(121) Besson, M.; Gallezot, P., Deactivation of metal catalysts in liquid phase organic reactions. *Catal. Today* **2003,** *81* 547–559.

(122) Sheldon, R. A.; Wallau, M.; Arends, I. W. C. E.; Schuchardt, U., Heterogeneous Catalysts for Liquid-Phase Oxidations: Philosophers' Stones or Trojan Horses? *Acc. Chem. Res.* **1998,** *31* 485–493.

(123) Lamm, A.; Gasteiger, H.; Vielstich, W., Vol. 2, Electrocatalysis. In *Fuel Cell Handbook*, Wiley-VCH: 2003.

(124) McCreery, R. L., Advanced Carbon Electrode Materials for Molecular Electrochemistry. *Chem. Rev.* **2008,** *108* 2646–2687.

(125) Davis, S. E.; Ide, M. S.; Davis, R. J., Selective oxidation of alcohols and aldehydes over supported metal nanoparticles. *Green Chem.* **2013,** *15* 17–45.

(126) Kwon, Y.; Lai, S. C.; Rodriguez, P.; Koper, M. T., Electrocatalytic oxidation of alcohols on gold in alkaline media: base or gold catalysis? *J. Am. Chem. Soc.* **2011,** *133* 6914–6917.

(127) Gangwal, V.; Vanderschaaf, J.; Kuster, B.; Schouten, J., Influence of pH on noble metal catalysed alcohol oxidation: reaction kinetics and modelling. *J. Catal.* **2005,** *229* 389−403.

(128) Ide, M. S.; Davis, R. J., The Important Role of Hydroxyl on Oxidation Catalysis by Gold Nanoparticles. *Acc. Chem. Res.* **2013,** *47* 825–833.

(129) Ketchie, W.; Murayama, M.; Davis, R., Selective oxidation of glycerol over carbon-supported AuPd catalysts. *J. Catal.* **2007,** *250* 264–273.

(130) De Nooy, A. E. J.; Besemer, A. C.; Bekkum, H. v., On the use of stable organic nitroxyl radicals for the oxidation of primary and secondary alcohols. *Synthesis* **1996,** *1996* 1153–1174.

(131) Ciriminna, R.; Pagliaro, M., Industrial Oxidations with Organocatalyst TEMPO and Its Derivatives. *Org. Process Res. Dev.* **2010,** *14* 245–251.

(132) Bobbitt, J. M., Oxoammonium Salt Oxidations of Alcohols. *ChemInform* **2011,** *146* 2–10.

(133) Sheldon, R. A.; Arends, I. W. C. E., Organocatalytic Oxidations Mediated by Nitroxyl Radicals. *Adv. Synth. Catal.* **2004,** *346* 1051–1071.

(134) Semmelhack, M. F.; Schmid, C. R.; Cortes, D. A., Mechanism of the oxidation of alcohols by 2,2,6,6-tetramethylpiperidine nitrosonium cation. *Tetrahedron Lett.* **1986,** *27* 1119–1122.

(135) Bailey, W. F.; Bobbitt, J. M.; Wiberg, K. B., Mechanism of the Oxidation of Alcohols by Oxoammonium Cations. *J. Org. Chem.* **2007,** *72* 4504–4509.

(136) de Nooy, A. E. J.; Besemer, A. C.; Bekkum, H. v., Selective Oxidation of Primary Alcohols Mediated by Nitroxyl Radical in Aqueous Solution. Kinetics and Mechanism. *Tetrahedron* **1995,** *51* 8023–8032.

(137) Demizu, Y.; Shiigi, H.; Oda, T.; Matsumura, Y.; Onomura, O., Efficient oxidation of alcohols electrochemically mediated by azabicyclo-N-oxyls. *Tetrahedron Lett.* **2008,** *49* 48–52.

(138) Lauber, M. B.; Stahl, S. S., Efficient Aerobic Oxidation of Secondary Alcohols at Ambient Temperature with an ABNO/NO_x Catalyst System. *ACS Catal.* **2013,** *3* 2612−2616.

(139) Anelli, P. L.; Montanari, F.; Quici, S., A General Synthetic Method for the Oxidation of Primary Alcohols to Aldehydes: (S)-(+)-2-Methylbutanal. *Org. Synth.* **1990,** *69* 212–218.

(140) Lv, G.; Wang, H.; Yang, Y.; Deng, T.; Chen, C.; Zhu, Y.; Hou, X., Graphene oxide: A Convenient Metal-free Carbocatalyst for Facilitating Aerobic Oxidation of 5-Hydroxymethylfurfural into 2,5-Diformylfuran. *ACS Catal.* **2015,** *5* 5636−5646.

(141) Lv, G.; Wang, H.; Yang, Y.; Li, X.; Deng, T. s.; Chen, C.-M.; Zhu, Y. l.; Hou, X., Aerobic Selective Oxidation of 5-Hydroxymethyl-furfural over Nitrogen-doped Graphene Material with 2,2,6,6-Tetramethylpiperidin-oxyl as Cocatalyst. *Catal. Sci. Technol.* **2015,** *6* 2377–2386.

(142) Dijksman, A.; Arends, I. W. C. E.; Sheldon, R. A., Efficient ruthenium–TEMPO-catalysed aerobic oxidation of aliphatic alcohols into aldehydes and ketones. *Chem. Comm.* **1999,** 1591–1592.

(143) Dijksman, A.; Arends, I. W. C. E.; Sheldon, R. A., The Ruthenium/TEMPO - Catalysed Aerobic Oxidation of Alcohols. *Platin. Met. Rev.* **2001,** *45* 15–19.

(144) Dijksman, A.; Marino-Gonzalez, A.; Payeras, A. M. i.; Arends, I. W. C. E.; Sheldon, R. A., Efficient and Selective Aerobic Oxidation of Alcohols into Aldehydes and Ketones Using Ruthenium/TEMPO as the Catalytic System. *J. Am. Chem. Soc.* **2001,** *123* 6826−6833.

(145) Semmelhack, M. F.; Schmid, C. R.; Cortes, D. A.; Chou, C. S., Oxidation of Alcohols to Aldehydes with Oxygen and Cupric Ion, Mediated by Nitrosonium Ion. *J. Am. Chem. Soc.* **1984,** *106* 3374−3376.

(146) Hoover, J. M.; Stahl, S. S., Highly practical copper(I)/TEMPO catalyst system for chemoselective aerobic oxidation of primary alcohols. *J. Am. Chem. Soc.* **2011,** *133* 16901−16910.

(147) Hoover, J. M.; Ryland, B. L.; Stahl, S. S., Mechanism of copper(I)/TEMPO-catalyzed aerobic alcohol oxidation. *J. Am. Chem. Soc.* **2013,** *135* 2357−2367.

(148) Gamez, P.; Arends, I. W. C. E.; Sheldon, R. A.; Reedijk, J., Room Temperature Aerobic Copper–Catalysed Selective Oxidation of Primary Alcohols to Aldehydes. *Adv. Synth. Catal.* **2004,** *346* 805–811.

(149) Semmelhack, M. F.; Chou, C. S.; Cortes, D. A., Nitroxyl-Mediated Electrooxidation of Alcohols to Aldehydes and Ketones. *J. Am. Chem. Soc.* **1983,** *105* 4492−4494.

(150) Rafiee, M.; Miles, K. C.; Stahl, S. S., Electrocatalytic Alcohol Oxidation with TEMPO and Bicyclic Nitroxyl Derivatives: Driving Force Trumps Steric Effects. *J. Am. Chem. Soc.* **2015,** *137* 14751−14757.

(151) Rafiee, M.; Karimi, B.; Alizadeh, S., Mechanistic Study of the Electrocatalytic Oxidation of Alcohols by TEMPO and NHPI. *ChemElectroChem* **2014,** *1* 455–462.

(152) Ciriminna, R.; Ghahremani, M.; Karimi, B.; Pagliaro, M., Electrochemical Alcohol Oxidation Mediated by TEMPO-like Nitroxyl Radicals. *ChemistryOpen* **2017,** *6* 5–10.

(153) Ciriminna, R.; Palmisano, G.; Pagliaro, M., Electrodes Functionalized with the 2,2,6,6-Tetramethylpiperidinyloxy Radical for the Waste-Free Oxidation of Alcohols. *ChemCatChem* **2015,** *7* 552–558.

(154) Das, A.; Stahl, S. S., Non-Covalent Immobilization of Molecular Electrocatalysts for Chemical Synthesis: Efficient Electrochemical Alcohol Oxidation with a Pyrene-TEMPO Conjugate. *Angewandte Chemie* **2017,** *56* 8892–8897.

(155) Vuyyuru, K. R.; Strasser, P., Oxidation of biomass derived 5-hydroxymethylfurfural using heterogeneous and electrochemical catalysis. *Catal. Today* **2012,** *195* 144–154.

(156) Birdja, Y. Y.; Koper, M. T., The Importance of Cannizzaro-Type Reactions during Electrocatalytic Reduction of Carbon Dioxide. *J. Am. Chem. Soc.* **2017,** *139* 2030–2034.

CHAPTER 2

SELECTIVE OXIDATION OF 1,2-PROPANEDIOL IN ALKALINE ANION-EXCHANGE MEMBRANE ELECTROCATALYTIC FLOW REACTORS: EXPERIMENTAL AND DFT INVESTIGATIONS

Modified from a paper published in ACS Catalysis*

David J. Chadderdon,[a] Le Xin,[a] Ji Qi,[a] Brian Brady,[b] Julie A. Miller,[b] Kai Sun,[c] Michael J. Janik,[b] and Wenzhen Li,[a]

[a] *Department of Chemical Engineering Michigan Technological University, Houghton, Michigan 49931, USA*

[b] *Department of Chemical Engineering Pennsylvania State University, University Park, Pennsylvania 16802, USA*

[c] *Department of Material Science and Engineering University of Michigan, Ann Arbor, Michigan 48109, USA*

Abstract

Electrocatalytic oxidation of polyhydric alcohols represents an important route for coproduction of biorenewable chemicals and energy. However, the governing factors leading to high product selectivity remain unclear. Herein, we investigate the selective oxidation of 1,2-propanediol (PDO) to pyruvate or lactate in electrocatalytic reactors over carbon-supported platinum (Pt/C) and gold (Au/C) anode catalysts. PDO-fed alkaline anion-exchange membrane fuel cells successfully cogenerated electricity and valuable chemicals with peak power densities of 46.3 mW cm^{-2} on Pt/C and 10.0 mW cm^{-2} on Au/C. Pt/C was highly selective for primary alcohol group oxidation to lactate (86.8%) under fuel cell conditions, but Au/C yielded significant amounts of pyruvate, a product that previously eluded heterogeneous catalytic

*Chadderdon, D. J.; Xin, L.; Qi, J.; Brady, B.; Miller, J. A.; Sun, K.; Janik, M. J.; Li, W., Selective Oxidation of 1,2-Propanediol in Alkaline Anion-Exchange Membrane Electrocatalytic Flow Reactors: Experimental and DFT Investigations *ACS Catal.* **2015,** *5* 6926−6936.

studies on Au. Sequential oxidation of lactate to pyruvate was not observed on Au/C but did occur slowly on Pt/C. The electrode potential dependent product distribution was investigated, and it was revealed that pyruvate selectivity on Au/C was sensitive to anode potential, and could be varied from 20% to 56%. On the basis of observed product distributions and linear sweep voltammetry of intermediate products, we proposed that the intermediates hydroxyacetone and pyruvaldehyde, which are not stable in high pH electrolyte, can be further oxidized to pyruvate on Au/C only if they are trapped within the thick diffusion layer of the carbon cloth supported catalyst layer. Density functional theory (DFT) calculations of reaction energies identified the most favorable reaction intermediates and provided insight into the likely reaction pathways.

2.1. Introduction

Renewable biomass has received great interest for its potential to replace petroleum as the primary feedstock for liquid fuels, chemicals, and polymeric materials. Biodiesel made by the transesterification of renewable oils and blended with petroleum diesel is a promising transportation fuel, and U.S. production reached over 1.2 billion gallons in 2014.[1] A major coproduct of biodiesel production is glycerol, which comprises approximately 10 wt% of the product stream.[2] It is attractive to find processes to upgrade renewable glycerol to more valuable chemicals, therefore improving the feasibility of biodiesel production and reducing our reliance on petroleum feedstocks. One promising glycerol conversion route is catalytic hydrogenolysis, which can achieve high selectivity to 1,2-propanediol (PDO),[3–5] a key chemical building block currently produced by petrochemical-based processing of propylene oxide.[6] A sustainability analysis found renewable PDO production from glycerol to be a viable and sustainable alternative to the petrochemical route, and this technology has been

commercialized by ADM and BASF.[7] PDO contains vicinal primary and secondary alcohol groups, and may be transformed by selective oxidation into industrially important chemicals, including lactic and pyruvic acids. Oxidation of the primary alcohol group gives lactic acid, which has potential as a major feedstock for sustainable production of polymers, fibers, and solvents,[8,9] while oxidation of the primary and secondary groups yields pyruvic acid, which has seen rising commercial demand as a health supplement,[10] and also as an important feedstock for chemical, pharmaceutical, and agrochemical industries.[11] Selective oxidation of primary and secondary alcohol groups of PDO through efficient catalytic processes represents an important route for biorenewable chemical production.

Selective oxidation of polyhydric alcohols (polyols) has been a long-term challenge in heterogeneous catalysis, and the dominant factors governing the oxidation of different functional groups remain unclear. PDO has been studied not only for the industrial significance of its oxidation products, but also as a model vicinal-diol molecule for selective oxidation. Initial work by Tsijino et al. demonstrated the oxidation of both primary and secondary alcohol groups of PDO using a carbon-supported palladium (Pd/C) catalyst under aqueous conditions (pH 8, 90 °C), with low selectivity to lactic acid, hydroxyacetone, and pyruvic acid.[12] They found that modifying Pd/C with lead, bismuth, or tellurium gave higher yields of pyruvate via sequential oxidation of lactate. Prati and Rossi compared supported Pd, Pt, and Au catalysts for PDO oxidation by O_2 in alkaline media and found that lactic acid formation was highly selective on these catalysts (89−100%) and occurred through a complex pathway of heterogeneous catalytic steps and homogeneous chemical transformations of intermediate species.[13] More recent efforts have focused on optimizing lactic acid yield with Au−Pd,[14] Au−Pt, or Pt−Pd bimetallic catalysts,[15] and under mild conditions with an Au−Pt catalyst on

activated carbon support.[16] An alternative to traditional heterogeneous catalysis is to selectively oxidize PDO under electrocatalytic conditions, in which the interfacial electrode potential directly affects the Gibbs free energy of reaction and Gibbs chemisorption energy of intermediates.[17]

Electrocatalytic oxidation in fuel cell reactors offers the potential economic advantage of coproducing electricity and chemical products simultaneously.[18] Polyols have been investigated as potential fuels because of their high energy densities and wide range of useful oxidation products, and may be viable feedstocks for cogeneration if a desired product can be generated with high selectively.[19–29] Horányi and Torkos identified the main oxidation products for PDO on a platinized platinum electrode in acidic media, and noted that the reaction scheme is complicated by the simultaneous presence of loosely adsorbed and strongly chemisorbed species on the electrode.[30] Alonso and Gonzalez-Velasco studied the electrooxidation of PDO on a bulk Au plate under basic conditions and identified lactic, acetic, and formic acids as stable products, while pyruvic acid was not detected.[31] A PDO-fed organometallic fuel cell has been demonstrated, which generated modest electrical power output and lactic acid with total selectivity, achieving simultaneous production of biorenewable energy and chemicals.[32]

A consistent trend among traditional heterogeneous and electrocatalytic studies has been that oxidation of PDO on Au-based catalysts in alkaline media does not yield significant amounts of pyruvic acid. Our group has investigated the selective electrocatalytic oxidation of polyols on porous carbon cloth supported Pt/C or Au/C electrodes, using glycerol as a model molecule.[23–25, 33–35] A key result was that the formation of mesoxalate, the product of oxidizing two primary and one secondary alcohol group, was achieved with 46% selectivity on Au/C,

whereas mesoxalate formation was not favored on Pt/C anode catalyst (<3% selectivity).[34] Later, we proposed a reaction intermediate trapping effect after demonstrating that the thick, porous structure of Au/C on carbon cloth supported electrodes facilitated deeper oxidation (to mesoxalate) than thin catalyst layers (<3 μm, on a glassy-carbon rotating disk electrode).[35] On the basis of the similar structures of PDO and glycerol, which both have vicinal primary and secondary alcohol groups, we hypothesized that electrocatalytic oxidation of PDO on a porous Au/C electrode could yield pyruvate analogously to glycerol oxidation to mesoxalate, and reveal more insight into the mechanisms and pathways for selective polyol oxidation.

Herein, the simultaneous cogeneration of electricity and chemical products (lactate or pyruvate) was demonstrated on self-prepared Pt/C and Au/C anode catalysts in a PDO-fed alkaline anion-exchange membrane fuel cell reactor with *ex situ* HPLC analysis of liquid products. A custom-made anion-exchange membrane electrocatalytic flow reactor with controllable anode potential was used to study the product selectivity over a wide range of electrode potentials. Linear sweep voltammetry was performed to compare the activity of PDO and proposed intermediate products. A reaction pathway of PDO oxidation for selective formation of lactate or pyruvate was proposed on the basis of results from electrocatalytic experiments and density functional theory (DFT) calculations of reaction energetics over Au(111) and Pt(111) surfaces.

2.2. Methods

2.2.1. Catalyst synthesis and characterization

Carbon-supported nanoparticle Pt/C and Au/C catalysts (40 wt %) were synthesized by a solution-phase reduction method. For Au/C synthesis, carbon black (148 mg, Cabot, Vulcan XC-72R) was pretreated by refluxing in 4.0 M nitric acid before being dispersed in a solution

of hexanes and ethanol in an ultrasonic bath. In a separate flask, the metal precursor, gold(III) chloride (0.5 mmol, Sigma-Aldrich, 99%), was dissolved in a mixture of 1-octadecene (16 mL, Sigma-Aldrich, 90%) and oleylamine (4 mL, Aldrich Chemistry, 70%). The solution was rapidly heated under nitrogen, and a strong reducing agent, lithium triethylborohydride (1.7 mL, Acros Organics, 1.0 M in THF), was quickly injected at 80 °C. The temperature was held for 10 min before cooling in an ice−water bath. The solution was added dropwise to the carbon black mixture under vigorous stirring. Ethanol (800 mL) was pumped slowly into the solution for 10 h. Catalyst was recovered by vacuum filtration and rinsed with ethanol to remove surfactants and solvents. Finally, the catalyst was dried overnight in a vacuum oven at 50 °C.

For Pt/C synthesis, pretreated carbon black (146 mg) was dispersed directly in benzyl ether (20 mL, Acros Organics) by ultrasonication, followed by the addition of platinum(II) acetylacetonate (0.5 mmol, Acros Organics, 97%) under magnetic stirring. The solution was heated under nitrogen, and oleic acid (200 μL, Sigma-Aldrich, 90%) and oleylamine (200 μL) were injected at 60 °C. After the precursors were completely dissolved, the solution was heated rapidly to 120 °C. When the solution was thermally stable, 1.7 mL of lithium triethylborohydride solution was injected. After 30 min, the temperature was increased to 180 °C for 1 h. Finally, the Pt/C was cooled, separated, cleaned, and dried in the same manner as for Au/C. Transmission electron microscopy (TEM) images of the as-prepared catalysts were collected on a JEOL 2010 instrument with an operating voltage of 200 kV. High-resolution TEM (HRTEM) images were collected on a JEOL 2010F instrument with an operating voltage of 300 kV. X-ray diffraction (XRD) patterns were obtained with a Scintag XDS-2000 θ/θ diffractometer using Cu Kα radiation (λ = 1.5406), with a tube current of 35 mA and a tube voltage of 45 kV.

2.2.2. Anion-exchange membrane electrocatalytic flow reactors

PDO oxidation was performed in an anion-exchange membrane fuel cell (AEMFC) using a commercial fuel cell fixture (area 5.0 cm^2, Fuel Cell Technologies) controlled by a fuel cell test system (850e, Scribner Associates Inc.). The anode was Pt/C or Au/C blended with PTFE (10 wt % PTFE) in isopropyl alcohol and applied to a carbon cloth liquid diffusion layer (Fuel Cell Store) with a target metal loading of 1.0 mg cm^{-2}. The cathode was prepared with a carbon supported transition-metal catalyst (4020 Series, Acta) blended with ionomer (AS-4, Tokuyama Corp.) and applied directly to an anion-exchange membrane (AEM A-201, Tokuyama Corp.) with a catalyst loading of 1.5 mg cm^{-2}. Carbon paper (T-060, Toray) was used as the cathode gas diffusion layer. An aqueous solution of 1.0 M PDO with 2.0 M KOH was pumped through the anode at 4.0 mL min^{-1} by peristaltic pump (Gilson Minipuls 3), while humidified, high-purity O2 (>99.99%, 30 psi) was fed into the cathode for the oxygen reduction reaction. The anode fuel, cathode fuel, and cell temperatures were maintained at 50 °C. Polarization curves were obtained by sweeping current from zero to the limiting condition.

Constant cell voltage tests were performed at 0.1 V, where 55 mL of PDO alkaline solution was circulated through the anode chamber in a closed loop for 2 h. The final product solution was analyzed by HPLC. The anode potential was monitored by a Hg/HgO (1.0 M KOH) reference electrode inserted into the anode chamber. All potentials herein are reported with respect to the reversible hydrogen electrode (RHE), calculated as $E_{RHE} = E_{Hg/HgO} + 0.098 + 0.059 \times pH$.[25] A custom-made anion-exchange membrane (AEM) electrocatalytic flow reactor with controllable anode potential was built as described in our previous works.[35,36] Pt/C and Au/C served as working electrode (anode) catalysts, and Pt/C was used as the counter electrode to catalyze the hydrogen evolution reaction. Carbon cloth liquid diffusion layers and membrane

were the same as those used in the AEMFC. A Hg/HgO (1.0 M KOH) reference electrode was inserted directly into the anode compartment, allowing the anode potential to be regulated by potentiostat (Versastat MC, Princeton Applied Research). An aqueous solution of 1.0 M PDO with 2.0 M KOH (25 mL) was circulated in a closed loop through the anode chamber, while 2.0 M KOH circulated through the counter chamber. Solution and reactor temperatures were maintained at 50 °C.

2.2.3. Product analysis

Initial and final reaction mixtures from AEM-based flow reactors were analyzed by HPLC (Agilent 1100) equipped with an Alltech OA-1000 column operated at 60 °C with 5.0 mM sulfuric acid mobile phase flowing at 0.3 mL min^{-1}. Refractive index (Agilent G1362A) and variable wavelength (Agilent G1314F) detectors were used. Products were identified and quantified by comparison to known standard samples. Acid products are reported in their deprotonated forms because the reactions were carried out at high pH conditions. PDO conversion was calculated by **Equation 2.1**:

$$\text{PDO Conversion } \% = \frac{N_{\text{PDO,initial}} - N_{\text{PDO}}}{N_{\text{PDO,initial}}} \times 100\% \tag{2.1}$$

where N_{PDO} is the amount of PDO (moles) determined by HPLC. Product selectivity was calculated as a molar fraction of total identified products by **Equation 2.2**:

$$\text{Product selectivity } \% = \frac{N_{\text{i}}}{\sum_i N_i} \times 100\% \tag{2.2}$$

where N_i is the amount of product species i (moles). Total carbon balances were calculated to confirm that the majority of products had been identified, given by **Equation 2.3**:

$$\text{Carbon balance } \% = \frac{3N_{\text{PDO}} + 3N_{\text{C3}} + 2N_{\text{C2}} + N_{\text{C1}}}{3N_{\text{PDO,initial}}} \times 100\% \tag{2.3}$$

where N is the molar amount of PDO, C_3, C_2, or C_1 products.

2.2.4. Linear sweep voltammetry

Linear sweep voltammetry (LSV) was performed in a glass electrochemical reactor (AFCELL3, Pine Instruments) in a three-electrode configuration. Catalysts were dispersed in isopropyl alcohol by ultrasonication to form a uniform ink (1.0 mg mL^{-1}). With a microsyringe, 20 μL of ink was deposited onto a mirror-polished glassy-carbon rotating disk electrode (Pine Instruments, 5.0 mm diameter). A Hg/HgO (1.0 M KOH) reference electrode and platinum-wire counter electrode were used. LSV was performed at a sweep rate of 1.0 mV s^{-1} in a nitrogen-purged solution of potassium hydroxide (Sigma-Aldrich, ≥85%), with and without addition of PDO (Sigma-Aldrich, ≥99.5%), in 18.2 MΩ cm deionized water. Additional tests were performed with lactic acid (Sigma-Aldrich, ≥98%), pyruvic acid (Sigma-Aldrich, 98%), formic acid (Fisher Scientific, 88%), acetic acid (Fisher Scientific, ≥99.7%), or hydroxyacetone (Sigma-Aldrich, 90%).

2.2.5. DFT calculations of electrocatalytic PDO oxidation

DFT calculations were performed with the Vienna ab initio simulation program (VASP), a molecular dynamics and ab initio energy program.[37–40] The exchange and correlation energies were calculated using the Perdew−Wang functional form (PW91) of the generalized gradient approximation (GGA).[41] A Monkhorst−Pack grid (3×3×1) was used for structure optimization, followed by single-point calculations using a 4×4×1 grid.[42] Forces on the reactant atoms were minimized to values lower than 0.05 eV $Å^{-1}$. The Au(111) and Pt(111) surfaces were modeled with a 3×3 unit cell with four atom layers in a vacuum slab model. The bottom two layers were frozen at their bulk fcc cell optimized positions and the top two layers relaxed during structural optimization.

Reaction energies were determined by evaluating the relative energy of each surface intermediate along the oxidation reaction path as a function of electrode potential. The energy of an electron and proton pair, generated during oxidation elementary steps, was determined using the computational hydrogen electrode model.[43,44] Rather than direct calculation of elementary reaction energies, a state relative energy was defined that can be used to construct an overall reaction energy diagram. We define a relative energy (*RE*) of any surface intermediate, $C_3O_xH_y$*, as the reaction energy to convert an adsorbed alkoxy species ($C_3O_2H_7$*) and a water molecule to oxidation products:

$$C_3O_2H_7^* + H_2O \longrightarrow C_3O_xH_y^* + n(H^+ + e^-) + (3-x)H_2O \quad (2.4)$$

$$RE_{C_3O_xH_y}(U) = E_{C_3O_xH_y^*} - E_{C_3O_2H_7^*} - E_{H_2O} + (3-x)E_{H_2O} + \frac{n}{2}G_{H_2} - neU \quad (2.5)$$

where E_i represents the DFT energy of a species, G_{H2} is the free energy of gaseous H_2 at standard conditions, *e* is the absolute value of the elementary electron charge, and *U* is the electrode potential on the RHE scale. The number of electrons and protons transferred to form the surface intermediate, $C_3O_xH_y$*, is labeled as *n* in **Equations 2.4** and **2.5** and is equal to $3 - y + 2x$. The lowest energy surface alkoxy species (PDO with one alcohol group deprotonated) is used as a reference in generating the reaction energy diagrams. By referencing a surface species, we avoid using an improper reference to a gas-phase propanediol reactant as well as the difficulty of estimating the free energy of the solution-phase propanediol reactant. As solvation of surface species was not considered and the number of strong hydrogen bonds to surface-bound species may differ along the reaction path, conclusions as to dominant reaction paths are only made when differences exceed 0.25 eV.

For the surface-bound intermediates, numerous adsorption sites and configurations were considered on the Au(111) surface. Only the most favorable adsorbed configuration and states

along the energetically preferred reaction path are reported. The (111) surface was used to model surface chemistry, as it is the lowest energy facet of fcc metals. The experimental catalysts will expose numerous facets, and consideration of the impact of higher index facets on catalytic chemistry is beyond the scope of our current work. As our analysis does not consider activation barriers, and all significant mechanistic conclusions are based on path comparisons that differ by greater than 0.25 eV, the conclusions reached will be relatively robust across surface terminations.

For PDO oxidation on Pt(111), our analysis was limited only to the intermediates found to be along the most preferred path on Au(111), and we presumed adsorption at the most favorable sites located on the Au(111) surface. Our aim was to consider whether differences in energetics along the same path would explain observed kinetic and selectivity differences between the two electrodes, and as discussed later, we conclude that differences in path must occur that are left for future work.

Entropic corrections were not added to the initial PDO or H_2O energies, and therefore the absolute value of the relative energy is less meaningful than the relative values between states. Entropic corrections were not added to surface species, as these are small in comparison to the energy differences of significance in discussing the results. Activation barriers were not calculated and are left as a subject of future work. Though activation barriers would provide greater clarity as to the kinetic differences between catalysts or reaction paths, the reaction energies provided are sufficient to provide useful insight into the experimental results observed.

2.3. Results and Discussion

2.3.1. Catalyst characterizations

XRD patterns were collected for self-prepared Pt/C and Au/C, and both catalysts displayed typical face-centered cubic (fcc) patterns with diffraction peaks at around 39°, 46°, 65°, and 78° assigned to the corresponding (111), (200), (220), and (311) facets, respectively (**Figure 2.1**). Average crystallite sizes were calculated from the (220) peaks by the Scherrer equation to be approximately 2.4 and 2.8 nm for Pt/C and Au/C, respectively. TEM images in **Figures 2.2a,c** show evenly dispersed nanoparticles on the carbon support. HRTEM images shown in **Figures 2.2b,d** confirm that the nanoparticles had well-developed crystalline structures. Particle size histograms revealed average particle diameters of 3.1 and 3.0 nm for Pt/C and Au/C, respectively (**Figures 2.2e,f**), which are slightly larger than the average crystallite sizes estimated by XRD.

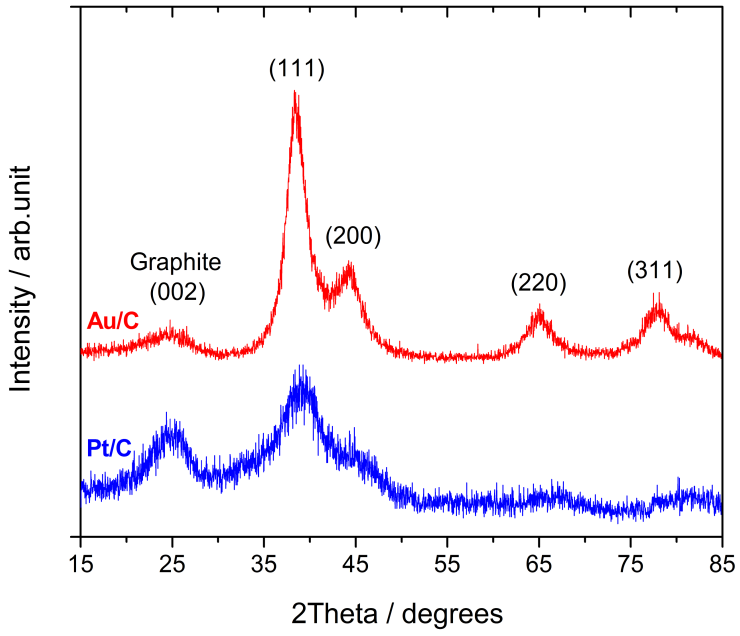

Figure 2.1. XRD patterns for Pt/C and Au/C catalysts.

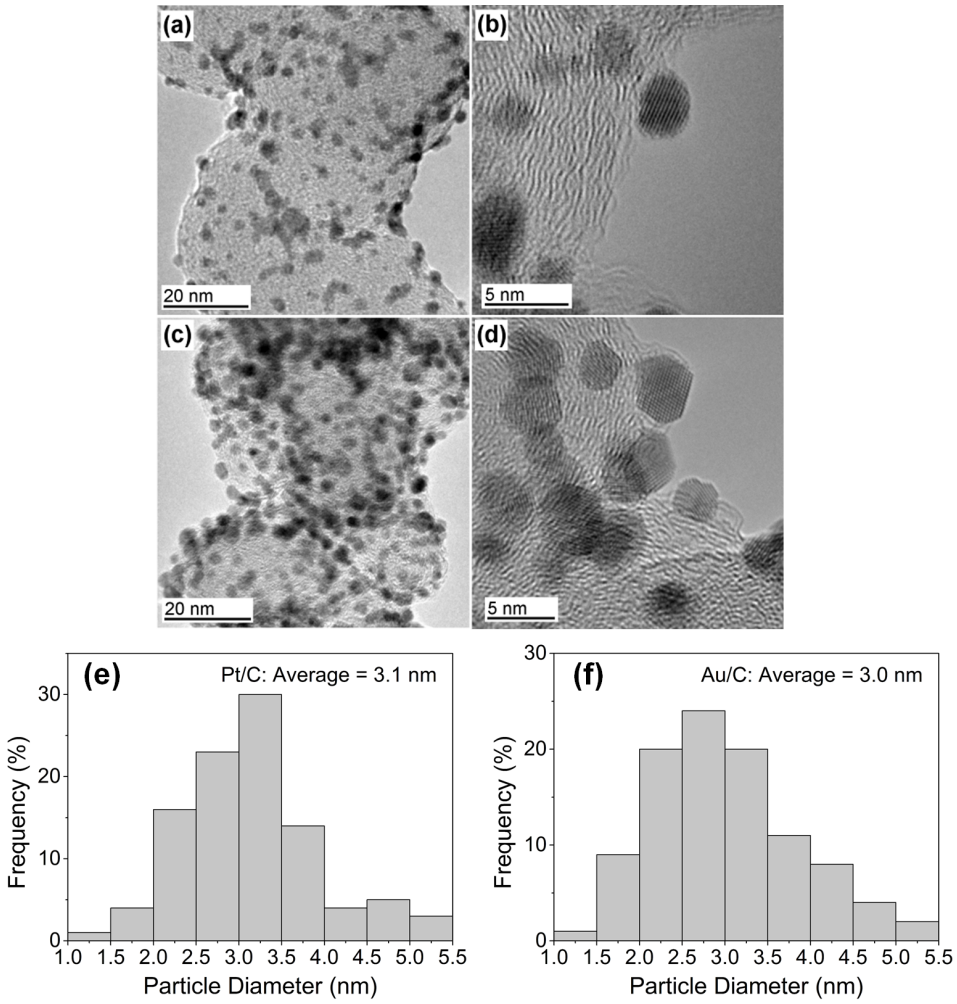

Figure 2.2. TEM and HRTEM images of (a, b) Pt/C and (c, d) Au/C catalysts; TEM particle size histograms for (e) Pt/C and (f) Au/C.

2.3.2. PDO oxidation in AEMFC reactors

Polarization curves shown in **Figure 2.3a** illustrate that AEMFCs with Pt/C and Au/C anode catalysts can spontaneously oxidize PDO and generate electrical power when they are coupled with the oxygen reduction cathode reaction. The cell had significantly greater open-circuit voltage for Pt/C (0.85 V) in comparison to Au/C (0.56 V), attributed to higher activity and lower activation losses for PDO oxidation on Pt/C. Similarly, peak power density on Pt/C (46.3 mW cm^{-2}) was nearly five times greater and limiting current density (310 mA cm^{-2}) was

over three times greater than those on Au/C, consistent with reported results of electrocatalytic oxidation of other polyols in AEMFCs, including glycerol and ethylene glycol, on similar catalysts.[27,45]

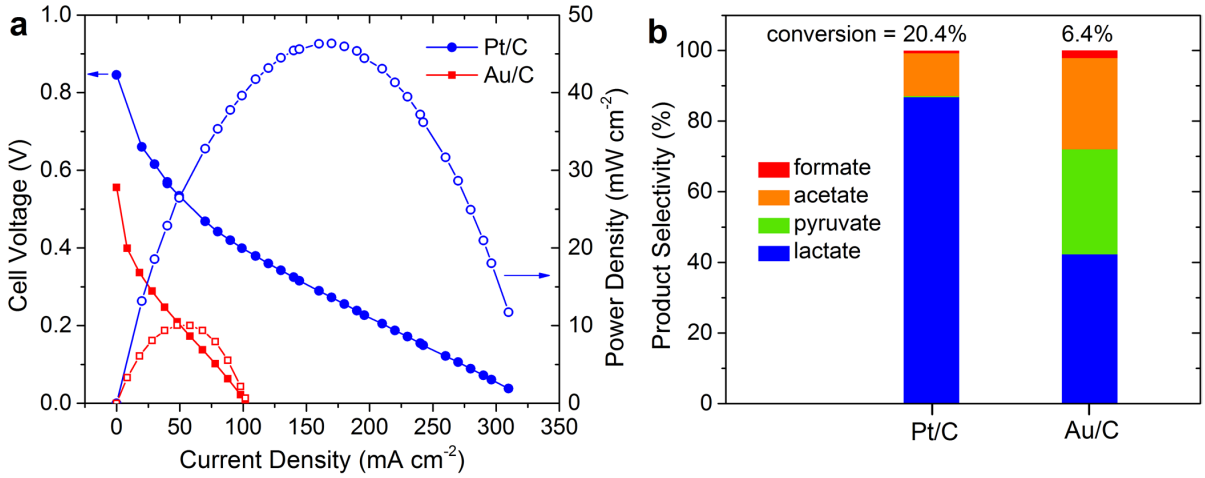

Figure 2.3. (a) Polarization curves showing cell voltage (solid points) and power density (open points) versus current density in PDO-fed AEMFCs and (b) oxidation product distribution after 2 h reaction at a cell voltage of 0.1 V. Conditions: 1.0 M PDO and 2.0 M KOH; 50 °C.

Figure 2.3b shows the oxidation product profiles as determined by HPLC analysis of the bulk liquid electrolyte after 2 h of reaction at a controlled cell voltage of 0.1 V. In agreement with the polarization curves, Pt/C showed greater activity for PDO oxidation, reaching about three times higher PDO conversion than Au/C. Lactate was the dominant product (86.8%) on Pt/C, whereas the more deeply oxidized C3 product pyruvate was detected in trace amounts (<1%). In contrast, significant amounts of pyruvate (30%) were observed on Au/C. This demonstrates that a PDO-fed AEMFC can coproduce important chemicals (lactate and pyruvate) and electrical power, and that product selectivity greatly depends on the anode catalyst. Acetate was the only observed C2 byproduct, with selectivity ranging from 12% to 26%, which indicates that C−C cleavage occurred under these conditions on both catalysts. It

is expected that C−C cleavage would yield equimolar C1 and C2 products (C3 =C1 + C2); however, formate, the only observed C1 product, was present in disproportionally low amounts (1−2%). Carbonate is likely another C1 byproduct, as its presence has been reported in past studies of PDO oxidation,[30] generated either by direct C−C cleavage of C3 species or by sequential oxidation of formate, although it is not included in this study.

A downfall of the AEMFC configuration is that anode potential is determined by the thermodynamics and kinetics of the overall cell, and is typically not directly controlled. Anode potential was monitored during the reactions and averaged 0.39 and 0.49 V versus RHE on Pt/C and Au/C electrodes, respectively. To study the effect of changing anode overpotential on the selective electrocatalytic oxidation of PDO, an alternative reactor design was implemented with a three-electrode setup, the AEM-electrocatalytic flow reactor, in which the anode potential was controlled directly by a potentiostat.

2.3.3. Potential-dependent PDO oxidation

Selective oxidation of PDO was investigated over a wide range of anode potentials in a custom-made AEM-electrocatalytic flow reactor, utilizing carbon cloth supported Pt/C or Au/C electrodes identical to those used in the AEMFC. A solution containing 1.0 M PDO and 2.0 M KOH was cycled through the anode chamber in a closed loop and oxidized at controlled anode potentials for 1 h. Liquid products were analyzed by HPLC, and the carbon balances ranged from 93% to 99%. All applied potentials (*E*) reported in this section are with respect to the RHE. **Figure 2.4a** shows product profiles of PDO oxidation on Pt/C at applied potentials from 0.2 to 0.7 V. PDO conversion steadily increased with increasing potentials to 12.3% at 0.7 V. Selectivity to lactate was insensitive to anode potential over the tested range, with nearly constant selectivity (86−90%). Acetate and formate were detected in approximately equal

amounts at low potentials, but at applied potentials of 0.4 V and higher almost no formate (<1%) was found, which is consistent with results in AEMFC (<1% formate, anode potential 0.39 V). Pyruvate was not detected at potentials lower than 0.4 V, and reached a maximum of 1.2% selectivity at the highest potential tested.

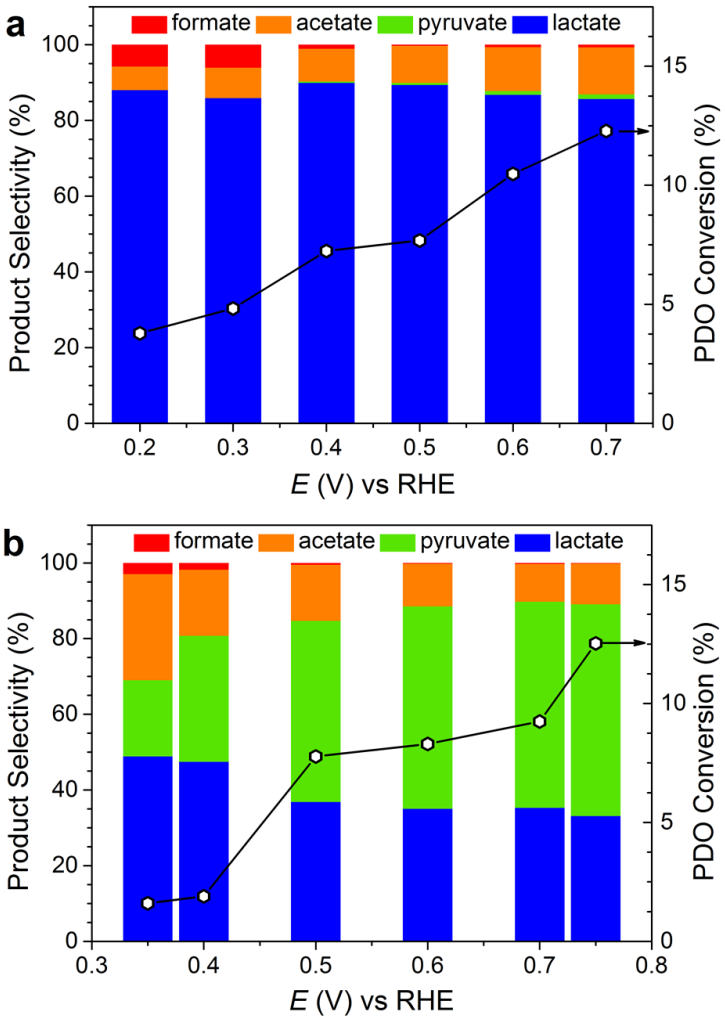

Figure 2.4. Potential-controlled oxidation of PDO on (a) Pt/C and (b) Au/C in AEM-electrocatalytic flow reactor. Conditions: 1.0 M PDO and 2.0 M KOH; 50 °C; 1 h reaction.

Figure 2.4b shows product profiles of PDO oxidation on Au/C at applied potentials from 0.35 to 0.75 V. The metal loading of Au in the anode catalyst layer was increased to 5.0 mg cm^{-2} to achieve sufficiently high PDO conversion for accurate product analysis. PDO

conversion on Au/C was comparable to that on Pt/C, and increased with increasing applied potentials to 12.5% at 0.75 V. Unlike Pt/C, product selectivity on Au/C was strongly dependent on the applied potential. Selectivity to pyruvate, a product not previously obtained from heterogeneous catalytic oxidation of PDO on Au catalysts, increased with increasing potential from 20.1% at 0.35 V to 55.9% at 0.75 V. The increased pyruvate selectivity correlated with decreased lactate and acetate selectivity. Formate was only detected in substantial quantities at potentials less than 0.6 V. Therefore, it is likely that carbonate, not formate, was the main C1 product of C−C cleavage at higher potentials. Further investigations of the activity of PDO and proposed reaction intermediates through linear sweep voltammetry and additional AEM-electrocatalytic flow cell reactions were performed to better understand the selective formation of lactate or pyruvate and the distribution of C1 and C2 products.

2.3.4. Linear sweep voltammetry of PDO and proposed intermediates

Linear sweep voltammetry (LSV) with a sweep rate of 1.0 mV s^{-1} was performed to evaluate the current density (*j*) as a function of potential for alkaline solutions containing PDO and proposed intermediate species. The onset potential was determined as the first potential when oxidation current became greater than the background current, measured in alkaline electrolyte only. PDO oxidation began at significantly more negative potentials on Pt/C than Au/C (**Figure 2.5**), which is consistent with higher open-circuit voltage for Pt/C measured by polarization tests in the AEMFC. The peak current density was reached on Pt/C at around 0.69 V, after which the current decreased sharply due to formation of surface oxides on the catalyst. In contrast, peak current density on Au/C occurred at 1.12 V, reflecting the higher onset potential for surface oxide formation for Au.[46] The results indicate that Au/C should be a very

active catalyst for PDO oxidation at high overpotentials; however, we note that such conditions were not achieved in the AEMFC reactor.

Figure 2.5 also shows linear sweep voltammograms in electrolyte containing 0.1 M of the proposed intermediates lactate, pyruvate, hydroxyacetone, formate, and acetate in 1.0 M KOH. Pyruvaldehyde was not tested, due to its highly unstable nature in alkaline conditions.[14] Qualitatively, LSV helps to elucidate the product selectivity observed in AEM-based flow reactors by revealing the relative reactivity of proposed reaction intermediates and products; however, some variation in onset potentials is expected due to the different reaction conditions, such as catalyst/substrate ratio, catalyst layer thickness, alkaline/substrate ratio, and temperature.

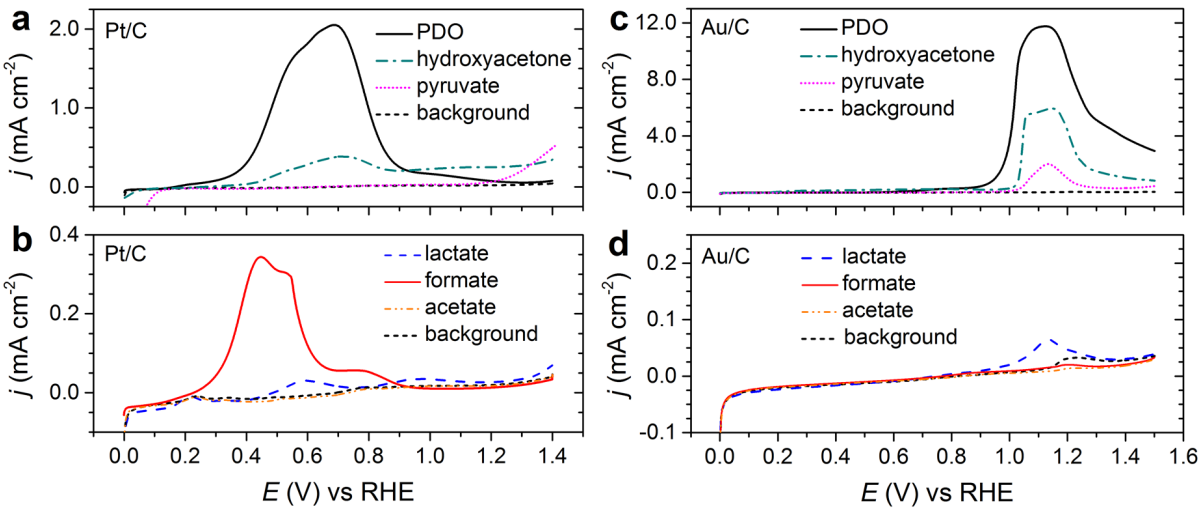

Figure 2.5. Linear sweep voltammograms recorded at 1.0 mV s^{-1} on (a,b) Pt/C and (c, d) Au/C catalysts for 0.1 M PDO or proposed intermediate products in 1.0 M KOH. The background voltammogram is 1.0 M KOH only.

Figure 2.5a shows that pyruvate was nonreactive on Pt/C until potentials greater than about 0.80 V, which is outside the potential range tested during PDO oxidation in AEM-based reactors, indicating that pyruvate is a stable product on Pt/C, and may require PtO_x surface

species and large overpotentials to be further oxidized. As previously shown, lactate was the major product of PDO oxidation on Pt/C in AEM-based reactors; thus, it was surprising that a small oxidation current was observed in the LSV of lactate at moderate potentials (0.4−0.8 V), indicating that lactate is a somewhat reactive species. AEM-electrocatalytic flow cell tests were performed with 1.0 M lactate (**Table 2.1**) and confirmed that further oxidation of lactate on Pt/C at 0.5 V and 0.6 V occurred slowly (lactate conversion about 1% after 1 h), and generated pyruvate. Therefore, we hypothesize that the trace amounts of pyruvate (0.3−1.2%) observed from PDO oxidation for Pt/C in AEM-based reactors at higher applied potentials resulted from sequential oxidation of lactate product. LSV of formate (**Figure 2.5b**) showed reactivity at relatively low potentials, which has been previously reported in alkaline media,[47] and indicates that further oxidation (to carbonate) is likely. This can explain the disproportionally low amount of formate detected on Pt/C. Acetate was found to be nonreactive at all potentials tested on Pt/C; thus, further oxidation of the C2 product is not expected.

Table 2.1. Oxidation of lactate and pyruvate in AEM-electrocatalytic flow cell[a]

catalyst	anolyte[b]	*E* (V) vs RHE	conversion (%)	selectivity (%)	product
Pt/C	lactate	<0.5	-	-	-
		0.5	0.7	100	pyruvate
		0.6	1.0	100	pyruvate
Au/C	lactate	<1.0	-	-	-
		1.0	2.5	98	acetate
		1.1	12.0	100	acetate
		1.2	22.0	100	acetate
Au/C	pyruvate	<1.1	-	-	-
		1.1	28	100	acetate

[a] 1 h reaction. [b] 1.0 M anolyte in aqueous solution with 2.0 M KOH electrolyte.

The LSVs for Au/C in **Figures 2.5c,d** show that the proposed intermediates have relatively low activity at mild potentials (i.e. <1.0 V). The onset potentials of lactate and pyruvate were about 0.83 and 0.81 V, respectively, which are outside the potential range tested in AEM-based reactors for PDO oxidation. Oxidation of 1.0 M lactate or pyruvate in alkaline electrolyte was conducted in the AEM-electrocatalytic flow cell, which confirmed that these species were nonreactive on Au/C at potentials less than about 1.0 to 1.1 V, and acetate was the only product detected (**Table 2.1**), resulting from C−C cleavage. No activity for acetate and formate oxidation was observed by LSV, and further conversion of these products is not expected in the AEM-based reactors. The relative stability of formate on Au/C supports the hypothesis that carbonate, not formate, was the main C1 product of C−C cleavage at higher potentials and explains the disproportionally low selectivity to formate in AEM-based reactors. LSV of hydroxyacetone (**Figure 2.5c**) showed the highest reactivity among proposed C3 intermediates, with a very low onset potential of about 0.15 V, a sharp current increase at about 1.0 V, and a broad peak around 1.1 V. The complexity of the voltammogram could be related to the instability of hydroxyacetone, which is in tautomeric equilibrium with lactaldehyde in alkaline solution through an enediol intermediate.[13] It is probable that the low onset potential observed is attributed to the oxidation of lactaldehyde to lactate. Low onset potentials for aldehyde oxidation (e.g. 0.31 V) have been reported on Au/C in alkaline media.[36] It is likely that hydroxyacetone was an intermediate of PDO oxidation on Au/C, but that it was not detected because of its instability under alkaline conditions.

2.3.5. Proposed reaction intermediates and pathways

On the basis of evidence from product analysis in electrocatalytic flow reactors and linear sweep voltammetry of PDO and intermediate species, we propose that Pt/C has a strong

preference for oxidization of the primary alcohol group of PDO through the O1 pathway of **Figure 2.6**, producing lactate with high selectivity. Formation of lactaldehyde is presumably much slower than its oxidation rate and was not observed in a product analysis of liquid products. Lactate accumulates in the bulk liquid and then very slowly forms pyruvate through secondary alcohol oxidation. C−C bond cleavage occurs with low selectivity to form acetate, a stable product on Pt/C, formate, which can be further oxidized under these conditions, or carbonate, which was not included in this study. On Au/C, lactate is the main product at low applied potentials, but pyruvate becomes more abundant at higher potentials. Since lactate was not further oxidized to pyruvate on Au/C (cf. **Table 2.1**), the pyruvate observed from PDO oxidation was most likely derived from hydroxyacetone by the O2 pathway of **Figure 2.6**.

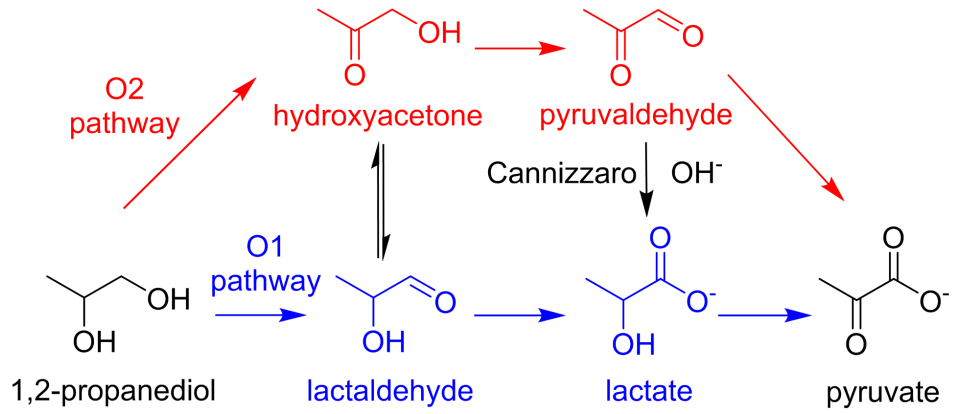

Figure 2.6. Proposed reaction network of PDO oxidation to lactate and pyruvate through O1 and O2 pathways in alkaline solution.

Hydroxyacetone has been proposed as an intermediate of PDO oxidation on Au/C in alkaline media on the basis of evidence from H/D exchange experiments,[13] and from in situ FTIR spectroscopy.[48] Under oxidizing conditions, Prati and Rossi observed completely selective conversion of hydroxyacetone to lactate on Au/C and hypothesized that

hydroxyacetone is either oxidized to pyruvaldehyde and then transformed to lactate through an intramolecular Cannizzaro-type reaction, or that hydroxyacetone is in equilibrium through an enediol intermediate with lactaldehyde, and the latter is rapidly oxidized to lactate.[13] We propose that the intermediates hydroxyacetone and pyruvaldehyde, which are not stable in high pH electrolyte, can be further oxidized to pyruvate on Au/C only if they are trapped (i.e. long residence times) within the thick diffusion layer of the carbon cloth supported catalyst layer. Electrocatalytic oxidation is accelerated with increasing anode potentials and becomes more competitive with the homogeneous reactions, thus explaining the increased pyruvate selectivity shown in **Figure 2.4b**. Additionally, high current densities give rise to decreased local pH within the catalyst layer from the consumption of hydroxide during oxidation reactions,[26] which may suppress the base-catalyzed homogeneous transformations.

We hypothesize that the thick electrode structure was crucial for pyruvate formation, which would explain why pyruvate was not reported previously when using Au/C dispersed in solution,[13,14] a thin film of Au/C on a glassy-carbon electrode,[48] or Au plate (polycrystalline Au) electrodes.[31] Our related study on the selective oxidation of glycerol on Au electrodes demonstrated that a thick catalyst layer was required to oxidize both primary and secondary alcohol groups to mesoxalate.[35] In fact, no mesoxalate was observed on thin catalyst flims (<3 μm, on glassy-carbon electrode). Direct evidence of the O2 pathway to pyruvate was not confirmed, as neither hydroxyacetone nor pyruvaldehyde were identified as intermediates by product analysis, likely due to their instability in the bulk alkaline solution. Furthermore, the equilibrium between lactaldehyde and hydroxyacetone makes a definite determination of the preferred pathway to pyruvate challenging without the use of rigorous theoretical calculations or advanced techniques such as in situ spectroscopy, which should be focuses of future studies.

2.3.6. Electrochemical oxidation mechanism on Au and Pt by DFT

The electrocatalytic selective oxidation of PDO was studied using DFT calculations to identify the most favorable reaction intermediates and provide more evidence of the likely path for the potential-dependent PDO oxidation on Au and Pt catalysts. The electrocatalytic oxidation of alcohol functional groups in alkaline media is largely believed to undergo an initial deprotonation step facilitated by OH^- in the electrolyte, followed by metal-catalyzed C−H and C−C bond breaking steps.[49] Therefore, DFT calculations were performed by starting from either the adsorbed terminal oxygen alkoxy (O1) or the secondary oxygen alkoxy (O2) on Au(111) or Pt(111), both presumed to form following a solution-mediated oxidative deprotonation step. Oxidations of up to six electrons to form pyruvic acid were considered. All potentials referred to in this section are with respect to RHE.

Figure 2.7a depicts the reaction energy diagram for PDO oxidation over the Au(111) surface at 0 V. Blue lines connect states reasonably connected by elementary reaction steps beginning with deprotonation and adsorption of primary alkoxide (O1), whereas red lines are for reactions initiated at the secondary position (O2). All reactions considered as elementary steps involve transfer of a single electron and breaking (deprotonation) or formation (C−OH formation) of a single bond on the surface intermediate. As the reaction energy diagrams in **Figure 2.7** reference the adsorbed alkoxy species, the generally weak binding of intermediates to the Au(111) surface is not evident. Without free energy corrections to the solvated propanediol reactant state, we cannot directly determine an equilibrium coverage of any species on the surface. We instead resort to a reference to the gas-phase species to illustrate the lack of favorability of adsorption to the Au(111) surface and encourage the reader to recognize that additional free energy corrections would act to further destabilize a surface-bound state in

comparison to a fluid-phase state. The O2 alkoxy species ($+H^+ + e^-$) is 1.39 eV higher in energy than gas-phase PDO at 0 V, and all species are at positive energies relative to the gas-phase PDO species at 0 V. This suggests that the Au surface will be devoid of PDO reaction intermediates at 0 V, in agreement with the lack of an oxidation current at this potential. At 0.75 V, the initial alkoxy species remains 0.64 eV higher in energy than a gas-phase PDO reference (**Figure 2.7b)**, suggesting that a low coverage of this initial reactive intermediate may limit the oxidation rate. Formation of oxidation surface intermediates beyond the initial alkoxy species is favorable at 0.75 V, confirming that favorable oxidation may occur at this potential, in agreement with an experimentally observed oxidation current.

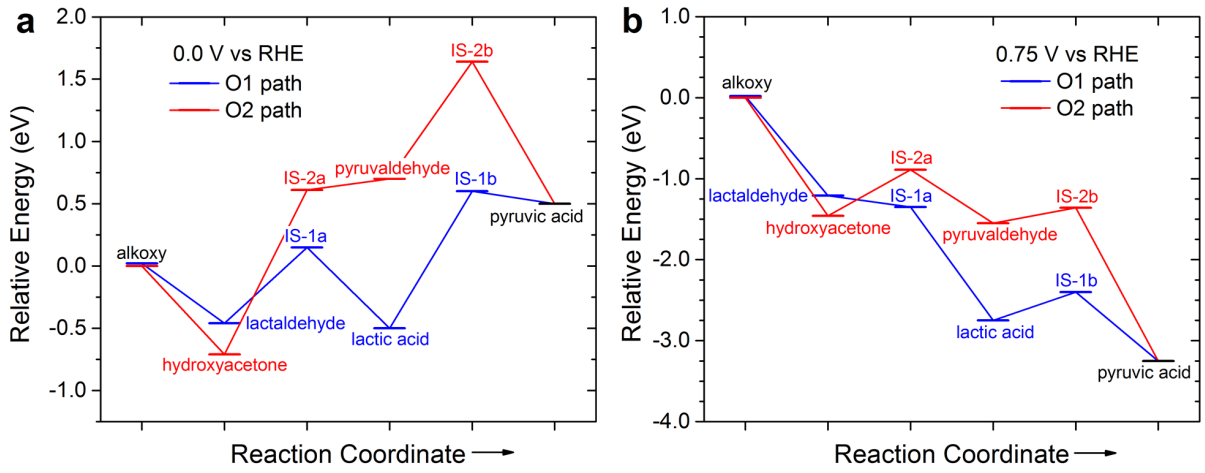

Figure 2.7. Reaction free energy diagrams of PDO oxidation through the O1 and O2 pathways at (a) 0.0 V and (b) 0.75 V on the Au(111) surface.

Formation of lactaldehyde, lactic acid, and pyruvic acid follow from progressively deeper oxidation of the initial O1-bound alkoxy species. On binding through O1, the terminal oxygen, lactaldehyde is formed by favorable C−H breaking of the alkoxide. Though this elementary reaction energy is favorable, this step can be expected to have a significant activation barrier at 0 V. Further oxidation breaks another primary C−H bond, generating an intermediate state

(IS-1a, CH_3−CHOH−C*O, where the asterisk indicates a direct interaction with the surface). The formation of this intermediate state is unfavorable, uphill in energy by 0.61 eV at 0 V, suggesting that lactate formation requires an overpotential to be accessible on the Au(111) surface. Formation of a C−OH bond (and oxidizing H_2O) to lactic acid is then favorable from the unstable IS-1a state. Further oxidation to pyruvic acid requires breaking a secondary C−H bond to form IS-1b (CH_3−C*OH−COOH). Formation of IS-1b from lactic acid has a reaction energy of 1.10 eV at 0 V, and the overall formation of pyruvic acid from lactic acid is unfavorable, corroborating the experimental results that lactate is the major product at low potentials.

If PDO is initially deprotonated at the secondary position, forming an alkoxide bound through O2, initial C−H breaking to form hydroxyacetone is highly favorable. Further oxidation from hydroxyacetone, which is found to preferentially occur through breaking a primary C−H bond, requires a large energy input of 1.32 eV at 0 V to reach IS-2a (CH3−CO−C*HOH). Though formation of hydroxyacetone (O2 path) is slightly thermodynamically favorable over lactaldehyde (O1 path), further oxidation of hydroxyacetone requires multiple high-energy steps to proceed. At low potentials, any hydroxyacetone formed would likely prefer the homogeneous transformation to lactaldehyde via tautomerism and then further oxidization through the O1 path. Further oxidations to pyruvaldehyde and through IS-2b to pyruvic acid are also unfavorable at low potentials. Pyruvaldehyde would be rapidly transformed to lactic acid through a homogeneous Cannizzaro-type reaction under alkaline conditions, as previously reported,[13] rather than continue on the O2 reaction path.

Figure 2.7b illustrates the PDO oxidation reaction energy diagram over the Au(111) surface at 0.75 V. At the higher potential, oxidation through the O1 path to lactic acid is favorable for all elementary steps. Oxidation of lactic acid to pyruvic acid appears favorable at this potential, though an uphill step through IS-1b remains. Both the O1 and O2 paths to pyruvic acid become more accessible as the potential increases, in agreement with the experimentally observed increase in pyruvate selectivity. Formation of IS-1b on the O1 path requires an uphill energy of 0.35 eV at 0.75 V. Both IS-2a (0.57 eV) and IS-2b (0.20 eV) require surmounting uphill energy steps to reach pyruvic acid along the O2 path at 0.75 V. Therefore, on the basis of the DFT calculations and experimental evidence, we propose that lactic acid formation on Au/C can form via two paths, binding through either the primary or secondary alcohols. At low potentials, lactic acid is the only viable stable oxidation product on Au electrodes. At higher overpotentials, DFT results suggest both the O1 and O2 paths to pyruvic acid on Au become viable, with the energetic differences too close (within 0.25 eV) to discern a preference, given the lack of solvation and single Au surface termination considered. Combining these considerations with the experimental observation that lactic acid does not oxidize at low potentials on Au electrodes (cf. **Table 2.1**), we conclude that the O2 path to pyruvic acid becomes operable at higher oxidation potentials.

Figure 2.8 shows the reaction energy diagrams for PDO oxidation over the Pt(111) surface. Relative to a gas-phase PDO species, the O2-bound alkoxy species (+0.93 eV) and all subsequent intermediates are unstable at 0 V, in agreement with the lack of an observed oxidation current at low overpotentials. All intermediates bind more strongly to Pt(111) than to Au(111), and all surface intermediates past the initial alkoxy species (0.18 eV) are stable relative to gas-phase PDO at 0.75 V. Differences in intermediate binding are especially evident

for the unstable (IS-1a, IS-1b, IS-2a, and IS-2b) intermediate states, with all elementary steps on the O1 path being downhill in energy at 0.75 V on Pt(111). The stronger binding of the unstable intermediates demonstrates the greater activity of the Pt catalyst, as the potential limiting steps of forming the IS states on Au are all more favorable on Pt. This agrees with the greater observed oxidation currents for Pt in comparison to those for Au electrodes.

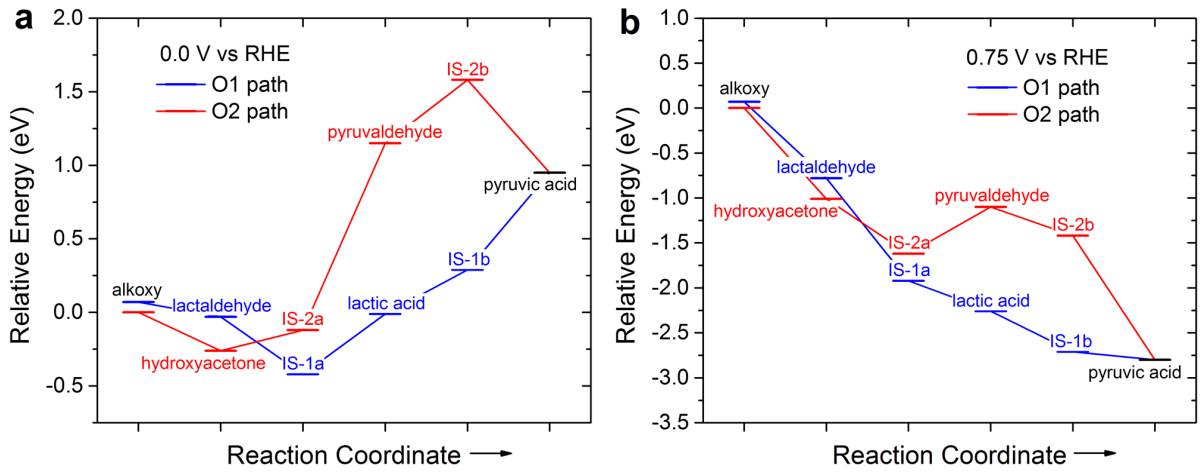

Figure 2.8. Reaction free energy diagrams of PDO oxidation through the O1 and O2 pathways at (a) 0.0 V and (b) 0.75 V on the Pt(111) surface.

Mechanistic causes of selectivity differences between Au and Pt catalysts, specifically Au forming pyruvate at higher potentials whereas Pt is selective to lactate, are not evident from the reaction energy diagrams. Pt(111) shows a more favorable formation of IS-1b for transformation of lactate to pyruvate at lower overpotentials in comparison to the Au(111) surface. The mechanistic source of this selectivity difference must stem from factors not considered in this study, which could include higher index facets of the surface, activation barriers not correlated with reaction energies, surface coverage or electrolyte effects, or differences in reaction paths between Au and Pt not considered herein. We speculate that the surface coverage of intermediates during PDO oxidation will differ significantly between Au

and Pt electrodes and that this is a likely cause of the selectivity differences. Numerous C1 to C3 intermediates could form, bind strongly on the Pt surface, and be resistant to rapid oxidation. A higher coverage of surface intermediates on the Pt surface could drive preferential oxidation at the terminal carbon atom, as the terminal carbon atom could more easily access a surface site in a high-coverage environment than the sterically inhibited secondary carbon. Direct consideration of coverage effects is beyond the scope of this study, but provides an interesting direction for future consideration of selective oxidation of PDO.

2.4. Conclusions

PDO-fed alkaline anion-exchange membrane fuel cells successfully cogenerated electricity and valuable chemical products with peak power densities of 46.3 mW cm^{-2} on Pt/C and 10.0 mW cm^{-2} on Au/C. Pt/C was highly selective for primary alcohol group oxidation to lactate (86.8%) under fuel cell conditions with very little activity of secondary alcohol oxidation to pyruvate. Au/C was less active than Pt/C, but gave significant amounts of pyruvate (30%), a product that previously eluded heterogeneous catalytic studies on Au catalysts. Pyruvate selectivity on Au/C was sensitive to anode potential, and was further increased to 56% by increasing the applied potential in an AEM-electrocatalytic flow reactor. Sequential oxidation of lactate to pyruvate was not observed on Au/C, but did occur slowly on Pt/C. On the basis of observed product distributions and linear sweep voltammetry of intermediate products, we proposed that the intermediates hydroxyacetone and pyruvaldehyde, which are not stable in alkaline electrolyte, can be further oxidized to pyruvate on Au/C only if they are trapped within the thick diffusion layer of the carbon cloth supported catalyst layer. We hypothesized that long residence times and local pH effects within the thick electrode structure were crucial for pyruvate formation, which can explain why pyruvate has not been previously reported on Au

catalysts. DFT calculations of reaction energies identified the most favorable reaction intermediates and concluded that the O2 pathway through hydroxyacetone becomes viable at high potentials, which is consistent with the experimentally observed increase in pyruvate selectivity with applied potential on Au/C. A definitive determination of reaction pathways is challenging due to the instability and interconversion of proposed reaction intermediates, and should be a focus of future studies.

2.5. Acknowledgements

The experimental portion of this work was supported by the National Science Foundation (CBET-1159448) and Michigan Technological University (REF-RS E49290). The computational portion of this work was supported by the National Science Foundation (CBET-1264104). J.Q. is grateful for financial support from the Chinese Scholarship Council. The authors thank Andrew Fogerty of Iowa State University for assistance in electrochemical measurements.

2.6. References

(1) U.S. Energy Information Administration, Monthly Biodiesel Production Report, July 31, 2015.

(2) Yang, F.; Hanna, M. A.; Sun, R., Value-added uses for crude glycerol–a byproduct of biodiesel production. *Biotechnol. Biofuels* **2012**, *5* 13−22.

(3) Dasari, M. A.; Kiatsimkul, P.-P.; Sutterlin, W. R.; Suppes, G. J., Low-pressure hydrogenolysis of glycerol to propylene glycol. *Appl. Catal., A* **2005**, *281* 225–231.

(4) Miyazawa, T.; Kusunoki, Y.; Kunimori, K.; Tomishige, K., Glycerol conversion in the aqueous solution under hydrogen over Ru/C + an ion-exchange resin and its reaction mechanism. *J. Catal.* **2006**, *240* 213–221.

(5) Maris, E.; Davis, R., Hydrogenolysis of glycerol over carbon-supported Ru and Pt catalysts. *J. Catal.* **2007**, *249* 328–337.

(6) Martin, A. E.; Murphy, F. H., Glycols, Propylene Glycols. In Kirk-Othmer Encyclopedia of Chemical Technology, John Wiley & Sons, Inc.: **2000**.

(7) Marinas, A.; Bruijnincx, P.; Ftouni, J.; Urbano, F. J.; Pinel, C., Sustainability metrics for a fossil- and renewable-based route for 1,2-propanediol production: A comparison. *Catal. Today* **2014**, 239 31−37.

(8) Auras, R.; Harte, B.; Selke, S., An overview of polylactides as packaging materials. *Macromol. Biosci.* 2004, *4* 835–864.

(9) Datta, R.; Henry, M., Lactic acid: recent advances in products, processes and technologies – a review. *J. Chem. Technol. Biotechnol.* **2006**, *81* 1119–1129.

(10) Xu, P.; Qiu, J.; Gao, C.; Ma, C., Biotechnological Routes to Pyruvate Production. *J. Biosci. Bioeng.* **2008**, *105* 169–175.

(11) Li, Y.; Chen, J.; Lun, S.-Y., Biotechnological production of pyruvic acid. *Appl. Microbiol. Biotechnol.* **2001**, *57* 451–459.

(12) Tsujino, T.; Ohigashi, S.; Sugiyama, S.; Kawashiro, K.; Hayashi, H., Oxidation of propylene glycol and lactic acid to pyruvic acid in aqueous phase catalyzed by lead-modified palladium-on-carbon and related systems. *J. Mol. Catal.* **1992**, *71* 25–35.

(13) Prati, L.; Rossi, M., Gold on Carbon as a New Catalyst for Selective Liquid Phase Oxidation of Diols. *J. Catal.* **1998**, *176* 552–560.

(14) Dimitratos, N.; Lopez-Sanchez, J. A.; Meenakshisundaram, S.; Anthonykutty, J. M.; Brett, G. L.; Carley, A. F.; Taylor, S. H.; Knight, D. W.; Hutchings, G. J., Selective formation of lactate by oxidation of 1,2-propanediol using gold palladium alloy supported nanocrystals. *Green Chem.* **2009**, *11* 1209–1216.

(15) Ryabenkova, Y.; Miedziak, P. J.; Dummer, N. F.; Taylor, S. H.; Dimitratos, N.; Willock, D. J.; Bethell, D.; Knight, D. W.; Hutchings, G. J., The Selective Oxidation of 1,2-Propanediol by Supported Gold-Based Nanoparticulate Catalysts. *Top. Catal.* **2012**, *55* 1283–1288.

(16) Ryabenkova, Y.; He, Q.; Miedziak, P. J.; Dummer, N. F.; Taylor, S. H.; Carley, A. F.; Morgan, D. J.; Dimitratos, N.; Willock, D. J.; Bethell, D.; Knight, D. W.; Chadwick, D.; Kiely, C. J.; Hutchings, G. J., The selective oxidation of 1,2-propanediol to lactic acid using mild conditions and gold-based nanoparticulate catalysts. *Catal. Today* **2013**, *203* 139–145.

(17) Vuyyuru, K. R.; Strasser, P., Oxidation of biomass derived 5-hydroxymethylfurfural using heterogeneous and electrochemical catalysis. *Catal. Today* **2012**, *195* 144–154.

(18) Alcaide, F.; Cabot, P.-L.; Brillas, E., Fuel cells for chemicals and energy cogeneration. *J. Power Sources* **2006**, *153* 47–60.

(19) Yuan, X.; Ma, Z.; Bueb, H.; Drillet, J. F.; Hagen, J.; Schmidt, V. M., Cogeneration of electricity and organic chemicals using a polymer electrolyte fuel cell. *Electrochim. Acta* **2005**, *50* 5172–5180.

(20) Bambagioni, V.; Bianchini, C.; Marchionni, A.; Filippi, J.; Vizza, F.; Teddy, J.; Serp, P.; Zhiani, M., Pd and Pt–Ru anode electrocatalysts supported on multi-walled carbon nanotubes and their use in passive and active direct alcohol fuel cells with an anion-exchange membrane (alcohol =methanol, ethanol, glycerol). *J. Power Sources* **2009**, *190* 241–251.

(21) Simões, M.; Baranton, S.; Coutanceau, C., Electro-oxidation of glycerol at Pd based nano-catalysts for an application in alkaline fuel cells for chemicals and energy cogeneration. *Appl. Catal., B* **2010**, *93* 354–362.

(22) Simões, M.; Baranton, S.; Coutanceau, C., Electrochemical Valorisation of Glycerol. *ChemSusChem* **2012**, *5* 2106–2124.

(23) Zhang, Z.; Xin, L.; Li, W., Electrocatalytic oxidation of glycerol on Pt/C in anion-exchange membrane fuel cell: Cogeneration of electricity and valuable chemicals. *Appl. Catal., B* **2012**, *119–120* 40–48.

(24) Zhang, Z.; Xin, L.; Li, W., Supported gold nanoparticles as anode catalyst for anion-exchange membrane-direct glycerol fuel cell (AEM-DGFC). *Int. J. Hydrogen Energy* **2012**, *37* 9393–9401.

(25) Qi, J.; Xin, L.; Chadderdon, D. J.; Qiu, Y.; Jiang, Y.; Benipal, N.; Liang, C.; Li, W., Electrocatalytic selective oxidation of glycerol to tartronate on Au/C anode catalysts in anion exchange membrane fuel cells with electricity cogeneration. *Appl. Catal., B* **2014**, *154–155* 360–368.

(26) Han, X.; Chadderdon, D. J.; Qi, J.; Xin, L.; Li, W.; Zhou, W., Numerical analysis of anion-exchange membrane direct glycerol fuel cells under steady state and dynamic operations. *Int. J. Hydrogen Energy* **2014**, *39* 19767–19779.

(27) Xin, L.; Zhang, Z.; Qi, J.; Chadderdon, D.; Li, W., Electrocatalytic oxidation of ethylene glycol (EG) on supported Pt and Au catalysts in alkaline media: Reaction pathway investigation in three-electrode cell and fuel cell reactors. *Appl. Catal., B* **2012**, *125* 85–94.

(28) Qi, J.; Xin, L.; Zhang, Z.; Sun, K.; He, H.; Wang, F.; Chadderdon, D. J.; Qiu, Y.; Liang, C.; Li, W., Surface dealloyed Pt nanoparticles supported on carbon nanotubes: facile synthesis and promising applications for direct crude glycerol anion-exchange membrane fuel cell. *Green Chem.* **2013**, *15* 1133–1137.

(29) Marchionni, A.; Bevilacqua, M.; Bianchini, C.; Chen, Y. X.; Filippi, J.; Fornasiero, P.; Lavacchi, A.; Miller, H.; Wang, L.; Vizza, F., Electrooxidation of Ethylene Glycol and Glycerol on Pd-(Ni-Zn)/C Anodes in Direct Alcohol Fuel Cells. *ChemSusChem* **2013**, *6* 518–528.

(30) Horanyi, G.; Torkos, K., Electrochemical behaviour of 1,2-propanediol and methyl-glyoxal at a platinized plantinum electrode in acidic media. *J. Electroanal. Chem.* **1981**, *125* 105–113.

(31) Alonso, C.; Gonzalez-Velasco, J., Study of the electrooxidation of 1,2-propanediol on an Au electrode in basic medium. *J. Electroanal. Chem.* **1988**, *248* 193–208.

(32) Bellini, M.; Bevilacqua, M.; Filippi, J.; Lavacchi, A.; Marchionni, A.; Miller, H. A.; Oberhauser, W.; Vizza, F.; Annen, S. P.; Grutzmacher, H., Energy and chemicals from the selective electrooxidation of renewable diols by organometallic fuel cells. *ChemSusChem* **2014**, *7* 2432–2435.

(33) Zhang, Z.; Xin, L.; Qi, J.; Wang, Z.; Li, W., Selective electro-conversion of glycerol to glycolate on carbon nanotube supported gold catalyst. *Green Chem.* **2012**, *14* 2150–2152.

(34) Xin, L.; Zhang, Z.; Wang, Z.; Li, W., Simultaneous Generation of Mesoxalic Acid and Electricity from Glycerol on a Gold Anode Catalyst in Anion-Exchange Membrane Fuel Cells. *ChemCatChem* **2012**, *4* 1105–1114.

(35) Zhang, Z.; Xin, L.; Qi, J.; Chadderdon, D. J.; Sun, K.; Warsko, K. M.; Li, W., Selective electro-oxidation of glycerol to tartronate or mesoxalate on Au nanoparticle catalyst via electrode potential tuning in anion-exchange membrane electro-catalytic flow reactor. *Appl. Catal., B* **2014**, *147* 871–878.

(36) Chadderdon, D. J.; Xin, L.; Qi, J.; Qiu, Y.; Krishna, P.; More, K. L.; Li, W., Electrocatalytic oxidation of 5-hydroxymethylfurfural to 2,5-furandicarboxylic acid on supported Au and Pd bimetallic nanoparticles. *Green Chem.* **2014**, *16* 3778–3786.

(37) Kresse, G.; Hafner, J., Ab initio molecular dynamics for liquid metals. *Phys. Rev. B* **1993**, *47* 558−561.

(38) Kresse, G.; Hafner, J., Ab initio molecular-dynamics simulation of the liquid-metal-amorphous-semiconductor transition in germanium. *Phys. Rev. B* **1994**, *49* 14251−14269.

(39) Kresse, G.; Furthmüller, J., Efficiency of ab-initio total energy calculations for metals and semiconductors using a plane-wave basis set. *Comput. Mat. Sci.* **1996**, *6* 15−50.

(40) Kresse, G.; Furthmüller, J., Efficient iterative schemes for ab initio total-energy calculations using a plane-wave basis set. *Phys. Rev. B* **1996**, *54* 11169−11186.

(41) Perdew, J. P.; Chevary, J. A.; Vosko, S. H.; Jackson, K. A.; Pederson, M. R.; Singh, D. J.; Fiolhais, C., Atoms, molecules, solids, and surfaces: Applications of the generalized gradient approximation for exchange and correlation. *Phys. Rev. B* **1992**, *46* 6671−6687.

(42) Monkhorst, H. J.; Pack, J. D., Special points for Brillouin-zone integrations. *Phys. Rev. B* **1976**, 13 5188–5192.

(43) Yeh, K. Y.; Janik, M. J., Computational Catalysis: Chapter 3: Density Functional Theory Methods for Electrocatalysts. The Royal Society of Chemistry: **2014**.

(44) Nørskov, J. K.; Rossmeisl, J.; Logadottir, A.; Lindqvist, L.; Kitchin, J. R.; Bligaard, T.; Jónsson, H., Origin of the Overpotential for Oxygen Reduction at a Fuel-Cell Cathode. *J. Phys. Chem. B* **2004**, *108* 17886–17892.

(45) Zhang, Z.; Xin, L.; Qi, J.; Chadderdon, D. J.; Li, W., Supported Pt, Pd and Au nanoparticle anode catalysts for anion-exchange membrane fuel cells with glycerol and crude glycerol fuels. *Appl. Catal., B* **2013**, *136–137* 29–39.

(46) Kwon, Y.; Schouten, K. J. P.; Koper, M. T. M., Mechanism of the Catalytic Oxidation of Glycerol on Polycrystalline Gold and Platinum Electrodes. *ChemCatChem* **2011**, *3* 7776–7785.

(47) John, J.; Wang, H.; Rus, E. D.; Abruña, H. D., Mechanistic Studies of Formate Oxidation on Platinum in Alkaline Medium. *J. Phys. Chem. C.* **2012**, *116* 5810–5820.

(48) Bott-Neto, J. L.; Garcia, A. C.; Oliveira, V. L.; de Souza, N. E.; Tremiliosi-Filho, G., Au/C catalysts prepared by a green method towards C3 alcohol electrooxidation: A cyclic voltammetry and in situ FTIR spectroscopy study. *J. Electroanal. Chem.* **2014**, *735* 57–62.

(49) Kwon, Y.; Lai, S. C.; Rodriguez, P.; Koper, M. T., Electrocatalytic oxidation of alcohols on gold in alkaline media: base or gold catalysis? *J. Am. Chem. Soc.* **2011**, *133* 6914–6917.

CHAPTER 3

ELECTROCATALYTIC OXIDATION OF 5-HYDROXYMETHYLFURFURAL TO 2,5-FURANDICARBOXYLIC ACID ON SUPPORTED GOLD AND PALLADIUM BIMETALLIC NANOPARTICLES

Modified from a paper published in Green Chemistry*

David J. Chadderdon,[a] Le Xin,[a] Ji Qi,[a] Yang Qiu,[a] Phani Krishna,[a] Karren L. More,[b] and Wenzhen Li[a]

[a] *Department of Chemical Engineering Michigan Technological University, Houghton, Michigan 49931, USA*

[b] *Materials Science and Technology Division Oak Ridge National Laboratory, Oak Ridge, Tennessee 37831, USA*

Abstract

This work explores the potential-dependent electrocatalytic oxidation of 5-hydroxymethylfurfural (HMF) in alkaline media over supported Au and Pd nanoparticles, and demonstrates the synergistic effects of bimetallic Pd-Au catalysts for the selective formation of 2,5-furandicarboxylic acid (FDCA). Results from electrolysis product analysis at various electrode potentials, along with cyclic voltammetry of HMF and its oxidation intermediates, revealed the different catalytic properties of Pd and Au for competitive oxidation of alcohol and aldehyde groups present in HMF. Aldehyde oxidation was greatly favored over alcohol oxidation on the Au/C catalyst, which was very active for HMF oxidation to 5-hydroxymethyl-2-furancarboxylic acid (HFCA). However, high electrode potentials were required for further oxidation of the alcohol group to FDCA. HMF oxidation on Pd/C followed two competitive routes to FDCA, and the favored pathway was dependent on electrode potential. Oxidation of

*Chadderdon, D. J.; Xin, L.; Qi, J.; Qiu, Y.; Krishna, P.; More, K. L.; Li, W., Electrocatalytic oxidation of 5-hydroxymethylfurfural to 2,5-furandicarboxylic acid on supported Au and Pd bimetallic nanoparticles. *Green Chem.* **2014,** *16* 3778–3786. Adapted with permission from The Royal Society of Chemistry.

aldehyde groups occurred much slower on Pd/C than Au/C at low potentials, but was greatly enhanced by increasing potential or by alloying with Au. It was found that bimetallic catalysts with 2:1 and 1:2 Pd-Au molar ratios (Pd_2Au_1/C and Pd_1Au_2/C) generated deeper oxidized products (i.e. FFCA and FDCA) at lower potentials than monometallic catalysts. The product distributions were dependent on electrode potential and surface composition. Bimetallic catalysts exhibited advantages of both single components with facile alcohol and aldehyde oxidation, resulting in greatly enhanced HMF conversion rate and selectivity to FDCA.

3.1. Introduction

Rapid growth of world population and declining petroleum reserves create a great need for renewable sources of carbon for production of chemicals in the future. Lignocellulosic biomass is an abundant, inexpensive, and sustainable resource from which many platform sugars can be derived. New scientific challenges arise in converting these platform sugars because, unlike petroleum feeds, biomass-derived chemicals are often highly-functionalized and new catalytic processes are needed to control the functionality of the final products.[1] Recent progress has achieved high yield of the important building-block molecule 5-hydroxymethylfurfural (HMF) from hexoses.[2-5] HMF, which features a furan ring with alcohol and aldehyde side groups, has attracted enormous attention, and US DOE has identified HMF as one of the most important intermediates for biorenewable chemicals and fuels.[6-7] Of particular interest is the selective oxidation product, 2,5-furandicarboxylic acid (FDCA), which is a suitable starting monomer for bio-derived polymeric materials.[6-9] The selective oxidation of HMF to FDCA must be studied not only due to the industrial significance of FDCA, but also as a model for effective catalytic processing of multi-functional molecules from biomass. There is an urgent need to

better understand catalyst selectivity and its relationship with reaction steps and pathways, in order to design green catalytic processes of the future.

Significant progress has been made in the selective oxidation of HMF in traditional heterogeneous catalytic systems.[10-17] Verdeguer et al. thoroughly studied the selective aerobic oxidation of HMF to FDCA on Pt/C and Pt-Pb/C catalysts under various temperatures and alkaline conditions.[10] They identified two pathways to FDCA (**Figure 3.1**), either through aldehyde oxidation of HMF to 5-hydroxymethyl-2-furancarboxylic acid (HFCA, Path A), or alcohol oxidation of HMF to 2,5-diformylfuran (DFF, Path B). They found that the final product distribution was highly dependent on temperature and pH. Casanova and others investigated Au as a catalyst for HMF oxidation and observed formation of FDCA with high selectivity through the HFCA intermediate.[11-12, 15, 17] Later, Davis et al. directly compared supported Au, Pd, and Pt catalysts and found that Pd/C and Pt/C were more selective to FDCA (71–79%) than Au/C at complete HMF conversion under identical conditions (6 h, 2:1 molar ratio HMF/KOH, 7 bar O_2, 295 K).[14] Incomplete oxidation yielding HFCA was observed on Au/C, and they concluded that higher O_2 pressures and alkaline concentrations were required to further oxidize the alcohol group of HFCA to the intermediate 2-formyl-5-furancarboxylic acid (FFCA), and then to FDCA. However, discussion of the mechanistic differences of HMF oxidation on Au/C or Pd/C and Pt/C considered only oxidation through the HFCA intermediate (i.e. **Figure 3.1**, Path A). Prati's group found that the activity of supported Au catalysts modified with Pt or Pd had extraordinarily enhanced activity and stability for HMF oxidation and selectivity to FDCA compared to the monometallic catalysts.[16] Furthermore, Pd-Au was more active than Au-Pt, and reached nearly full conversion to FDCA (2 h, 2:1 molar ratio HMF-KOH, 3 bar O_2, 333 K). Prati attributed the higher FDCA yield on bimetallic catalysts

to an increased resistance to poisoning by adsorbed intermediate species. However, the specific benefits of Pd (or Pt) addition to Au for competitive alcohol and aldehyde group oxidation and the synergistic effect of the bimetallic catalysts remain unclear.

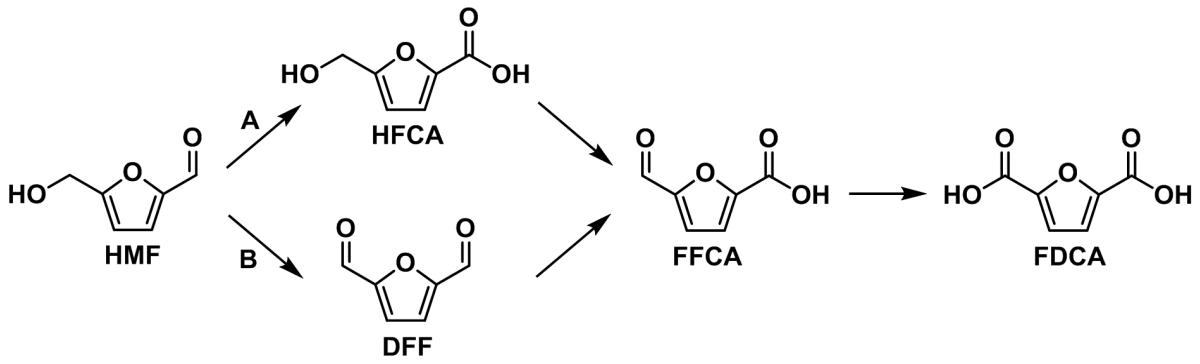

Figure 3.1. Possible reaction pathways of HMF oxidation to FDCA.

Electrocatalytic oxidation is an alternative to traditional aerobic oxidation, in which the driving force is an electrochemical potential. The regulation of electrode potential varies the driving force, and the rates of surface reactions can be monitored by current measurement. Also, electrochemical systems give rise to the fuel cell, which can simultaneous produce chemical products and renewable electricity.[18-22] Electrocatalytic oxidation of HMF on supported noble metal catalysts has received attention, however the work was limited to a bulk Pt foil electrode, and full oxidation to FDCA was not achieved.[23] The application of supported metal nanoparticle electrocatalysts for HMF oxidation allows parallel research between heterogeneous and electrocatalytic oxidation and the potential to advance both fields. In the past, our group has determined the electrode potential-dependent reaction pathways for selective oxidation of poly-alcohols including ethylene glycol and glycerol on supported nanoparticle catalysts.[18-19, 22, 24-26] This research approach is readily extended to study oxidation of compounds containing multiple functional groups, such as HMF.

In the present work, self-prepared monometallic Au/C and Pd/C and bimetallic Pd_2Au_1/C and Pd_1Au_2/C (subscripts indicate molar ratios) were applied as electrocatalysts for oxidation of HMF in anion-exchange membrane (AEM) electrolysis flow cells to determine the potential-dependent product distributions and yields. This study elucidates the effects of electrode potential and catalyst metal on the competitive oxidation of aldehyde and alcohol side groups, isolated by a stable furan-ring structure. A reaction pathway is proposed for the aqueous-phase HMF electrocatalytic oxidation on Au/C and Pd/C in alkaline media. The advantages of bimetallic Pd-Au catalysts for FDCA production are demonstrated by electrochemical methods and discussed in terms of the proposed reaction pathway and the surface composition and morphology of metallic nanoparticles.

3.2. Results and Discussion

3.2.1. Physical characterizations

Carbon black supported monometallic Pd/C and Au/C and bimetallic Pd-Au catalysts with 2:1 and 1:2 molar ratios (i.e. Pd_2Au_1/C and Pd_1Au_2/C) were prepared by an organic-phase reduction method.[20, 25, 27] The same synthesis conditions, such as surfactant concentration and reduction temperature and duration were used to prepare each catalyst, while only the type or amount of metal precursors changed with catalyst composition. The morphology, structure, and composition of the as-prepared catalysts were analyzed by X-ray diffraction (XRD), transmission electron microscopy (TEM), high-angle annular dark field via aberration-corrected scanning transmission electron microscopy (HAADF-STEM), scanning transmission electron microscopy coupled with high-spatial resolution energy dispersive spectroscopy (STEM-EDS), and inductively coupled plasma atomic emission spectroscopy (ICP-AES).

XRD patterns for all catalysts were collected from 15° to 90° and displayed typical face-centered cubic (fcc) patterns with diffraction peaks around 39°, 46°, 67°, and 80° assigned to the corresponding (111), (200), (220), and (311) facets, respectively (**Figure 3.2**). There was a clear shift in XRD peak position with changing metal composition, implying that alloyed crystal structures were present in Pd_2Au_1/C and Pd_1Au_2/C. Average crystallite sizes were estimated from the (220) peaks using the Scherrer equation, and are summarized in **Table 3.1**. Typical TEM and HAADF-STEM images, together with corresponding particle size histograms are shown in **Figure 3.3**. All catalysts featured small metal nanoparticles which were uniformly distributed on the carbon support. The average particle sizes evaluated from TEM were 2.1 nm, 2.0 nm, 2.9 nm and 2.6 nm for Pd/C, Pd_2Au_1/C, Pd_1Au_2/C, and Au/C, respectively, which are in good agreement with average crystallite sizes estimated from XRD (cf. **Table 3.1**). The organic-phase reduction method produced very small Pd nanoparticles under these synthesis conditions, whereas the Au-containing particles were slightly larger and more developed, as observed in the HAADF-STEM images. Bulk metal compositions of bimetallic catalysts (Pd_2Au_1/C and Pd_1Au_2/C) were determined by ICP-AES and STEM-EDS, and shown in **Table 3.1**. Bulk compositions were near the target ratios, indicating that the Pd and Au precursors were fully reduced during nanoparticle synthesis. Further characteristics such as the nature of the phases and the surface compositions of Pd_2Au_1/C and Pd_1Au_2/C were explored later through electrochemical methods.

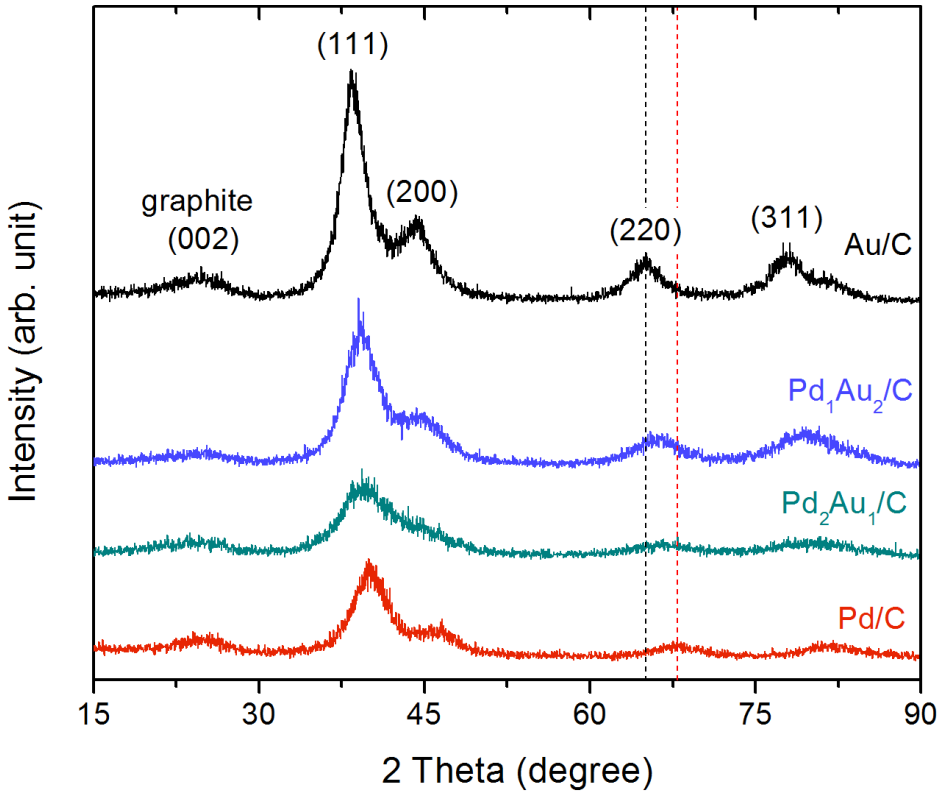

Figure 3.2. XRD patterns of self-prepared Pd/C, Pd_2Au_1/C, Pd_1Au_2/C, and Au/C catalysts. Peak position shift was observed as metal composition was varied, indicating that alloyed crystal structures were present in the Pd_2Au_1/C and Pd_1Au_2/C samples. The peaks for Pd_2Au_1/C and Pd_1Au_2/C were between Pd/C and Au/C, as noted by dashed lines for the (220) peak.

Table 3.1. XRD, TEM, ICP-AES and STEM-EDS results for self-prepared catalysts

Catalyst	Average crystallite size [a] (nm)	Average particle size [b] (nm)	Pd:Au molar ratio [c]	Pd:Au molar ratio [d]
Pd/C	2.6	2.1	-	-
Pd_2Au_1/C	2.2	2.0	1.8 : 1	1.7 : 1
Pd_1Au_2/C	2.5	2.9	1 : 1.8	1 : 2.3
Au/C	2.8	2.6	-	-

[a] from XRD [b] from TEM [c] from ICP-AES [d] from STEM-EDS

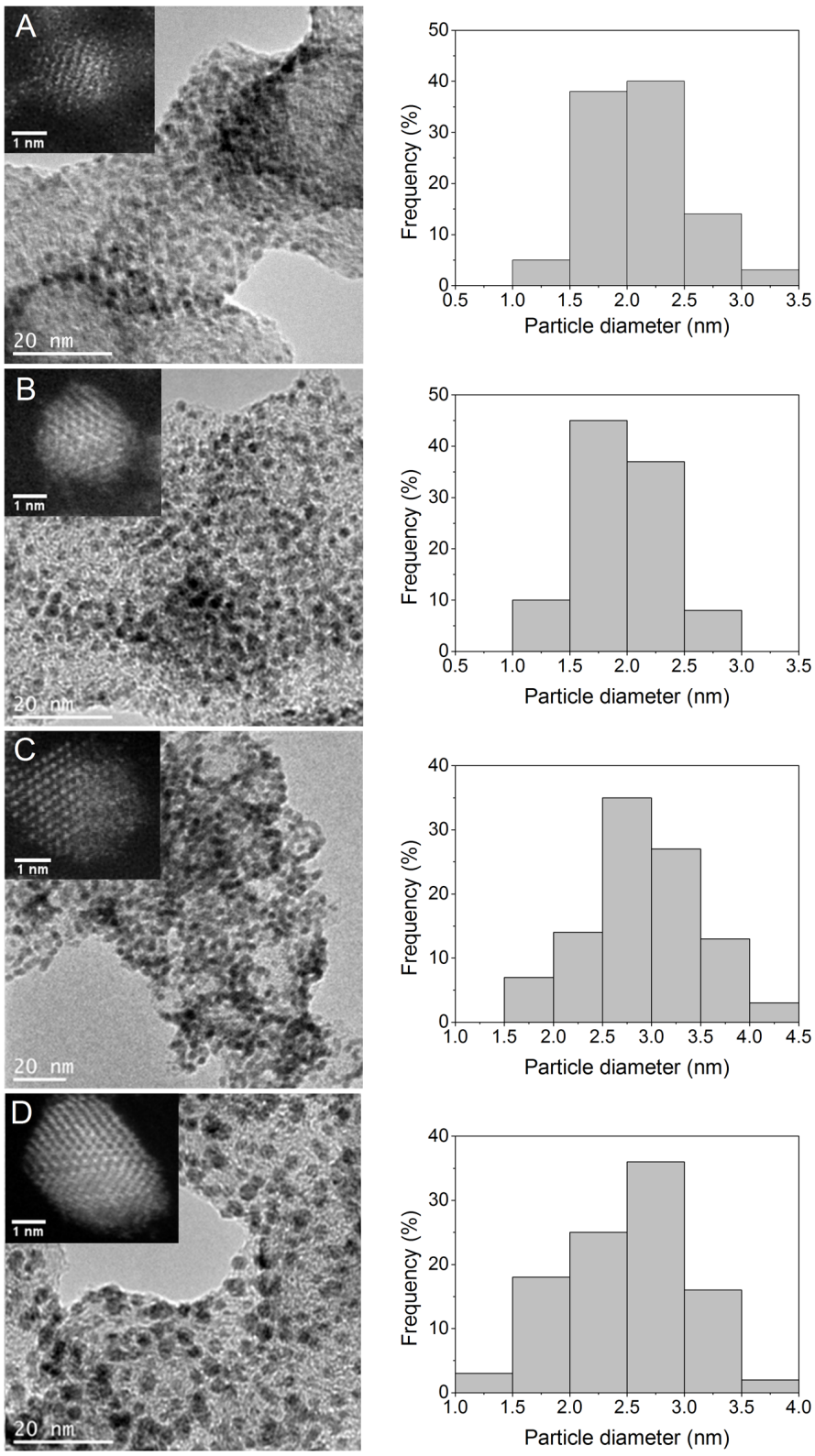

Figure 3.3. TEM, HAADF-STEM, and particle size histograms for (a) Pd/C (b) Pd_2Au_1/C (c) Pd_1Au_2/C and (d) Au/C catalysts.

3.2.2. Effects of electrode potential and catalyst metal composition

The prepared catalysts were investigated for the electrocatalytic oxidation of HMF in an AEM-electrolysis flow cell reactor at applied anode potentials of 0.6 V, 0.9 V, and 1.2 V versus RHE. The catalyst metal loading was 1 mg cm^{-2}. Alkaline solution (0.1 M KOH) containing 0.02 M HMF was passed through the anode reaction chamber and product samples were collected for HPLC analysis. HMF conversion and product selectivity of these runs after 1 h are shown in **Table 3.2**. For all catalysts and tested potentials, FDCA was observed; however, HMF conversion and product selectivity were highly dependent on applied anode potential and metal composition. The bimetallic catalysts showed higher HMF conversion and much greater selectivity to FDCA than monometallic catalysts, with Pd_1Au_2/C slightly better than Pd_2Au_1/C. Remarkably, oxidation on Pd_1Au_2/C at 0.9 V achieved nearly 83% molar yield of FDCA after

Table 3.2. HMF oxidation product analysis in AEM-electrolysis flow cell [a]

Catalyst	Potential (V vs. RHE)	C_{HMF} (%)	S_{HFCA} (%)	S_{DFF} (%)	S_{FFCA} (%)	S_{FDCA} (%)	Y_{FDCA} (%)
Pd/C	0.6	75.3	24.5	0.5	63.8	11.2	8.4
Pd_2Au_1/C	0.6	86.7	30.0	0.4	62	7.5	6.5
Pd_1Au_2/C	0.6	99.9	59.1	-	16.2	24.6	24.6
Au/C	0.6	100	98.3	-	0.3	1.4	1.4
Pd/C	0.9	96.8	70.0	-	0.6	29.4	28.5
Pd_2Au_1/C	0.9	100	35.0	-	0.8	64.1	64.1
Pd_1Au_2/C	0.9	100	16.4	-	0.9	82.7	82.7
Au/C	0.9	100	98.8	-	0.2	1.0	1.0
Pd/C	1.2	31.8	71.0	-	25.6	3.4	1.1
Pd_2Au_1/C	1.2	81.5	61.5	-	17.2	21.4	17.4
Pd_1Au_2/C	1.2	100	59.8	-	3.9	36.3	36.3
Au/C	1.2	100	80.8	-	5.1	14.2	14.2

[a] Reaction conditions: 1 hour; 25 mL of 0.02 M HMF, 0.1 M KOH solution; flow 20 mL min^{-1}; 25 °C; anode catalyst metal loading 1 mg cm^{-2}. *C* is conversion. *S* is molar selectivity. *Y* is molar yield.

1 h, which was almost three times higher than Pd/C. In contrast, the Au/C catalyst was nearly inactive for FDCA formation at this potential.

Figure 3.4 illustrates the strong impact of electrode potential on HMF conversion and product distribution on the Pd_1Au_2/C catalyst. The highest yield to FDCA was achieved at 0.9 V. It should be noted that HMF conversion rate and FDCA selectivity dropped off drastically on Pd-rich catalysts at 1.2 V versus RHE (**Table 3.2**), at which the potential was sufficient for the formation of metal-oxide species. On the other hand, Au/C resists oxidation under the same electrochemical conditions. HMF was fully converted (>99%) after 1 h on Au/C at the three tested potentials, however HFCA was the major observed product. For Au/C, the selectivity to FFCA and FDCA significantly increased at 1.2 V, indicating that further oxidation of the alcohol group of HFCA required high potential. In contrast, HMF oxidation on Pd/C was relatively slow and did not reach complete conversion after 1 h of reaction. However, Pd/C achieved higher FDCA production than Au/C at lower potentials. Interestingly, at 0.6 V on Pd/C, the major observed product was FFCA (S_{FFCA} = 64%), whereas at 0.9 V the main product was HFCA (S_{HFCA} = 70%). These differences in product distribution between Pd/C and Au/C indicate that the preferred reaction pathway of HMF electrocatalytic oxidation was dependent on catalyst metal and electrode potential. Additional studies of electrocatalytic oxidation of reaction intermediates were conducted to clarify these differences and give insight into the advantages of Pd-Au bimetallic catalysts for highly active and selective oxidation of HMF to FDCA.

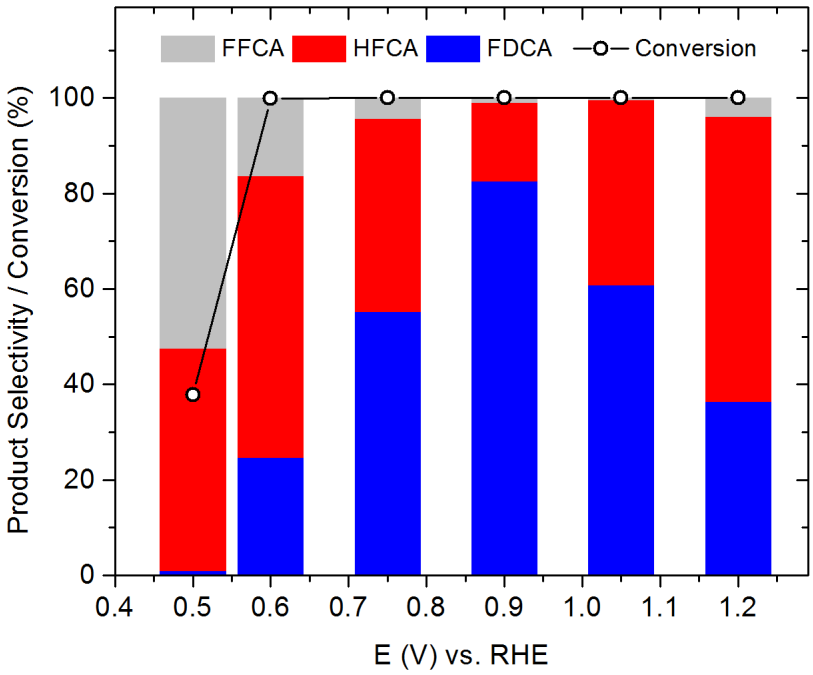

Figure 3.4. Product distribution on Pd_1Au_2/C for the oxidation of 0.02 M HMF in 0.1 M KOH. Reaction conditions: 1 h; AEM-electrolysis flow cell; 25 °C.

3.2.3. Onset potential and net peak current densities

To further investigate the pathways of HMF oxidation, cyclic voltammetry (CV) was conducted for aqueous solutions of 0.1 M KOH with and without addition of 0.02 M HMF, HFCA, or FFCA. The catalytic activities for oxidation of HMF and intermediates were compared on the basis of onset potential and peak net current density. **Figure 3.**5 shows net current density, as defined herein as the difference of the anodic-sweep current density and background current density (i.e. in 0.1 M KOH only). Onset of HMF oxidation occurred at much lower potentials (i.e. ~260 mV lower) on Au/C than Pd/C, whereas the onset potentials on the bimetallic catalysts were in between the monometallic catalysts (**Figure 3.5a**). In the low potential range, net current density for HMF oxidation on Au/C was significantly higher than on the Pd-containing catalysts, however the bimetallic catalysts were notably higher than Pd/C. Similar trends were observed in the voltammetry of FFCA (**Figure 3.5c**). This indicates

that aldehyde oxidation was much easier on Au/C than Pd/C, and that the addition of Au to the Pd-based catalysts greatly facilitated aldehyde oxidation at low potentials. On the other hand, the onset potential for HFCA oxidation was about 100 mV lower on Pd/C than on Au/C, and was even lower on the Pd-Au catalysts (**Figure 3.5b**). Peak net current density for HFCA oxidation on the bimetallic catalysts was higher than monometallic catalysts, reaching about two times higher than Pd/C and eight times higher than Au/C. Together, these results indicate that the bimetallic catalysts have enhanced activity for alcohol oxidation compared to monometallic catalysts. Evidence from the voltammetry of HMF and its oxidation intermediates provides new insight into the synergistic effect of Pd-Au bimetallic catalysts for selective oxidation, which has been previously studied in both aerobic chemical and electrochemical oxidation systems.[28-34] The advantages of Pd-Au for selective oxidation of HMF to FDCA were demonstrated by voltammetry to be a combination of facilitated aldehyde oxidation at low potentials and higher activity to alcohol oxidation.

It is worth noting that the voltammograms for FFCA oxidation showed a sharp increase in current around 0.8 V versus RHE on Pd/C and Pd_2Au_1/C, and to a lesser extent on Pd_1Au_2/C. This may indicate a change in reaction mechanism at higher potentials that leads to enhanced aldehyde oxidation on Pd-based catalysts. Enhanced aldehyde oxidation may have an effect on reaction pathways, by altering the competitive oxidation of the aldehyde and alcohol groups present in HMF. For comparison, the current density of FFCA oxidation on Au/C reached its highest value at 0.71 V versus RHE and gradually decreased at higher potentials.

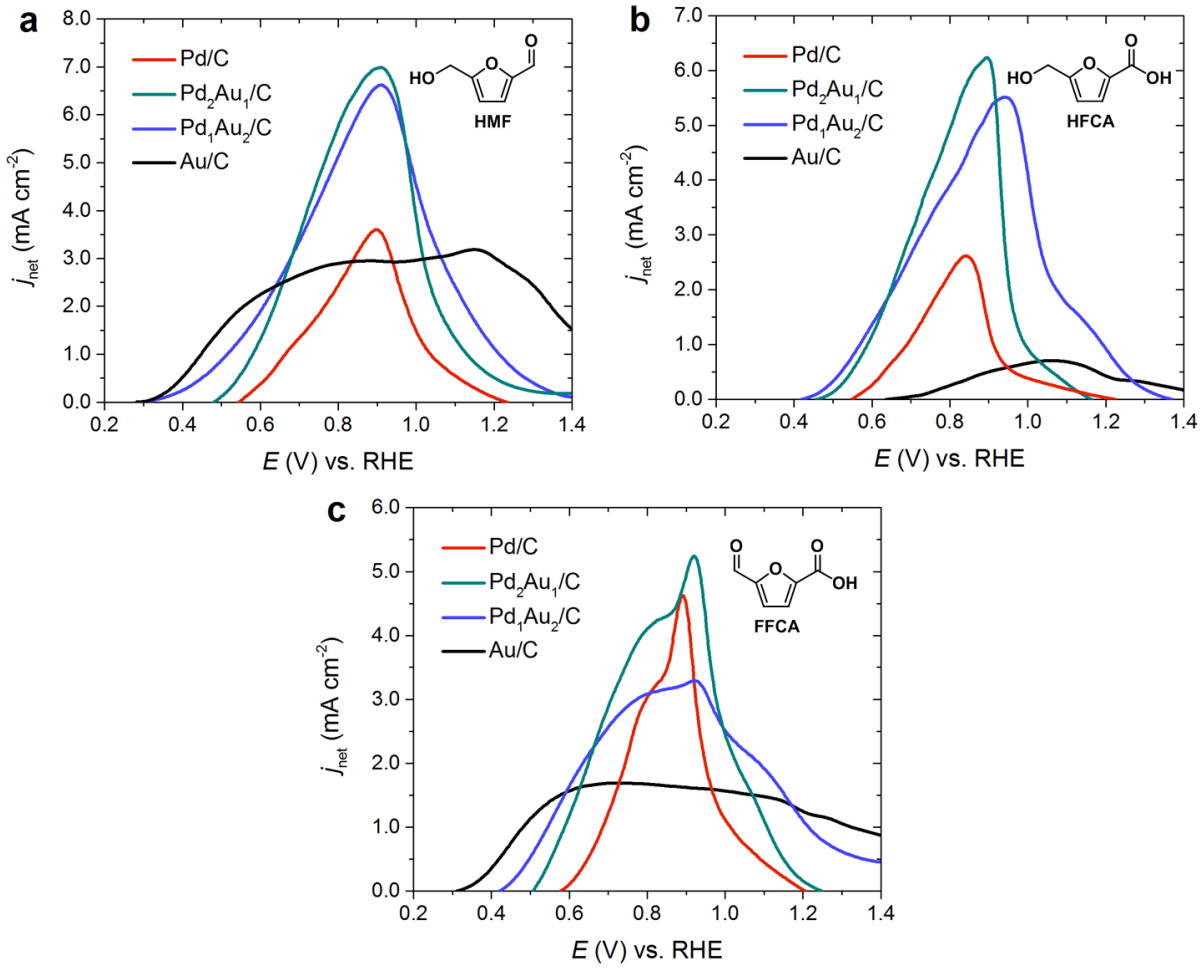

Figure 3.5. Anodic-sweep from voltammograms of 0.1 M KOH with 0.02 M of (a) HMF, (b) HFCA and (c) FFCA. Net current density (j_{net}) is the difference between anodic-sweep current density and background current density (i.e. in 0.1 M KOH). Reaction conditions: 50 mL solution; 25 °C; sweep rate 50 mV s^{-1}.

3.2.4. Reaction pathways of potential-dependent HMF oxidation

A closer look at time-dependent product distributions reveals more insight into the influence of catalyst metal on reaction mechanism and pathway. Time-dependent HMF conversion and product selectivity for a two hour reaction at 0.6 V versus RHE on Au/C and Pd/C are reported in **Figure 3.6**. On Au/C, HMF was nearly completely converted to HFCA (S_{HFCA} = 98%) after only 30 min, followed by very slow formation of FDCA (S_{FDCA} = 6% at 2h). In contrast, HMF conversion on Pd/C was notably slower, but resulted in more deeply

oxidized products, even at very short reaction times. FFCA was the main observed product (S_{FFCA} = 52% at 2 h) under these conditions, with also significant amounts of HFCA and FDCA formed. The intermediate DFF was initially present (S_{DFF} = 2.5% at 10 min) but not detected after two hours of reaction. The high selectivity to FFCA and presence of both DFF and HFCA intermediates is evidence that HMF oxidation proceeds by parallel pathways on Pd/C under these conditions. Similar evidence for two competitive pathways has been reported in non-electrochemical catalytic HMF oxidation on Pt/C and $Ru(OH)_x$ on Mg-based supports.[35-36]

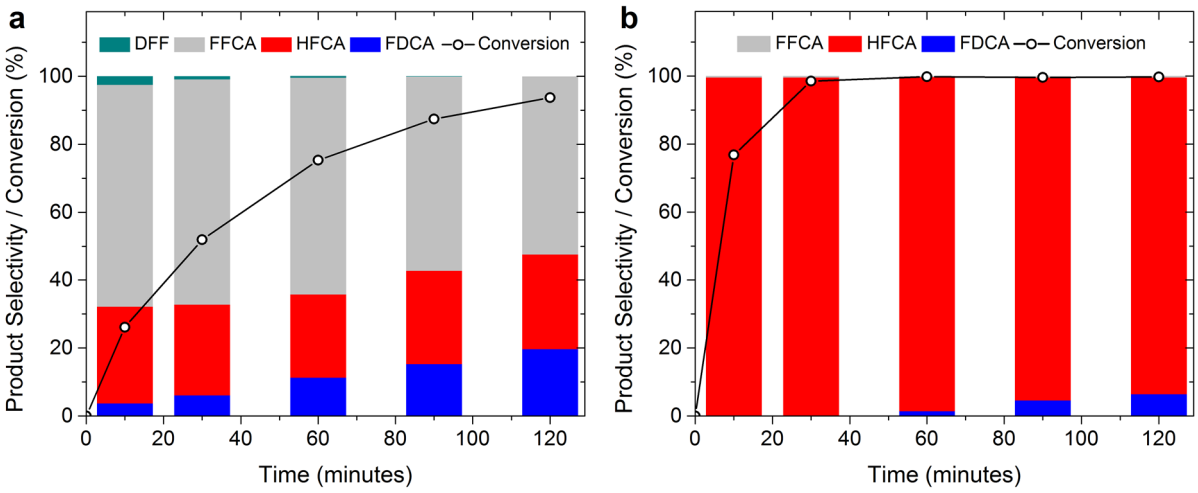

Figure 3.6. Reaction product profiles for oxidation of HMF over (a) Pd/C and (b) Au/C including HMF conversion and product selectivity. Reaction conditions: 25 mL of 0.02 M HMF, 0.1 M KOH solution; flow 20 mL min^{-1}; 25 °C; anode potential 0.6 V versus RHE.

The scheme in **Figure 3.7** shows the proposed potential-dependent reaction pathways of HMF oxidation in alkaline conditions for Pd/C and Au/C catalysts. Aldehyde oxidation was highly favored compared to alcohol oxidation on Au/C, as evidenced by the much lower onset potential for oxidation of FFCA compared to HFCA, and the fact that HFCA was the major observed intermediate. As a result, electrocatalytic oxidation of HMF on Au/C proceeded mainly by a single pathway, through aldehyde oxidation to HFCA, followed by a potential-

sensitive oxidation of the alcohol group to FFCA. Finally, FFCA was further oxidized to FDCA. In sharp contrast to Au/C, electrocatalytic oxidation of HMF on Pd/C followed potential-dependent parallel reaction pathways, attributed to its similar onset potentials for alcohol oxidation (i.e. HFCA, ~0.55 V) and aldehyde oxidation (i.e. FFCA, ~0.58 V), and the enhanced rate of aldehyde oxidation at higher potentials (cf. **Figure 3.5c**). At low potentials, both initial pathways via oxidation of the aldehyde or alcohol group of HMF were possible on Pd/C, evidenced by the detection of both HFCA and DFF intermediates. However, DFF was only detected in early reaction samples (**Figure 3.6a**), so it is hypothesized that its formation was followed by very fast oxidation to FFCA. At 0.6 V, the major observed product was FFCA, and further oxidation of the aldehyde group to FDCA was relatively slow under these conditions (**Figure 3.5a**). It should be noted that the non-electrochemical conversion of aldehyde-containing species by Cannizzaro-type reactions is possible in alkaline solution;[14, 23, 37] however, it was determined to not be a significant factor under these conditions (data not shown). At higher potentials, aldehyde oxidation was greatly enhanced on Pd/C, as evidenced by the voltammetry of FFCA (**Figure 3.5c**), making the initial oxidation of HMF to HFCA more favorable compared to the DFF pathway. The alcohol group of HFCA was relatively nonreactive, and consequently HFCA was the major observed product on Pd/C at 0.9 V (**Table 3.2**: S_{HFCA} = 70%, 1 h). Meanwhile, the route of HMF oxidation through DFF was a more minor pathway at higher potentials, and any DFF or FFCA formed would be rapidly be oxidized to FDCA as a result of the accelerated aldehyde oxidation. This can explain the lack of aldehyde-containing intermediates detected on Pd/C at 0.9 V (**Table 3.2**: $S_{FFCA} < 1\%$, S_{DFF} = 0%, 1 h at 0.9 V).

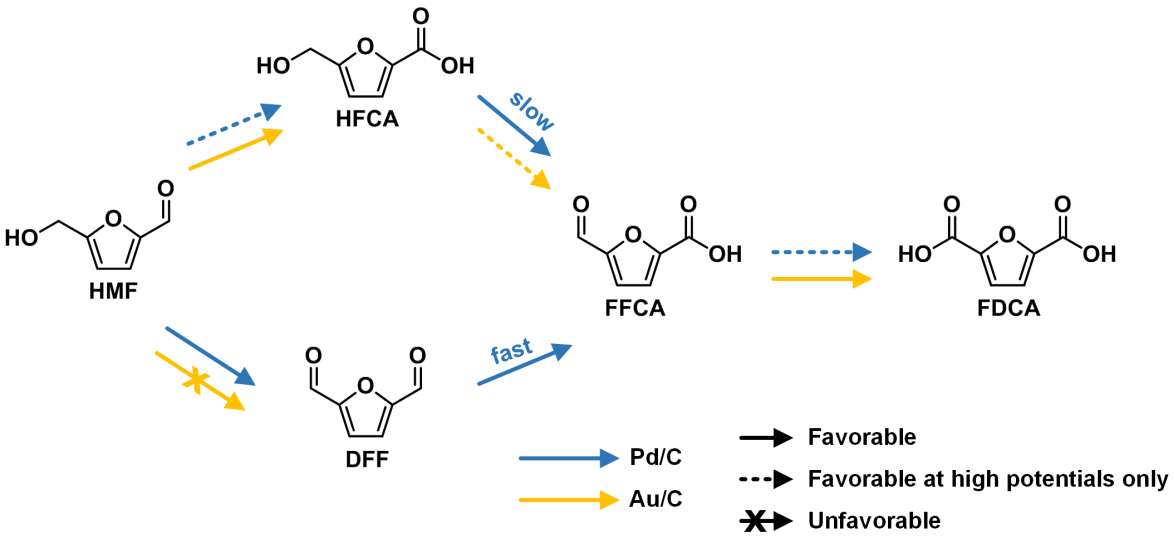

Figure 3.7. Proposed reaction pathways of HMF oxidation on Pd/C and Au/C electrocatalysts in alkaline media.

After clarifying the reaction pathways and slow steps for Au/C and Pd/C, some conclusions can be made about the advantages of bimetallic Pd-Au catalysts for FDCA production. At low potentials, HMF oxidation with Pd/C catalysts led to FFCA formation. As shown from cyclic voltammetry, the addition of Au greatly enhanced aldehyde oxidation at lower potentials. This resulted in more favorable aldehyde oxidation, both for HMF to HFCA and FFCA to FDCA. Both bimetallic catalysts had increased HMF conversion rate and FDCA selectivity, and the Au-rich Pd_1Au_2/C facilitated significant oxidation of FFCA to FDCA, even at a low potential of 0.6 V (S_{FDCA} = 25% at 1 h). At higher potentials, HMF oxidation on both Pd/C and Au/C catalysts yielded HFCA as the major product. From cyclic voltammetry, oxidation of the alcohol group in HFCA on bimetallic catalysts was shown to have much lower onset potential and higher peak current density than both Au and Pd, indicating a synergistic effect for the bimetallic catalysts. In the AEM-electrolysis flow cell reactors, this led to enhanced activity to HFCA oxidation and greatly increased selectivity to FDCA.

3.2.5. Surface morphology of Pd-Au bimetallic electrocatalysts

It is well known that bimetallic Pd-Au catalysts have greatly enhanced activity over their monometallic components for many applications; however, the promotional role of Pd or Au remains under debate. Bimetallic systems can introduce morphological and structural changes including the dilution of one atom type on the surface, different lattice parameters, possible electron charge transfer between different metal atoms, and formation of phase boundaries.[38] Previous works have proposed that isolated Pd atoms are highly active catalytic sites, due to decreased species adsorption energy compared to pure Pd crystals, therefore suggesting that the role of Au is dilute and stabilize surface Pd.[38-42] Surface metal composition, which may vary greatly from bulk composition, is a critical factor for catalyst activity and selectivity, therefore additional analysis was conducted to characterize the surface morphology of supported Pd-Au bimetallic catalysts for HMF oxidation.

The surface atomic compositions of Pd-Au bimetallic catalysts were determined by electrochemical methods first proposed by Rand and Woods.[43] In cyclic voltammetry, distinct reduction peaks are observed in the cathodic sweep, corresponding to the reduction of metal oxides formed on the catalyst surface during the anodic sweep. The peak position is dependent on the catalyst surface composition, and therefore can be used to determine the nature of surface alloys present in Pd-Au.[43-44] Cyclic voltammetry was performed in 0.1 M KOH electrolyte and the resulting voltammograms for bimetallic catalysts and Pd/C and Au/C are shown in **Figure 3.8**.

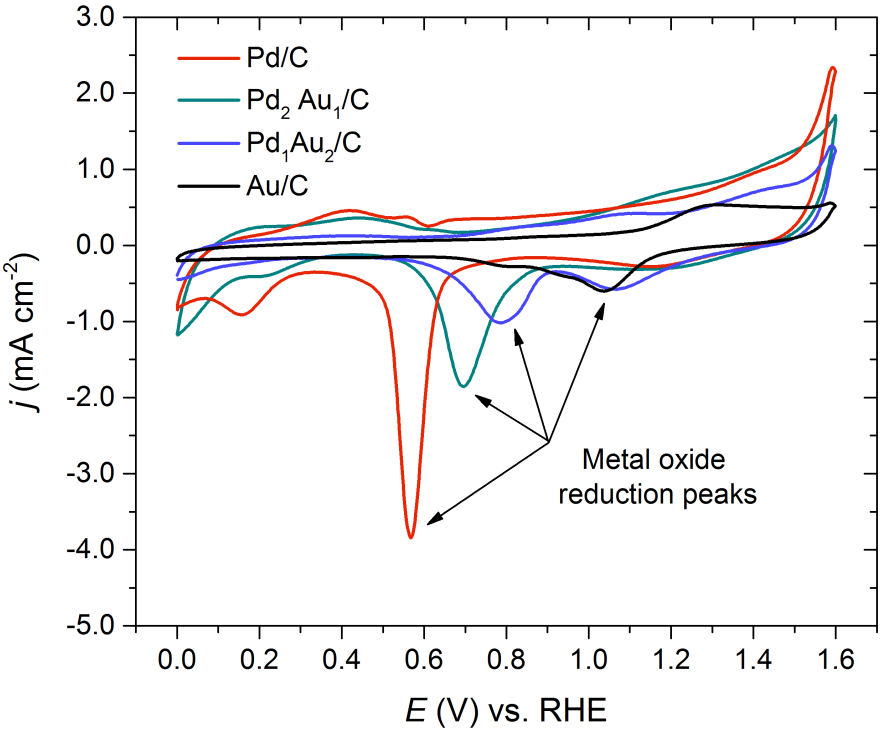

Figure 3.8. Cyclic voltammograms in 0.1 M KOH for monometallic and bimetallic catalysts. Conditions: 50 mL electrolyte; 25 °C; 20 μg catalyst loading on the glassy carbon electrode; sweep rate 50 mV s^{-1}.

Pd/C exhibited a sharp Pd-oxide reduction peak at 0.57 V, whereas Au/C showed a broad Au-oxide reduction peak around 1.04 V. These are in good agreement with our previously reported results.[27] The bimetallic catalysts had reduction peaks shifted away from the monometallic catalysts at 0.70 and 0.79 V. According to Rand and Wood's method, which predicts a linear variation of reduction peak potential with Pd content, these reduction peak positions correspond to Pd surface contents of 72% and 53% (atomic basis) for Pd_2Au_1/C and Pd_1Au_2/C, respectively.[43] These surfaces were found to be more Pd-rich than the bulk composition (cf. **Table 3.1**), a phenomenon which has previously been reported for Pd-Au nanoparticles.[45-46] Furthermore, a second reduction peak was observed for Pd_1Au_2/C at the signature potential for Au, indicating that two phases were present on the catalyst surface, one

alloyed Pd-Au phase and one non-alloyed Au phase. However, only one reduction peak was observed for Pd_2Au_1/C, suggesting that a single alloyed phase was present on the catalyst surface and monometallic phases were absent.

The proposed beneficial role of Au is to isolate and stabilize Pd sites on the surface. Therefore, higher surface Au composition is desired to increase the fraction of isolated Pd sites and catalytic activity. This was evidenced by Prati's group, who found increased turn over frequencies for glycerol oxidation with increasing Au-content up to 90%, beyond which the rates decreased sharply.[42] Enhanced activity for HMF oxidation on Pd_1Au_2/C compared to Pd_2Au_1/C therefore might be attributed to its higher surface Au composition in the alloy phase and increased number of isolated Pd sites. Additionally, electrochemical techniques provided evidence of a pure Au phase on the Pd_1Au_2/C surface, leading to a unique two-phase catalyst, which we hypothesize may further contribute to its superior activity and selectivity. Au/C was found to be highly active for aldehyde oxidation at all potentials but poor for alcohol oxidation at low potentials, so we propose that pure Au regions can promote aldehyde adsorption and oxidation, while Pd-rich alloyed regions promote alcohol oxidation. The intimate contact of Au and alloyed Pd-Au regions provides a bifunctional surface for aldehyde and alcohol oxidations, which are both necessary to obtain FDCA efficiently.

3.3. Conclusions

Electrocatalytic oxidation of HMF in AEM-electrolysis flow cell reactors with product analysis at varying electrode potentials, along with cyclic voltammetry of HMF, HFCA, and FFCA, provided direct evidence of a Pd-Au synergistic effect for HMF oxidation for FDCA production. The unique catalytic properties of Pd and Au for competitive oxidation of alcohol and aldehyde groups present in HMF were also revealed. The observed product distributions

from the AEM-electrolysis flow cell reactions were highly dependent on electrode potential and catalyst surface composition. We have proposed the electrode potential-dependent pathways for electrocatalytic oxidation of HMF in alkaline media over supported Au and Pd nanoparticles. Under these electrochemical conditions, Au/C favored HMF oxidation to HFCA, whereas oxidation on Pd/C followed two competitive pathways to FDCA. Aldehyde oxidation was greatly favored over alcohol oxidation on Au/C, but required higher potentials to proceed rapidly on Pd/C. Bimetallic catalysts (Pd_2Au_1/C and Pd_1Au_2/C) achieved much higher FDCA yield, attributed to altered surface composition and morphology. Introducing Au to the Pd surface led to more facile aldehyde oxidation at low potentials and enhanced alcohol oxidation activity compared to monometallic catalysts. The advantages of Pd-Au bimetallic catalysts for the selective production of FDCA from HMF were demonstrated in electrochemical systems. This approach may be extended to guide the rational design of other highly active and selective catalysts for green oxidation of multifunctional molecules.

3.4. Experimental Methods

3.4.1. Catalyst synthesis

Carbon black supported Pd, Pd-Au, and Au nanoparticles were synthesized by reduction of metal precursors $Pd(acac)_2$ (Sigma-Aldrich, 99%) and $AuCl_3$ (Sigma-Aldrich, 99%) followed by deposition on carbon black support (Vulcan XC-72R, Cabot). Typically, precursors were dissolved in 16 mL 1-octadecene (Sigma Aldrich, 90%) and 4 mL oleylamine (Aldrich Chemistry, 70%) and heated to 80°C under nitrogen flow. The precursors were added to give 2:1 and 1:2 Pd/Au molar ratios for the bimetallic nanoparticles. 1.7 mL $LiEt_3BH$ (1.0 M in THF, Acros Organics) was injected to rapidly precipitate metal nanoparticles, and after 10 min the solution was cooled to room temperature before drop-wise transfer to a well-stirred

dispersion of carbon black in hexane and ethanol. The amount of carbon black was controlled to give approximately 40 wt.% metal in the catalyst. The final catalysts were cleaned with ethanol, separated by vacuum filtration and dried overnight.

3.4.2. Catalyst characterizations

Catalysts were characterized by TEM (JEOL 2010) with an operating voltage of 200 kV. HAADF-STEM and STEM-EDS were performed on a Hitachi HF-3300 TEM-STEM with Bruker silicon drift detector (SDD). XRD patterns were obtained with a Scintag XDS-2000 θ/θ diffractometer using CuKα radiation (λ = 1.5406 Å), with a tube current of 35 mA and a tube voltage of 45 kV. Catalysts were digested in aqua regia (HCl:HNO_3 volume ratio 3:1) and analyzed by a PerkinElmer ICP-AES, model 7000 DV to verify bulk metal loading and composition.

3.4.3. Cyclic voltammetry

Cyclic voltammetry was performed in a glass reactor with a three-electrode setup controlled by potentiostat (Versastat MC, Princeton Applied Research). Prepared catalysts were dispersed in isopropanol by ultrasonication to form a uniform ink (1.0 mg mL^{-1}). With a micro-syringe, 20 µL of ink was deposited onto a polished and cleaned glassy-carbon electrode with geometric area of 0.196 cm^2. Hg/HgO (1.0 M KOH) reference electrode and Pt-wire counter electrode were used. Typically, the cell was loaded with 50 mL solution of 1.0 mmol HMF (Sigma-Aldrich, ≥99%) and 5.0 mmol KOH (Sigma-Aldrich, ≥85%) in deionized water. Cyclic voltammetry was performed at a sweep rate of 50 mV sec^{-1} in alkaline solution with and without addition of HMF at 25°C with nitrogen purging. Additional tests were performed with 1.0 mmol HFCA (Matrix Scientific, ≥99%) or FFCA (TCI America, ≥98%) intermediates.

3.4.4. AEM-electrolysis flow cell experiments

A custom-made reactor was built consisting of a solid anion-exchange membrane (AEM, A-201 Tokuyama Corp.) mechanically sandwiched between anode and cathode catalyst layers on carbon cloth. Self-prepared Pd/C, Pd-Au/C, and Au/C served as anode catalysts, while commercial Pt/C (40 wt.% Pt, ETEK) was the cathode catalyst. Catalyst and PTFE were dispersed in isopropanol by ultrasonication to form a uniform ink (10 mg catalyst mL^{-1}), which was applied onto the carbon cloth with a spray gun. The mass of catalyst on the carbon cloth was controlled to give a metal (Au, Pd, Pt) loading of 1 mg cm^{-2}. After drying, the catalyst to PTFE mass ratio was 9:1. Hg/HgO (1.0 M KOH) reference electrode was inserted through a hole in the anode compartment, allowing the anode potential to be regulated and monitored by potentiostat (Versastat MC, Princeton Applied Research). Additional details of electrolysis flow cell design can be found in our previous works.[26] Product samples were taken throughout the test for analysis by HPLC (Agilent 1100, Alltech OA-1000 column, 60°C) equipped with RID (Agilent G1362A) and VWD (Agilent G1314A, 220 nm) and a 5.0 mM aqueous H_2SO_4 mobile phase (0.3 mL min^{-1}).

3.5. Acknowledgements

We acknowledge partial financial support from the US National Science Foundation (CBET-1159448) and Michigan Tech Research Excellence Fund (E49290). J. Qi is grateful to the Chinese Scholarship Council for support.

3.6. References

(1) Medlin, W. J., Understanding and Controlling Reactivity of Unsaturated Oxygenates and Polyols on Metal Catalysts. *ACS Catal.* **2011,** *1* 1284-1297.

(2) Chheda, J. N.; Huber, G. W.; Dumesic, J. A., Liquid-Phase Catalytic Processing of Biomass-Derived Oxygenated Hydrocarbons to Fuels and Chemicals. *Angew. Chem. Int. Ed.* **2007,** *46* 7164-7183.

(3) Chheda, J. N.; Roman-Leshkov, Y.; Dumesic, J. A., Production of 5-hydroxymethylfurfural and furfural by dehydration of biomass-derived mono- and poly-saccharides *Green Chem.* **2007,** *9* 342-350.

(4) Corma, A.; Iborra, S.; Velty, A., Chemical Routes for the Transformation of Biomass into Chemicals. *Chem. Rev.* **2007,** *107* 2411-2502.

(5) Roman-Leshkov, Y.; Chheda, J. N.; Dumesic, J. A., Phase Modifiers Promote Efficient Production of Hydroxymethylfurfural from Fructose. *Science* **2006,** *213* 1933-1937.

(6) Werpy, T.; Peterson, G., Top Value Added Chemicals from Biomass. *NREL/TP-510-35523* **2004**.

(7) Bozell, J. J.; Petersen, G. R., Technology development for the production of biobased products from biorefinery carbohydrates-the US Department of Energy's "Top 10" revisited. *Green Chem.* **2010,** *12* 539-554.

(8) Gandini, A.; Silvestre, A. J. D.; Neto, C. P.; Sousa, A. F.; Gomes, M., The furan counterpart of poly(ethylene terephthalate): An alternative material based on renewable resources. *J. Polym. Sci., Part A: Polym. Chem* **2009,** *47* 295-298.

(9) Tong, X.; Ma, Y.; Li, Y., Biomass into chemicals: Conversion of sugars to furan derivatives by catalytic processes. *Appl. Catal., A* **2010,** *385* 1-13.

(10) Verdeguer, P.; Merat, N.; Gaset, A., Catalytic oxidation of HMF to FDCA. *J. Mol. Catal.* **1993,** *85* 327-344.

(11) Casanova, O.; Iborra, S.; Corma, A., Biomass into Chemicals: Aerobic Oxidation of 5-Hydroxymethyl-2-furfural into 2,5-Furandicarboxylic Acid with Gold Nanoparticle Catalysts. *ChemSusChem* **2009,** *2* 1138-1144.

(12) Gorbanev, Y. Y.; Klitgaard, S. K.; Woodley, J. M.; Christensen, C. H.; Riisager, A., Gold-Catalyzed Aerobic Oxidation of 5-Hydroxymethylfurfural in Water at Ambient Temperature. *ChemSusChem* **2009,** *2* 672-675.

(13) Rosatella, A. A.; Simeonov, S. P.; Fradea, R. F. M.; Afonso, C. A. M., 5-Hydroxymethylfurfural (HMF) as a building block platform: Biological properties, synthesis and synthetic applications. *Green Chem.* **2010,** *13* 754-793.

(14) Davis, S. E.; Houk, L. R.; Tamargo, E. C.; Datye, A. K.; Davis, R. J., Oxidation of 5-hydroxymethylfurfural over supported Pt, Pd, and Au catalysts. *Catal. Today* **2011,** *160* 55-60.

(15) Pasini, T.; Piccinini, M.; Blosi, M.; Bonelli, R.; Albonetti, S.; Dimitratos, N.; Lopez-Sanchez, J. A.; Sankar, M.; He, Q.; Kiely, C. J.; Hutchings, G. J.; Cavania, F., Selective oxidation of 5-hydroxymethyl-2-furfural using supported gold–copper nanoparticles. *Green Chem.* **2011,** *13* 2091-2099.

(16) Villa, A.; Schiavoni, M.; Campisi, S.; Veith, G. M.; Prati, L., Pd-modified Au on Carbon as an Effective and Durable Catalyst for the Direct Oxidation of HMF to 2,5-Furandicarboxylic Acid. *ChemSusChem* **2013,** *6* 609-612.

(17) Taarning, E.; Nielsen, I. S.; Egeblad, K.; Madsen, R.; Christensen, C. H., Chemicals from Renewables: Aerobic Oxidation of Furfural and Hydroxymethylfurfural over Gold Catalysts. *ChemSusChem* **2008,** *1* 75-78.

(18) Xin, L.; Zhang, Z.; Wang, Z.; Li, W., Simultaneous Generation of Mesoxalic Acid and Electricity from Glycerol on a Gold Anode Catalyst in Anion-Exchange Membrane Fuel Cells. *ChemCatChem* **2012,** *4* 1105-1114, S1105/1101-S1105/1106.

(19) Zhang, Z.; Xin, L.; Li, W., Electrocatalytic oxidation of glycerol on Pt/C in anion-exchange membrane fuel cell: Cogeneration of electricity and valuable chemicals. *Appl. Catal., B* **2012,** *119-120* 40-48.

(20) Zhang, Z.; Xin, L.; Li, W., Supported gold nanoparticles as anode catalyst for anion-exchange membrane-direct glycerol fuel cell (AEM-DGFC). *Int. J. of Hydrogen Energy* **2012,** *37* 9393-9401.

(21) Qi, J.; Xin, L.; Zhang, Z.; Sun, K.; He, H.; Wang, F.; Chadderdon, D.; Qiu, Y.; Liang, C.; Li, W., Surface dealloyed PtCo nanoparticles supported on carbon nanotube: facile synthesis and promising application for anion exchange membrane direct crude glycerol fuel cell. *Green Chem.* **2013,** *15* 1133-1137.

(22) Qi, J.; Xin, L.; Chadderdon, D. J.; Qiu, Y.; Jiang, Y.; Benipal, N.; Liang, C.; Li, W., Electrocatalytic Selective Oxidation of Glycerol to Tartronate on Au/C Anode Catalysts in Anion Exchange Membrane Fuel Cells with Electricity Cogeneration. *Appl. Catal., B* **2014,** *154-155* 360-368.

(23) Vuyyuru, K. R.; Strasser, P., Oxidation of biomass derived 5-hydroxymethylfurfural using heterogeneous and electrochemical catalysis. *Catal. Today* **2012,** *195* 144-154.

(24) Xin, L.; Zhang, Z.; Qi, J.; Chadderdon, D. J.; Li, W., Electrocatalytic oxidation of ethylene glycol (EG) on supported Pt and Au catalysts in alkaline media: Reaction pathway investigation in three-electrode cell and fuel cell reactors. *Appl. Catal., B* **2012,** *125* 85-94.

(25) Zhang, Z.; Xin, L.; Qi, J.; Wang, Z.; Li, W., Selective electro-conversion of glycerol to glycolate on carbon nanotube supported gold catalyst. *Green Chem.* **2012,** *14* 2150-2152.

(26) Zhang, Z.; Xin, L.; Qi, J.; Chadderdon, D. J.; Sun, K.; Warsko, K. M.; Li, W., Selective electro-oxidation of glycerol to tartronate or mesoxalate on Au nanoparticle catalyst via electrode potential tuning in anion-exchange membrane electro-catalytic flow reactor. *Appl. Catal., B* **2014,** *147* 871-878.

(27) Zhang, Z.; Xin, L.; Qi, J.; Chadderdon, D. J.; Li, W., Supported Pt, Pd and Au nanoparticle anode catalysts for anion-exchange membrane fuel cells with glycerol and crude glycerol fuels. *Appl. Catal., B* **2013,** *136–137* 29-39.

(28) Bianchi, C. L.; Canton, P.; Dimitratos, N.; Porta, F.; Prati, L., Selective oxidation of glycerol with oxygen using mono and bimetallic catalysts based on Au, Pd and Pt metals. *Catal. Today* **2005,** *102-103* 203-212.

(29) Dimitratos, N.; Porta, F.; Prati, L., Au, Pd (mono and bimetallic) catalysts supported on graphite using the immobilisation method: Synthesis and catalytic testing for liquid phase oxidation of glycerol. *Appl. Catal., A* **2005,** *291* 210-214.

(30) Dimitratos, N.; Villa, A.; Wang, D.; Porta, F.; Su, D.; Prati, L., Pd and Pt catalysts modified by alloying with Au in the selective oxidation of alcohols. *J. Catal.* **2006,** *244* 113-121.

(31) Enache, D. I.; Edwards, J. K.; Landon, P.; Solsona-Espriu, B.; Carley, A. F.; Herzing, A. A.; Watanabe, M.; Kiely, C. J.; Knight, D. W.; Hutchings, G. J., Solvent-Free Oxidation of Primary Alcohols to Aldehydes Using Au-Pd/TiO2 Catalysts. *Science* **2006,** *311* 362-365.

(32) Wook Lee, Y.; Kim, M.; Kim, Y.; Wook Kang, S.; Lee, J.-H.; Woo, H., Synthesis and Electrocatalytic Activity of Au−Pd Alloy Nanodendrites for Ethanol Oxidation. *J. Phys. Chem. C* **2010,** *114* 7689-7693.

(33) Brett, G. L.; He, Q.; Hammond, C.; Miedziak, P. J.; Dimitratos, N.; Sankar, M.; Herzing, A. A.; Conte, M.; Lopez-Sanchez, J. A.; Kiely, C. J.; Knight, D. W.; Taylor, S. H.; Hutchings, G. J., Selective Oxidation of Glycerol by Highly Active Bimetallic Catalysts at Ambient Temperature under Base-Free Conditions. *Angew. Chem. Int. Ed.* **2011,** *123* 10318-10321.

(34) Kesavan, L.; Tiruvalam, R.; Rahim, M. H. A.; bin Saiman, M. I.; Enache, D. I.; Jenkins, R. L.; Dimitratos, N.; Lopez-Sanchez, J. A.; Taylor, S. H.; Knight, D. W.; Kiely, C. J.; Hutchings, G. J., Solvent-Free Oxidation of Primary Carbon-Hydrogen Bonds in Toluene Using Au-Pd Alloy Nanoparticles. *Science* **2011,** *331* 195-199.

(35) Gorbanev, Y. Y.; Kegnæs, S.; Riisager, A., Selective Aerobic Oxidation of 5-Hydroxymethylfurfural in Water Over Solid Ruthenium Hydroxide Catalysts with Magnesium-Based Supports. *Catal. Lett.* **2011,** *141* 1752-1760.

(36) Rass, H. A.; Essayem, N.; Besson, M., Selective aqueous phase oxidation of 5-hydroxymethylfurfural to 2,5-furandicarboxylic acid over Pt/C catalysts: influence of the base and effect of bismuth promotion. *Green Chem.* **2013,** *15* 2240-2251.

(37) Kang, E.-S.; Chae, D. W.; Kim, B.; Kim, Y. G., Efficient preparation of DHMF and HMFA from biomass-derived HMF via a Cannizzaro reaction in ionic liquids. *J. Ind. Eng. Chem.* **2012,** *18* 174-177.

(38) Maroun, F.; Ozanam, F.; Magnussen, O. M.; Behm, R. J., The Role of Atomic Ensembles in the Reactivity of Bimetallic Electrocatalysts. *Science* **2001,** *293* 1811-1814.

(39) Meyer, R.; Lemire, C.; Shaikhutdinov, S. K.; Freund, H. J., Surface Chemistry of Catalysis by Gold. *Gold Bull.* **2004,** *37* 72-124.

(40) Mejia-Rosales, S. J.; Fernandez-Navarro, C.; Perez-Tijerina, E.; Blom, D. A.; Allard, L. F.; Yacaman, M. J., On the Structure of Au/Pd Bimetallic Nanoparticles. *J. Phys. Chem. C* **2007,** *111* 1256-1260.

(41) Chen, M.; Goodman, D. W., Promotional Effects of Au in Pd-Au Catalysts for Vinyl Acetate Synthesis. *Chin. J. Catal.* **2008,** *29* 1178-1186.

(42) Wang, D.; Villa, A.; Porta, F.; Prati, L.; Su, D., Bimetallic Gold/Palladium Catalysts: Correlation between Nanostructure and Synergistic Effects. *J. Phys. Chem. C.* **2008,** *112* 8617-8622.

(43) Rand, D.; Woods, R., Determination of the surface composition of smooth noble metal alloys by cylic voltammetry. *J. Electroanal. Chem.* **1972,** 57-69.

(44) Mougenot, M.; Caillard, A.; Simoes, M.; Baranton, S.; Coutanceau, C.; Brault, P., PdAu/C catalysts prepared by plasma sputtering for the electro-oxidation of glycerol. *Appl. Catal., B* **2011,** *107* 372-379.

(45) Simoes, M.; Baranton, S.; Coutanceau, C., Electrooxidation of Sodium Borohydride at Pd, Au, and PdxAu1-x Carbon-Supported Nanocatalysts. *J. Phys. Chem. C* **2009,** *113* 13369–13376.

(46) Simoes, M.; Baranton, S.; Coutanceau, C., Electro-oxidation of glycerol at Pd based nano-catalysts for an application in alkaline fuel cells for chemicals and energy cogeneration. *Appl. Catal., B* **2010,** *93* 354-362.

CHAPTER 4

HETEROSTRUCTURED BISMUTH VANADATE PHOTOELECTRODES FOR TEMPO-MEDIATED ALCOHOL OXIDATION

A manuscript in preparation for future publication.

David J. Chadderdon,[ab] Li-Pin Wu,[a] Zachary A. McGraw, [a] Matthew G. Panthani,[a*] and Wenzhen Li[ab*]

[a] *Department of Chemical and Biological Engineering*
Iowa State University, Ames, IA 50011, USA

[b] *U.S. Department of Energy, Ames Laboratory, Ames, Iowa 50011, USA*

[*] *Corresponding authors*

Abstract

Bismuth vanadate (BVO) photoelectrodes were modified with cobalt phosphate (CoPi) to facilitate TEMPO-mediated selective oxidation of alcohols (TEMPO = 2,2,6,6-tetramethylpiperidine-1-oxyl). Tuning CoPi electrodeposition time enabled the preference for TEMPO oxidation or oxygen evolution reaction (OER) to be tailored; photoanodes optimized for TEMPO oxidation reduced the required potential by 0.5 V and increased net charge injection efficiency by seven-fold, while also suppressing undesired OER compared to unmodified BVO. Transient photocurrent measurements suggested that CoPi alleviates recombination losses resulting from the back reduction of oxidized TEMPO. TEMPO-mediated oxidation of 5-hydroxymethylfurfural (HMF) with BVO/CoPi achieved 88% yield to 2,5-furandicarboxylic acid (FDCA) under mild conditions, whereas <1% FDCA was generated with BVO. These findings will promote development of more efficient photoelectrochemical devices for biomass upgrading and renewable energy conversion.

4.1. Introduction

Photoelectrochemistry may play a key role in moving our society toward a sustainable energy future. Photoelectrochemical cells (PECs) use light-absorbing semiconductor photoelectrodes to drive reactions with solar energy, often aided by external electricity input which can be supplied from renewable sources. In typical PECs, low-value molecules such as H_2O or CO_2 are reduced at metal/semiconductor cathodes to generate hydrogen gas (i.e., the hydrogen evolution reaction, HER) or carbon-based fuels and chemicals.[1-3] However, such PECs commonly suffer from poor energy conversion efficiency. This can largely be attributed to the slow kinetics and large overpotentials associated with the oxygen evolution reaction (OER) that occurs at the anode. Platinum-group metal catalysts are generally used to overcome the kinetic limitations; however, the high cost and low abundance of these materials limit their large-scale application.[4] Furthermore, the oxygen produced at the anode is not valuable. Therefore, it is desirable to find a more favorable anode reaction that utilizes low-cost and Earth-abundant electrode materials, and that generates value-added products.

A promising approach to improve the feasibility of PECs and related electrochemical cells is to pair HER at the cathode with anodic oxidation of biomass-derived chemicals (e.g., alcohols and aldehydes).[5-7] Alcohol oxidation is thermodynamically favorable compared to OER,[8-9] therefore reducing operating cell voltages and improving energy efficiency. Moreover, electrochemical alcohol oxidation can be tuned to selectively target desired products,[10-11] enabling the generation of high-purity valuable chemicals from renewable carbon sources. For example, 5-hydroxymethylfurfural (HMF), a platform molecule derived from C6 carbohydrates,[12] can be selectively oxidized to 2,5-furandicarboxylic acid (FDCA), a valuable precursor for biobased polymers.[13-14] In a breakthrough study, Cha et al. demonstrated the

photoelectrochemical conversion of HMF to FDCA using a bismuth vanadate (BVO) photoanode and a homogeneous redox mediator, TEMPO (2,2,6,6-tetramethylpiperidine-1-oxyl).[5] This work achieved remarkable selectivity and faradaic efficiency; however, a considerable external bias was required to support separation of photogenerated charge carriers and achieve high photocurrent densities. Although BVO has emerged as one of the most promising metal oxide-based photoanodes for OER,[15] it has been established that surface modifications, for example with catalysts such as cobalt phosphate (CoPi),[16-17] Co_3O_4,[18] or transition metal oxyhydroxides,[19-23] are required to mitigate charge recombination losses. However, such modifications have not been applied to BVO photoanodes for enhancing redox-mediated alcohol oxidations because it was presumed that they would promote OER in favor over mediator oxidation.[5, 24]

In this study, we challenge these previous presumptions by showing that BVO photoanodes modified with CoPi, a well-known OER electrocatalyst, can be tailored to selectively enhance TEMPO-mediated alcohol oxidation. We demonstrate for heterostructured BVO/CoPi photoanodes that OER activity is sensitive to CoPi electrodeposition time: short times (e.g. 1 min) reduce the onset potential and increase photocurrent for OER, whereas longer depositions severely suppress OER activity. We exploit the latter phenomenon to oxidize TEMPO without any faradaic efficiency loss to OER. Furthermore, TEMPO oxidation is enhanced for BVO/CoPi photoanodes in terms of reduced onset potential and increased photocurrent compared to BVO. Transient photocurrent measurements provide insight into interfacial charge transfer and recombination processes, elucidating the likely role of CoPi. Finally, we use BVO/CoPi photoanodes to drive TEMPO-mediated oxidation of HMF to FDCA and

demonstrate the viability of using heterostructured photoanodes for efficient biomass upgrading in PECs.

4.2. Results and Discussion

BVO films were synthesized on fluorine-doped tin oxide (FTO) glass substrates by electrodeposition and thermal processing according to literature.[21] Scanning electron microscopy (SEM) revealed the BVO films were nanoporous and about 2 μm thick (**Figure 4.1a-b**). Energy-dispersive spectroscopy (EDS) confirmed the composition of the films and indicated a Bi/V ratio of approximately 1:1 (**Table S4.1**). X-ray diffraction (XRD) patterns were consistent with a monoclinic BVO crystal structure (**Figure S4.1**). UV-vis diffuse absorbance spectra and corresponding Tauc analysis (**Figure S4.2**) confirmed a bandgap of about 2.47 eV, which matches those reported in literature.[25]

Photoelectrochemical measurements were performed in sodium borate electrolytes (pH 9.2) under simulated solar illumination (AM1.5, 100 mW cm^{-2}). **Figure 1c** shows the linear sweep voltammogram (LSV) for BVO in electrolyte containing sodium sulfite, which is known to be a good hole acceptor,[26] and is expected to extract nearly all photogenerated holes that reach the semiconductor/electrolyte interface. Thus, the sulfite oxidation photocurrent density ($j_{sulfite}$) provides an estimate for the total rate of holes reaching the interface. For TEMPO-mediated oxidations, it is desirable that a photoanode facilitates TEMPO oxidation at low potentials but has poor activity for OER, the main competing oxidation reaction in aqueous electrolytes.[27] **Figure 4.1c** shows the LSV collected in electrolyte without sulfite – in which case the photocurrent is from OER. The onset potential for OER was increased by about 150 mV compared to that for sulfite oxidation, and the photocurrent density (j_{OER}) was markedly lower than $j_{sulfite}$. The net charge injection efficiency (the fraction of surface-reaching holes

that are utilized for oxidation of species in the electrolyte) was estimated by the ratio $j_{OER}/j_{sulfite}$ to be 6.3% at 0.64 V. This suggests that the vast majority of the surface-reaching holes were lost to recombination processes. The photocurrent was even lower with TEMPO present in the electrolyte; most notably in the low potential region (i.e. < 1.0 V).

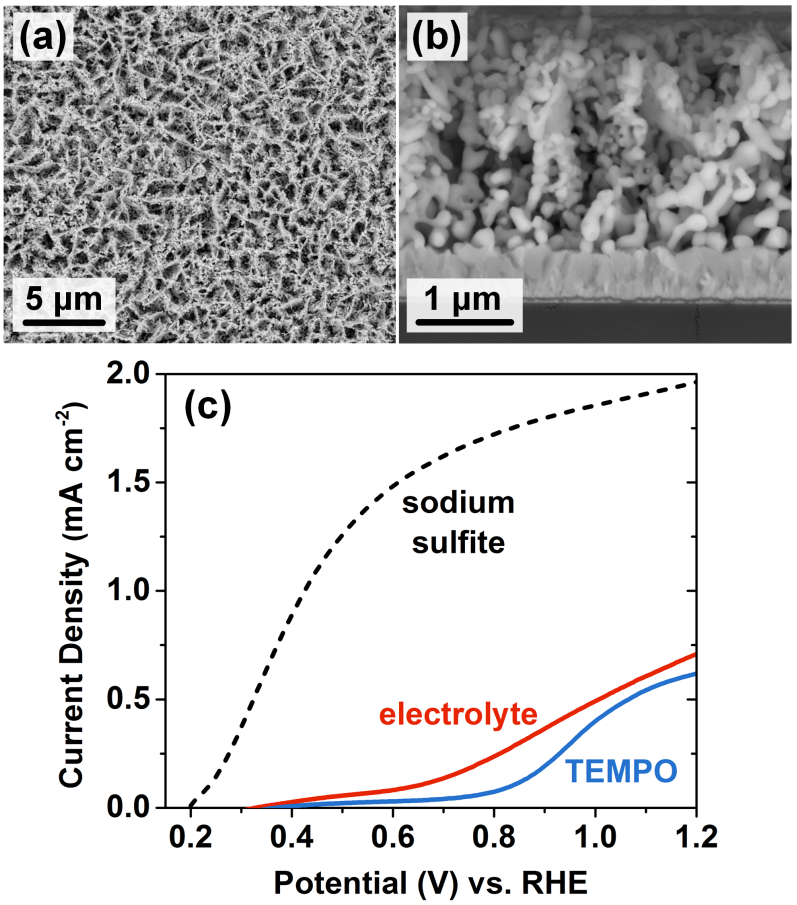

Figure 4.1. SEM micrographs of BVO films on FTO glass including (a) top and (b) cross-sectional views. (c) LSVs with AM1.5 illumination for BVO photoanodes in electrolytes with or without 5.0 mM TEMPO or 0.2 M sodium sulfite.

CoPi was deposited onto BVO electrodes using the electrodeposition method described by Kanan and Nocera.[28] Briefly, CoPi was electrodeposited from a solution of cobalt(II) nitrate (0.5 mM) and potassium phosphate (0.1 M, pH 7.0) at 1.1 V versus a Ag/AgCl reference electrode. Deposition time was varied between 1 and 30 min to obtain a range of CoPi loadings.

SEM revealed that the film morphology was unchanged after CoPi deposition (**Figure S4.3**), suggesting that the deposition was uniform over the electrode. The Co/P atomic ratio estimated by EDS was approximately 1.9:1.0, which is consistent with previous reports.[28] There was no appreciable change in the optical bandgap energy, indicating that inclusion of CoPi did not affect light absorption properties of photoanode.

Modifying BVO with a short CoPi deposition (i.e. 1 min) reduced the onset potential and increased photocurrent for OER compared to BVO (**Figure 4.2a**). However, longer depositions suppressed OER; photocurrent for BVO/CoPi-30 (i.e. BVO with 30 min CoPi deposition) was reduced by 95% compared to BVO at 1.04 V. It has been suggested that photoanodes modified with thicker CoPi layers have low OER performance due to increased interfacial recombination of conduction band electrons with accumulated CoPi holes,[29] or recombination via direct shunting of CoPi to the conductive back contact (i.e. FTO).[30] Nevertheless, we found that photocurrent for TEMPO oxidation was greatly enhanced with increased CoPi deposition times (**Figure 4.2b**), suggesting that TEMPO oxidation was able to compete with CoPi-induced charge recombination pathways. The potential required for TEMPO oxidation was reduced by nearly 0.5 V (e.g. 475 mV at 0.1 mA cm^{-2}) for BVO/CoPi-30 compared to BVO. Increasing CoPi deposition time beyond 30 min did not lead to further enhancement (data not shown).

The faradaic efficiency to OER was determined by quantifying evolved O_2 under steady-state conditions (**Figure 4.2c**). OER did not contribute to the photocurrents at 0.64 V, which can therefore be assigned to TEMPO oxidation (j_{TEMPO}). The net charge injection efficiency for TEMPO oxidation (i.e. $j_{TEMPO}/j_{sulfite}$) at 0.64 V was 15.4% for BVO/CoPi-30, a seven-fold increase compared to BVO (2.1%). OER prevailed at higher potentials for BVO and BVO/CoPi prepared with short CoPi deposition times; the faradaic efficiencies to OER at 1.24

V were 70% for BVO and 57% for BVO/CoPi with 1 min deposition. This was likely due to mass transport limitations for TEMPO oxidation at higher potentials. Remarkably, O_2 was not detected for BVO/CoPi-30 in electrolytes containing TEMPO at any potential tested. These findings show that BVO/CoPi-30 has the ability to enhance TEMPO oxidation photocurrent compared to BVO while also completely suppressing undesired OER.

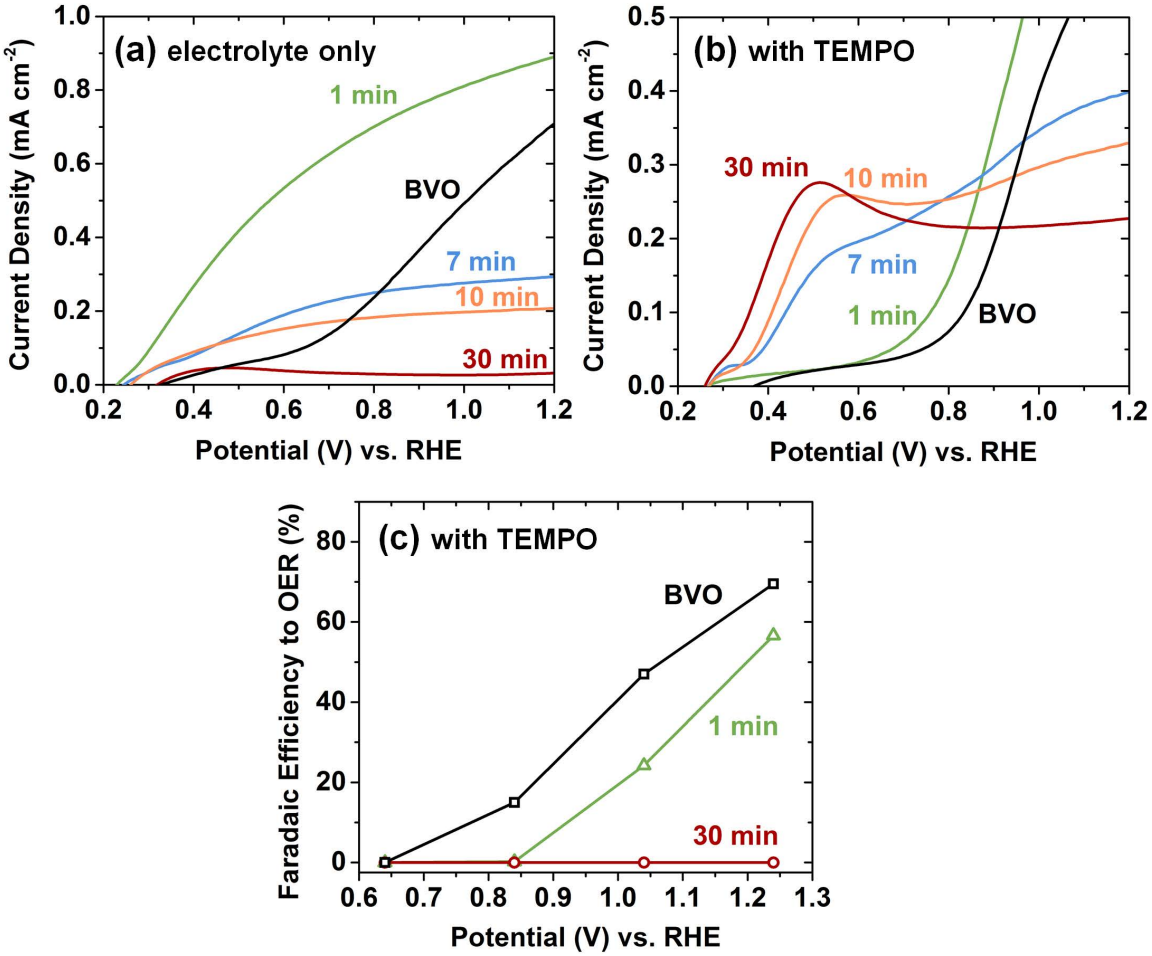

Figure 4.2. LSVs with AM1.5 illumination for BVO and BVO/CoPi photoanodes with varying CoPi deposition times (denoted within figures) in electrolyte (a) without TEMPO and (b) with 5.0 mM TEMPO. (c) Faradaic efficiency to OER in electrolyte with 5.0 mM TEMPO.

The low OER faradaic efficiencies observed at mild potentials in electrolytes with TEMPO (e.g. ~0% at 0.64 V) indicate that TEMPO oxidation was kinetically favored over OER.

However, the photocurrent for BVO in electrolytes with TEMPO was actually lower than in electrolytes without TEMPO (e.g. ~67% lower at 0.64 V). These seemingly inconsistent observations suggest that photocurrents were not limited by slow TEMPO oxidation kinetics, but by other factors. By extension, it is very unlikely that the higher TEMPO oxidation photocurrents observed for BVO/CoPi-30 resulted from enhanced charge transfer kinetics (i.e. electrocatalysis).

Photocurrents for BVO may have been limited by solution-mediated charge recombination via the back reduction of oxidized TEMPO (i.e. $TEMPO^+$), as depicted in **Figure 4.3a**. In principle, back reduction can occur by transfer of electrons from the conduction band or surface states of the semiconductor, or from the conductive substrate (e.g. FTO).[31] Cyclic voltammograms measured in the dark revealed that TEMPO exhibits quasi-reversible electrochemical oxidation/reduction on BVO and bare FTO electrodes **(Figure 4.3b)**. The midpoint potential was around 1.28 V, indicating that $TEMPO^+$ is susceptible to electrochemical reduction over most of the potential range of interest for photoelectrochemical TEMPO oxidation. In the dark, the low concentration of holes in n-type semiconductors (such as BVO) prevents them from facilitating oxidations.[32] Accordingly, the dark oxidation current observed for BVO electrodes can be attributed mainly to the underlying FTO substrate.[33] The dark oxidation currents for BVO and bare FTO were of similar magnitudes, suggesting that a substantial fraction of the underlying FTO was accessible to the electrolyte through the nanoporous BVO films. The exposed FTO could potentially facilitate electrochemical back reduction of $TEMPO^+$ at potentials more negative than 1.28 V.

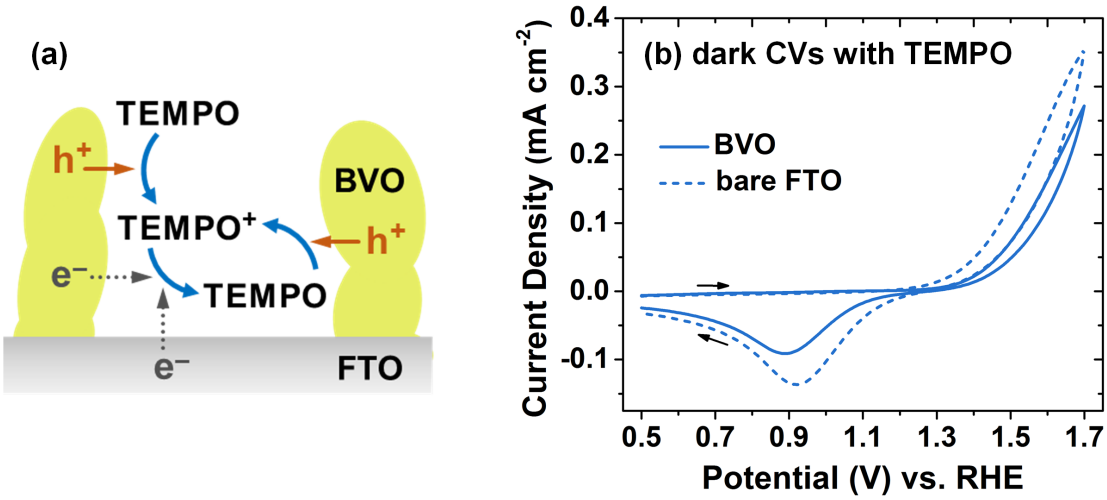

Figure 4.3. (a) Depiction of possible solution-mediated charge recombination pathways. Photogenerated holes oxidize TEMPO to $TEMPO^+$, which may be reduced back to TEMPO via electron transfer from the BVO conduction band or surface states, or from the exposed FTO substrate. (b) Dark cyclic voltammograms (CVs) for BVO or bare FTO electrodes in electrolyte with 5.0 mM TEMPO.

We used transient photocurrent measurements to gain more insight about charge transfer and recombination dynamics. **Figure 4.4a** shows LSVs for BVO under chopped AM1.5 illumination. In pure electrolyte (i.e. without TEMPO), transient current spikes were observed upon light "on" and "off", which are generally assigned to the back recombination of electrons with accumulated holes.[34] The spikes were most prominent at low potentials and diminished at increasingly anodic potentials. Negative transient current was negligible at potentials higher than about 0.8 V. This behavior has been attributed to enhanced band bending and charge separation at strongly anodic potentials.[35] The positive and negative current spikes were more pronounced in electrolyte containing TEMPO. Notably, substantial negative current spikes that were not observed in pure electrolyte initiated around 0.6 V and persisted up to about 1.2 V. Within that same potential range, the anodic photocurrents decayed to values lower than in pure electrolyte. We attribute this transient behavior to the electrochemical back reduction of $TEMPO^+$, which is operable over this potential range (cf. **Figure 4.3b**).

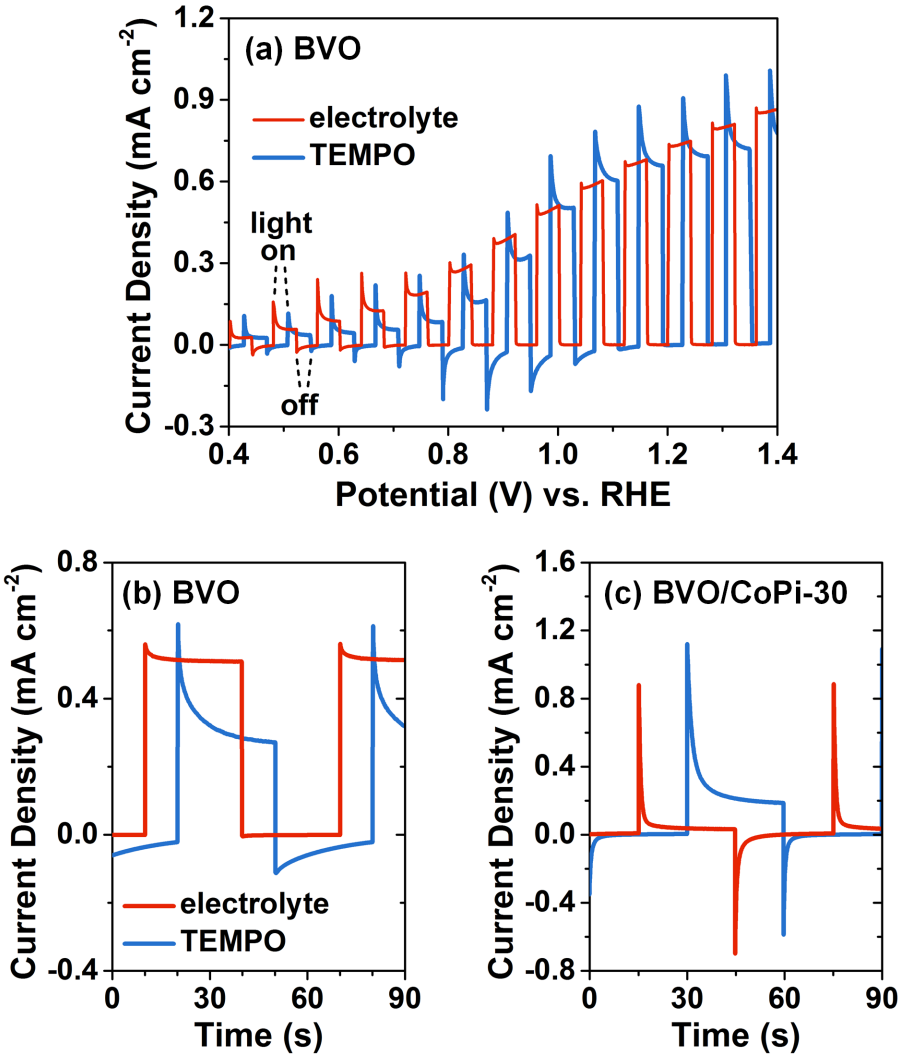

Figure 4.4. Transient photocurrent measurements with chopped AM1.5 illumination. (a) LSVs for BVO in pure electrolyte and electrolyte with 5.0 mM TEMPO. (b-c) Transient photocurrents at 1.04 V versus RHE for BVO and BVO/CoPi-30, respectively. For clarity, the traces in (b) and (c) are offset with respect to time.

Figures 4.4b-c show transient photocurrent measurements for BVO and BVO/CoPi-30 at a fixed potential of 1.04 V. BVO displayed behavior consistent with the LSVs under chopped illumination; quasi-steady-state photocurrents were smaller and negative transient currents were much larger for electrolytes with TEMPO compared to pure electrolytes. The negative current decayed very slowly ($t_{1/2} \approx 13$ s) and did not reach steady state during the dark periods. As previously mentioned, we assign the negative current mainly to the back reduction of

$TEMPO^+$ that accumulates in solution during illuminated periods. In pure electrolyte, BVO/CoPi-30 exhibited high anodic current initially after illumination; however, the photocurrent rapidly decayed to nearly zero. Also, sharp negative transients were observed when illumination was turned off. This behavior has been attributed to CoPi oxidation by photogenerated holes and subsequent back recombination of electrons with accumulated oxidized CoPi species.[36-37] In electrolytes with TEMPO, quasi-steady-state anodic current was greatly increased (i.e. 5.7-fold) and the negative transient current was diminished compared to pure electrolytes. Most notably, the slowly-decaying negative current assigned to $TEMPO^+$ back reduction was not observed for BVO/CoPi-30. On this basis, it is likely that the enhanced TEMPO oxidation photocurrents observed for CoPi-modified BVO photoanodes are at least in part due to the ability of CoPi to inhibit solution-mediated charge recombination.

Finally, we used the BVO/CoPi photoelectrodes for TEMPO-mediated oxidation of biomass-derived chemicals. Due to its high value for biomass conversion, we targeted HMF as an exemplary multifunctional substrate containing both alcohol and aldehyde functionalities (**Figure 4.5a**). LSVs for BVO/CoPi-30 show that photocurrent increased after adding HMF to a TEMPO-containing electrolyte (**Figure 4.5b**), resulting from the regeneration of TEMPO following the reaction between the oxoammonium cation (i.e. $TEMPO^+$) and HMF. No increase was observed in the absence of TEMPO, indicating that the non-mediated HMF oxidation was negligible under these conditions. TEMPO-mediated photoelectrolysis of HMF was performed at 0.64 V for 2.7 hours. Relatively low HMF conversion (15.2%) and yield to FDCA (~0.1%) were obtained using a BVO photoanode at such a mild potential (**Table S4.3**). In contrast, BVO/CoPi-30 achieved 88% yield to FDCA (**Figure 4.5c**), which we attribute to its greatly enhanced TEMPO oxidation performance. We highlight that the role of the

photoanode in this system is to oxidize TEMPO to $TEMPO^+$, which then oxidizes the substrate (i.e. HMF) homogeneously in the electrolyte. Therefore, this approach is not uniquely suited for HMF conversion, but rather we expect it to be readily applicable for the TEMPO-mediated oxidation of a wide range of biologically-derived substrates.

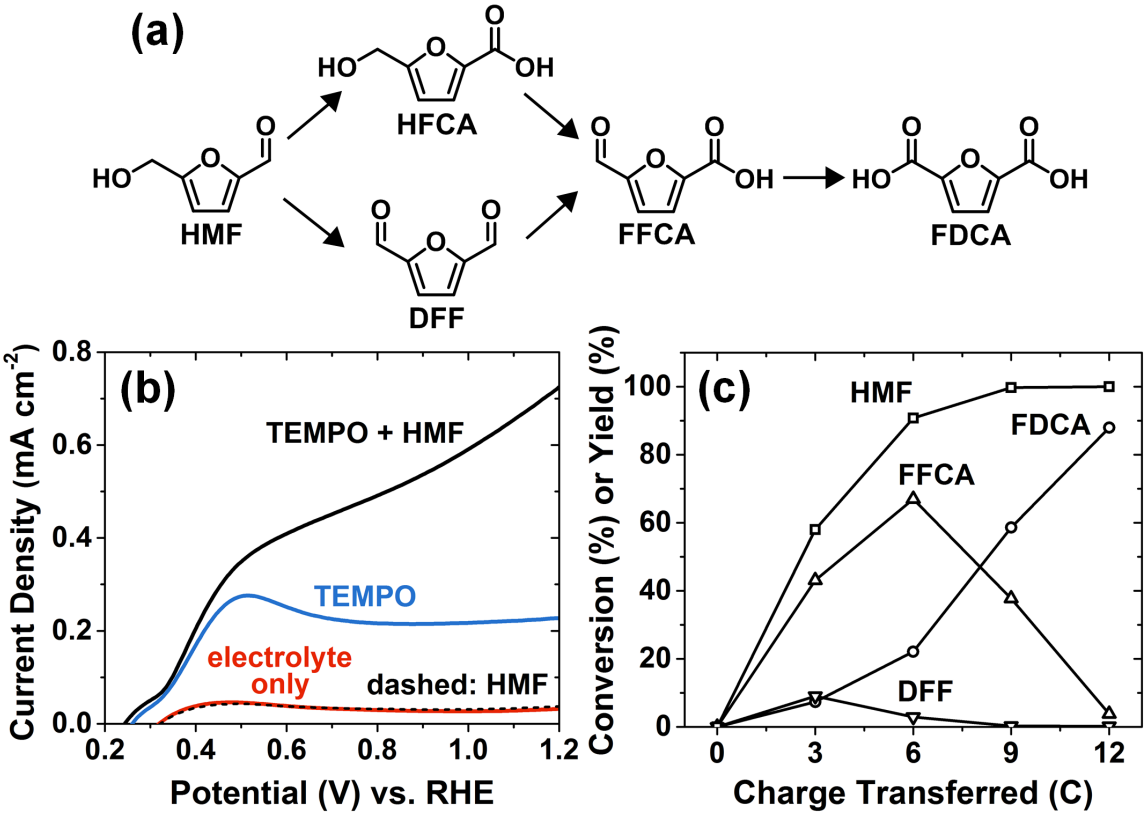

Figure 4.5. (a) Possible reaction pathways for HMF oxidation to FDCA. (b) LSVs under AM1.5 illumination for BVO/CoPi-30 in electrolyte only, electrolyte with 5.0 mM TEMPO, electrolyte with 5.0 mM TEMPO and 5.0 mM HMF, and electrolyte with 5.0 mM HMF without TEMPO. (c) HMF conversion and product yields for photoelectrolysis at 0.64 V versus RHE for BVO/CoPi-30.

4.3. Conclusions

In summary, we developed heterostructured photoelectrodes composed of nanoporous BVO films modified with CoPi for TEMPO-mediated alcohol oxidation. CoPi

electrodeposition time was a critical parameter for selectively promoting TEMPO oxidation in favor over OER. BVO/CoPi prepared by a 30 min CoPi deposition reduced the potential required for TEMPO oxidation by about 0.5 V and greatly enhanced the photocurrents for TEMPO oxidation compared to BVO. In situ O_2 measurements confirmed that TEMPO oxidation with BVO/CoPi-30 proceeded without any faradaic efficiency loss to OER. Transient photocurrent measurements suggested that CoPi alleviates solution-mediated recombination losses resulting from the back reduction of oxidized TEMPO, which we identified as a major limiting factor for BVO photoanode performance. BVO/CoPi-30 facilitated TEMPO-mediated oxidation of HMF, an exemplary biomass-derived alcohol, to FDCA with high yield at mild conditions. This work will promote the development of rationally-designed heterostructured photoanodes and the exploration of new strategies to more fully utilize renewable electricity, solar energy, and renewable feedstocks.

4.4. Experimental Methods

4.4.1. Materials

Boric acid (≥99.5%), dimethyl sulfoxide (DMSO, ≥99.9%), nitric acid, potassium iodide (≥99%), anhydrous sodium sulfite (≥99%), and sulfuric acid were purchased from Fisher Scientific. Bismuth(III) nitrate pentahydrate (98%), cobalt(II) nitrate hexahydrate (≥98%), dimethyl sulfoxide (DMSO, ≥99.5%), potassium dibasic phosphate (≥98%), potassium monobasic phosphate (≥99%), sodium hydroxide (≥97%), TEMPO (2,2,6,6-tetramethylpiperidine-1-oxyl) (98%), vanadyl acetylacetonate (98%), 1,4-benzoquinone (≥99%), 5-hydroxymethylfurfural (HMF, ≥99%), 2,5-diformylfuran (DFF, ≥99%), and 2,5-furandicarboxylic acid (FDCA, 97%) were purchased from Sigma-Aldrich. 5-hydroxymethyl-2-furancarboxylic acid (HFCA, ≥99%) was purchased from Matrix Scientific. 5-formylfuran-

2-carboxylic acid (FFCA, ≥98%) was purchased from TCI America. All electrolytes were prepared using deionized water (18.2 MΩ cm).

4.4.2. Fabrication of BVO photoanodes

BVO films were synthesized by a procedure adapted from Kim et al.[20-21] First, a 50 ml solution containing 0.4 M potassium iodide was adjusted to pH 1.7 with nitric acid, followed by the addition of 0.04 M bismuth(III) nitrate. The solution was mixed with a magnetic stir bar. After the bismuth precursor was fully dissolved, a 20 ml solution of 0.23 M 1,4-benzoquinone in ethanol was added. Electrodeposition was performed in a two-electrode configuration using fluorine-doped tin oxide (FTO) glass and platinum foil as working and counter electrodes, respectively. The area of FTO exposed to the electrolyte was approximately 5.75 cm^2. Deposition of bismuth oxyiodide (BiOI) was conducted at –4.0 mA for 328 s, corresponding to a charge transfer of approximately 0.23 C cm^{-2}. The BiOI films were washed with copious deionized water and dried under a nitrogen stream. A solution of 0.2 M vanadyl acetylacetonate in DMSO (0.8 ml) was drop-cast onto the top side of the BiOI film. Thermal treatment was performed in a muffle furnace at 450 °C (ramp rate 2 °C per minute) for 2 h, followed by naturally cooling to ambient temperature. Excess V_2O_5 was removed by placing the electrode in a stirred solution of 1.0 M sodium hydroxide for 30 min. The final BVO films were washed with deionized water and dried under a nitrogen stream at ambient temperature.

4.4.3. Electrodeposition of CoPi

CoPi was deposited onto BVO electrodes using the electrodeposition method described by Kanan and Nocera.[28] CoPi layers were deposited from a solution of 0.5 mM cobalt(II) nitrate in 0.1 M potassium phosphate (pH 7.0) at 1.1 V versus a Ag/AgCl reference electrode. Deposition time was varied between 1 and 30 min. **Figure S4** shows the typical current density

versus time plot for CoPi deposition. The photoanodes were designated BVO/CoPi-*t*, in which *t* is the CoPi deposition time in minutes.

4.4.4. Characterizations

X-ray diffraction (XRD) patterns were collected with a Siemens D500 diffractometer operated with a Cu K_α source (λ = 1.5418 Å) at 45 kV and 30 mA and equipped with a diffracted beam monochromator (carbon). Diffuse transmittance (*T*) and reflectance (*R*) measurements were taken using Lambda 750 UV-vis spectrophotometer with a 100 mm integrating sphere. Absorbance (*A*) was calculated by the relationship: $A = 1 - T - R$. Scanning electron microscopy (SEM) and energy dispersive X-ray spectroscopy (EDS) were performed on an FEI Quanta 250 field-emission scanning electron microscope equipped with an Oxford Aztec EDS. Samples for SEM were sputter-coated with Au films approximately 5 nm thick. SEM micrographs in **Figure 4.1** were collected with a backscattered electron detector.

4.4.5. Photoelectrochemical experiments

Photoelectrochemical measurements were performed in a custom-made undivided cell using a three-electrode configuration. Pt wire and Ag/AgCl (3.5 mm, Pine Research Instrumentation) served as counter and reference electrodes, respectively. Unless noted otherwise, all potentials (*E*) are reported versus RHE, as calculated by **Equation 4.1**.

$$E(\text{vs. RHE}) = E(\text{vs. Ag/AgCl}) + 0.199\ \text{V} + 0.059\ \text{V} \cdot \text{pH} \qquad (4.1)$$

Electrochemical measurements were conducted using a WaveDriver 20 system (Pine Research Instrumentation). Irradiation was achieved with a Sciencetech A1 Lightline solar simulator equipped with a 300 W xenon lamp and an AM1.5 filter. Light intensity was calibrated to approximately 1 sun equivalent (100 mW cm^{-2}) using a reference cell certified by National Renewable Energy Laboratories (NREL), USA. The photoanodes were irradiated through the

FTO glass substrate, i.e. “back-side” illumination. Photoanodes were masked with an aperture (1.0 cm diameter) to set the irradiated area to be the same as the area exposed to electrolyte. Current density values are reported with respect to geometric surface area (0.785 cm^2). All experiments were performed in 0.2 M sodium borate buffer electrolyte (pH 9.2). Linear sweep voltammograms (LSVs) and cyclic voltammograms (CVs) were collected at a sweep rate of 10 mV s^{-1}. Transient photocurrent measurements were collected using a mechanical shutter.

4.4.6. Oxygen quantification

The amount of evolved oxygen (O_2) was determined using an oxygen sensor system (NEOFOX-KIT-PROBE, Ocean Optics). Oxygen measurements were conducted in a glass H-type cell with an airtight silicone stopper on the anode chamber. The anode and cathode chambers were separated by an anion-exchange membrane (A-201, Tokuyama Corp.). The active area of the photoanode was approximately 5.75 cm^2. Irradiation passed through the glass wall of the reactor and electrolyte before striking the photoanode, so the light intensity was not exactly equivalent to 1 sun. A fluorescence-based oxygen probe and thermistor were submerged into the anode electrolyte to measure the temperature-compensated dissolved oxygen concentration. Agitation was provided by a magnetic stirrer. Before measurements, the cell was thoroughly purged with argon gas (99.99%, Airgas) and then sealed. The baseline oxygen concentration was monitored and subtracted from the measurements taken under photoelectrochemical conditions. The amount of O_2 produced (n_{O2}) was calculated by multiplying dissolved oxygen concentration by the electrolyte volume. The faradaic efficiency to OER was calculated by **Equation 4.2**:

$$FE_{O2}\ \% = 4F \cdot n_{O2} / \ Q \cdot 100\% \qquad (4.2)$$

in which n_{O2} is the measured amount of O_2 (mol), 4 is the electron transfer number for O_2 evolution, F is the Faraday constant (96485.3 C mol^{-1}), and Q is the charge transferred in coulombs calculated as the time integral of current. The theoretical amount of O_2 produced assuming 100% faradaic efficiency was calculated by **Equation S4.3**:

$$n_{O2,theoretical} = Q / (4F) \quad (4.3)$$

For electrolytes without TEMPO, the measured and theoretical amounts of O_2 produced were in good agreement, as shown in **Figure S4.5**.

4.4.7. Net charge injection efficiency

Net charge injection efficiency (ϕ_{inj}) is the fraction of the surface-reaching holes that are utilized for electrochemical reactions, rather than being lost to recombination processes. The total rate at which holes reach the surface can be estimated by measuring photocurrent in the presence of a hole scavenger. Sodium sulfite is a good hole accepter, capable of extracting nearly all holes that reach the semiconductor/electrolyte interface due to its fast, irreversible, oxidation kinetics.[26, 38] Therefore, the photocurrent measured for sulfite oxidation ($j_{sulfite}$) provides an estimate for the total rate of holes reaching the interface. Net charge injection efficiencies (ϕ_{inj}) for OER and TEMPO oxidation were determined by **Equations 4.4 and 4.5**.

$$\phi_{inj,OER}\,\% = j_{OER} / j_{sulfite} \cdot 100\% \quad (4.4)$$

$$\phi_{inj,TEMPO}\,\% = j_{TEMPO} / j_{sulfite} \cdot 100\% \quad (4.5)$$

Current density values were extracted from LSVs at 0.64 V versus RHE. Current density for OER (j_{OER}) was taken from LSVs measured in electrolyte without TEMPO or sodium sulfite present (cf. **Figure 4.2a**). Note that at 0.64 V versus RHE, the contribution of OER to the total measured photocurrent (i.e. faradaic efficiency to OER) was negligible for BVO and

BVO/CoPi when TEMPO was present in the electrolyte (cf. **Figure 4.2c**). Therefore, it is reasonable to assume that the measured current density (j) was from TEMPO oxidation under that condition (i.e. $j = j_{TEMPO}$). The value of $j_{sulfite}$ measured for BVO was used in all calculations. Net charge injection efficiencies are summarized in **Table S4.2**.

4.4.8. TEMPO-mediated photoelectrolysis

TEMPO-mediated photoelectrolysis of HMF was performed in a glass H-type cell at a constant potential of 0.64 V versus RHE. The anode and cathode chambers were separated by an anion-exchange membrane (A-201, Tokuyama Corp.). The anode electrolyte volume was 20 ml, and it contained 5.0 mM TEMPO and 1.0 mM HMF. Agitation was provided by a magnetic stirrer. The active area of the photoanode was approximately 5.25 cm^2. Irradiation passed through the glass wall of the reactor and electrolyte before illuminating the photoanode, and as a result the light intensity was not exactly equivalent to 1 sun. For BVO/CoPi-30, the reaction was concluded when the amount of charge transferred reached 12 C, which occurred after about 2.7 h of reaction. This amount of charge corresponds to about 103% of the theoretical charge transfer required for complete conversion of HMF to FDCA (i.e. 11.59 C). Additional experiments were conducted using a BVO photoanode for a duration of 2.7 h.

4.4.9. Product analysis

Product analysis was performed with an Agilent 1200 high-performance liquid chromatograph, equipped with a Bio-Rad Aminex HPX-87H column (50 °C) and a variable wavelength detector (Agilent G1314F, 260 nm). The mobile phase was 0.01 M sulfuric acid with a flow rate of 0.5 ml min^{-1}. Reactants and products were identified and quantified by comparison with authentic samples. HMF conversion (C) was calculated by **Equation 4.6**:

$$C = (n_{HMF} - n_{HMF,initial}) / n_{HMF,initial} \quad (4.6)$$

in which n_{HMF} is the amount of HMF (mol). The product selectivity (S) and yield (Y) were calculated for product i by **Equations 4.7 and 4.8,** in which n_i is amount of product i (mol).

$$S_i = n_i / (n_{\mathrm{HMF}} - n_{\mathrm{HMF,initial}}) \quad (4.7)$$

$$Y_i = n_i / n_{\mathrm{HMF,initial}} \quad (4.8)$$

4.5. Acknowledgements

WL and DC acknowledge support from the Bailey Research Career Development Award. The authors thank Warren Straszheim and Scott Schlorholtz of Iowa State University for assistance with SEM and XRD. This work was supported in part by the U.S. Department of Energy, Office of Science, and Office of Workforce Development for Teachers and Scientists (WDTS) under the Science Undergraduate Laboratory Internship (SULI) program. LW is grateful to the DOE for the assistantship and opportunity to participate in the SULI program.

4.6. References

(1) Centi, G.; Perathoner, S., Towards solar fuels from water and CO_2. *ChemSusChem* **2010,** *3* 195–208.

(2) Walter, M. G.; Warren, E. L.; McKone, J. R.; Boettcher, S. W.; Mi, Q.; Santori, E. A.; Lewis, N. S., Solar Water Splitting Cells. *Chem. Rev.* **2010,** *110* 6446–6473.

(3) Kim, D.; Sakimoto, K. K.; Hong, D.; Yang, P., Artificial photosynthesis for sustainable fuel and chemical production. *Angew. Chem. Int. Ed.* **2015,** *54* 3259−3266.

(4) Jiao, Y.; Zheng, Y.; Jaroniec, M.; Qiao, S. Z., Design of electrocatalysts for oxygen- and hydrogen-involving energy conversion reactions. *Chem. Soc. Rev.* **2015,** *44* 2060−2086.

(5) Cha, H. G.; Choi, K.-S., Combined biomass valorization and hydrogen production in a photoelectrochemical cell. *Nat. Chem.* **2015,** *7* 328–333.

(6) You, B.; Liu, X.; Liu, X.; Sun, Y., Efficient H_2 Evolution Coupled with Oxidative Refining of Alcohols via A Hierarchically Porous Nickel Bifunctional Electrocatalyst. *ACS Catal.* **2017,** 4564−4570.

(7) You, B.; Jiang, N.; Liu, X.; Sun, Y., Simultaneous H_2 Generation and Biomass Upgrading in Water by an Efficient Noble-Metal-Free Bifunctional Electrocatalyst. *Angew. Chem. Int. Ed.* **2016,** *55* 9913–9917.

(8) Chen, Y. X.; Lavacchi, A.; Miller, H. A.; Bevilacqua, M.; Filippi, J.; Innocenti, M.; Marchionni, A.; Oberhauser, W.; Wang, L.; Vizza, F., Nanotechnology makes biomass electrolysis more energy efficient than water electrolysis. *Nat. Commun.* **2014,** *5* 4036.

(9) González-Cobos, J.; Baranton, S.; Coutanceau, C., Development of Bi-Modified PtPd Nanocatalysts for the Electrochemical Reforming of Polyols into Hydrogen and Value-Added Chemicals. *ChemElectroChem* **2016,** *3* 1694–1704

(10) Zalineeva, A.; Serov, A.; Padilla, M.; Martinez, U.; Artyushkova, K.; Baranton, S.; Coutanceau, C.; Atanassov, P. B., Self-supported Pd($_x$)Bi catalysts for the electrooxidation of glycerol in alkaline media. *J. Am. Chem. Soc.* **2014,** *136* 3937–3945.

(11) Chadderdon, D. J.; Xin, L.; Qi, J.; Brady, B.; Miller, J. A.; Sun, K.; Janik, M. J.; Li, W., Selective Oxidation of 1,2-Propanediol in Alkaline Anion-Exchange Membrane Electrocatalytic Flow Reactors: Experimental and DFT Investigations. *ACS Catal.* **2015,** *5* 6926−6936.

(12) Wang, T.; Nolte, M. W.; Shanks, B. H., Catalytic dehydration of C_6 carbohydrates for the production of hydroxymethylfurfural (HMF) as a versatile platform chemical. *Green Chem.* **2014,** *16* 548−572.

(13) Binder, J. B.; Raines, R. T., Simple Chemical Transformation of Lignocellulosic Biomass into Furans for Fuels and Chemicals. *J. Am. Chem. Soc.* **2009,** *131* 1979–1985.

(14) Dijkman, W. P.; Groothuis, D. E.; Fraaije, M. W., Enzyme-catalyzed oxidation of 5-hydroxymethylfurfural to furan-2,5-dicarboxylic acid. *Angew. Chem. Int. Ed.* **2014,** *53* 6515−6518.

(15) Park, Y.; McDonald, K. J.; Choi, K. S., Progress in bismuth vanadate photoanodes for use in solar water oxidation. *Chem. Soc. Rev.* **2013,** *42* 2321–2337.

(16) Zhong, D. K.; Choi, S.; Gamelin, D. R., Near-complete suppression of surface recombination in solar photoelectrolysis by "Co-Pi" catalyst-modified W:$BiVO_4$. *J. Am. Chem. Soc.* **2011,** *133* 18370–18377.

(17) Pilli, S. K.; Furtak, T. E.; Brown, L. D.; Deutsch, T. G.; Turner, J. A.; Herring, A. M., Cobalt-phosphate (Co-Pi) catalyst modified Mo-doped $BiVO_4$ photoelectrodes for solar water oxidation. *Energy Environ. Sci.* **2011,** *4* 5028–5034.

(18) Chang, X.; Wang, T.; Zhang, P.; Zhang, J.; Li, A.; Gong, J., Enhanced Surface Reaction Kinetics and Charge Separation of p-n Heterojunction Co_3O_4/$BiVO_4$ Photoanodes. *J. Am. Chem. Soc.* **2015,** *137* 8356–8359.

(19) Seabold, J. A.; Choi, K. S., Efficient and stable photo-oxidation of water by a bismuth vanadate photoanode coupled with an iron oxyhydroxide oxygen evolution catalyst. *J. Am. Chem. Soc.* **2012,** *134* 2186–2192.

(20) McDonald, K. J.; Choi, K.-S., A new electrochemical synthesis route for a BiOI electrode and its conversion to a highly efficient porous $BiVO_4$ photoanode for solar water oxidation. *Energy Environ. Sci.* **2012,** *5* 8553–8557.

(21) Kim, T. W.; Choi, K.-S., Nanoporous $BiVO_4$ Photoanodes with Dual-Layer Oxygen Evolution Catalysts for Solar Water Splitting. *Science* **2014,** *343* 990–994.

(22) Kim, T. W.; Ping, Y.; Galli, G. A.; Choi, K. S., Simultaneous enhancements in photon absorption and charge transport of bismuth vanadate photoanodes for solar water splitting. *Nat. Commun.* **2015,** *6* 8769.

(23) Zhang, B.; Wang, L.; Zhang, Y.; Ding, Y.; Bi, Y., Ultrathin FeOOH Nanolayers with Rich Oxygen Vacancies on $BiVO_4$ Photoanodes for Efficient Water Oxidation. *Angew. Chem. Int. Ed.* **2018,** *57* 2248–2252.

(24) Li, T.; Kasahara, T.; He, J.; Dettelbach, K. E.; Sammis, G. M.; Berlinguette, C. P., Photoelectrochemical oxidation of organic substrates in organic media. *Nat. Commun.* **2017,** *8* 390.

(25) Cooper, J. K.; Gul, S.; Toma, F. M.; Chen, L.; Glans, P.-A.; Guo, J.; Ager, J. W.; Yano, J.; Sharp, I. D., Electronic Structure of Monoclinic $BiVO_4$. *Chem. Mater.* **2014,** *26* 5365–5373.

(26) Kang, D.; Kim, T. W.; Kubota, S. R.; Cardiel, A. C.; Cha, H. G.; Choi, K. S., Electrochemical Synthesis of Photoelectrodes and Catalysts for Use in Solar Water Splitting. *Chem. Rev.* **2015,** *115* 12839–12887.

(27) Couper, A. M.; Pletcher, D.; Walsh, F. C., Electrode Materials for Electrosynthesis. *Chem. Rev.* **1990,** *90* 837–865

(28) Kanan, M. W.; Nocera, D. G., In Situ Formation of an Oxygen-Evolving Catalyst in Neutral Water Containing Phosphate and Co^{2+}. *Science* **2008,** *231* 1072–1075.

(29) Carroll, G. M.; Gamelin, D. R., Kinetic analysis of photoelectrochemical water oxidation by mesostructured Co-Pi/α-Fe_2O_3 photoanodes. *J. Mater. Chem. A* **2016,** *4* 2986–2994.

(30) Qiu, J.; Hajibabaei, H.; Nellist, M. R.; Laskowski, F. A. L.; Oener, S. Z.; Hamann, T. W.; Boettcher, S. W., Catalyst Deposition on Photoanodes: The Roles of Intrinsic Catalytic Activity, Catalyst Electrical Conductivity, and Semiconductor Morphology. *ACS Energy Letters* **2018,** 961–969.

(31) Cameron, P. J.; Peter, L. M.; Hore, S., How Important is the Back Reaction of Electrons via the Substrate in Dye-Sensitized Nanocrystalline Solar Cells? *J. Phys. Chem. B* **2005,** *109* 930–936.

(32) Bard, A. J.; Faulkner, L. R., *Electrochemical Methods: Fundamentals and Applications*. 2nd ed.; John Wiley & Sons, Inc.: New York, 2001.

(33) Eisenberg, D.; Ahn, H. S.; Bard, A. J., Enhanced photoelectrochemical water oxidation on bismuth vanadate by electrodeposition of amorphous titanium dioxide. *J. Am. Chem. Soc.* **2014,** *136* 14011–14014.

(34) Peter, L. M.; Wijayantha, K. G. U.; Tahir, A. A., Kinetics of light-driven oxygen evolution at α-Fe_2O_3 electrodes. *Faraday Discuss.* **2012,** *155* 309–322.

(35) Ma, Y.; Pendlebury, S. R.; Reynal, A.; Le Formal, F.; Durrant, J. R., Dynamics of photogenerated holes in undoped $BiVO_4$ photoanodes for solar water oxidation. *Chem. Sci.* **2014,** *5* 2964−2973.

(36) Klahr, B.; Gimenez, S.; Fabregat-Santiago, F.; Bisquert, J.; Hamann, T. W., Photoelectrochemical and impedance spectroscopic investigation of water oxidation with "Co-Pi"-coated hematite electrodes. *J. Am. Chem. Soc.* **2012,** *134* 16693−16700.

(37) Ma, Y.; Kafizas, A.; Pendlebury, S. R.; Le Formal, F.; Durrant, J. R., Photoinduced Absorption Spectroscopy of CoPi on $BiVO_4$: The Function of CoPi during Water Oxidation. *Adv. Funct. Mater.* **2016,** *26* 4951−4960.

(38) Govindaraju, G. V.; Wheeler, G. P.; Lee, D.; Choi, K.-S., Methods for Electrochemical Synthesis and Photoelectrochemical Characterization for Photoelectrodes. *Chem. Mater.* **2017,** *29* 355−370.

4.6. Supplementary Information

Table S4.1. Relative abundance (at%) of Bi, V, Co, and P in BVO determined by SEM-EDS.

	Bi	V	Co	P
BVO	51.9	48.1	-	-
BVO/CoPi-30	46.4	43.8	6.5	3.4

Table S4.2. Net charge injection efficiencies (ϕ_{inj}) for OER and TEMPO oxidation at 0.64 V.

	j_{OER} (mA cm^{-2})	$\phi_{inj,OER}$ (%)	j_{TEMPO} (mA cm^{-2})	$\phi_{inj,TEMPO}$ (%)
BVO	0.098	6.3	0.033	2.1
BVO/CoPi-1 [a]	0.572	37.0	0.040	2.6
BVO/CoPi-30	0.035	2.3	0.238	15.4

[a] BVO/CoPi-1 is BVO modified with CoPi deposition of 1 min.

Table S4.3. Product analysis for photoelectrochemical TEMPO-mediation HMF oxidation.[a]

	Q (C) [b]	C_{HMF} (%) [c]	S_{DFF} (%) [d]	S_{FFCA} (%)	S_{FDCA} (%)
BVO	0.52	15.2	50.9	30.6	0.7
BVO/CoPi-30	12.0	98.8	0.2	3.8	89.0

[a] Conditions: 5.0 mM TEMPO and 1.0 mM HMF in 20 ml electrolyte; applied potential = 0.64 V versus RHE; reaction duration 2.7 h. [b] Q is charge transferred in external circuit in coulombs. [c] C is HMF conversion [d] S is product selectivity.

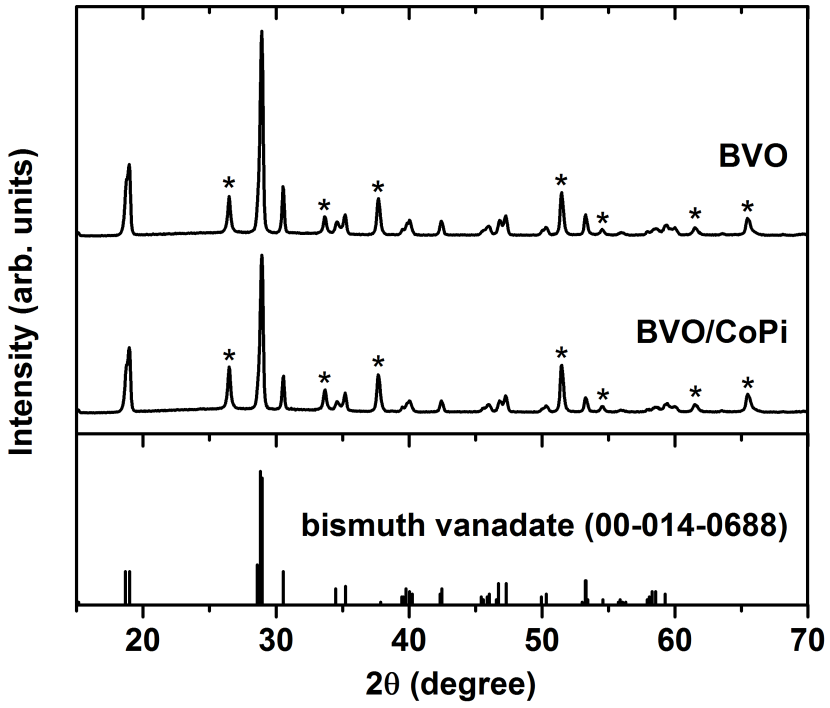

Figure S4.1. XRD patterns of BVO and BVO/CoPi-30 showing typical peaks for monoclinic scheelite structure (JCPDS No. 00-014-0688). Peaks from FTO substrate are indicated with asterisks (∗).

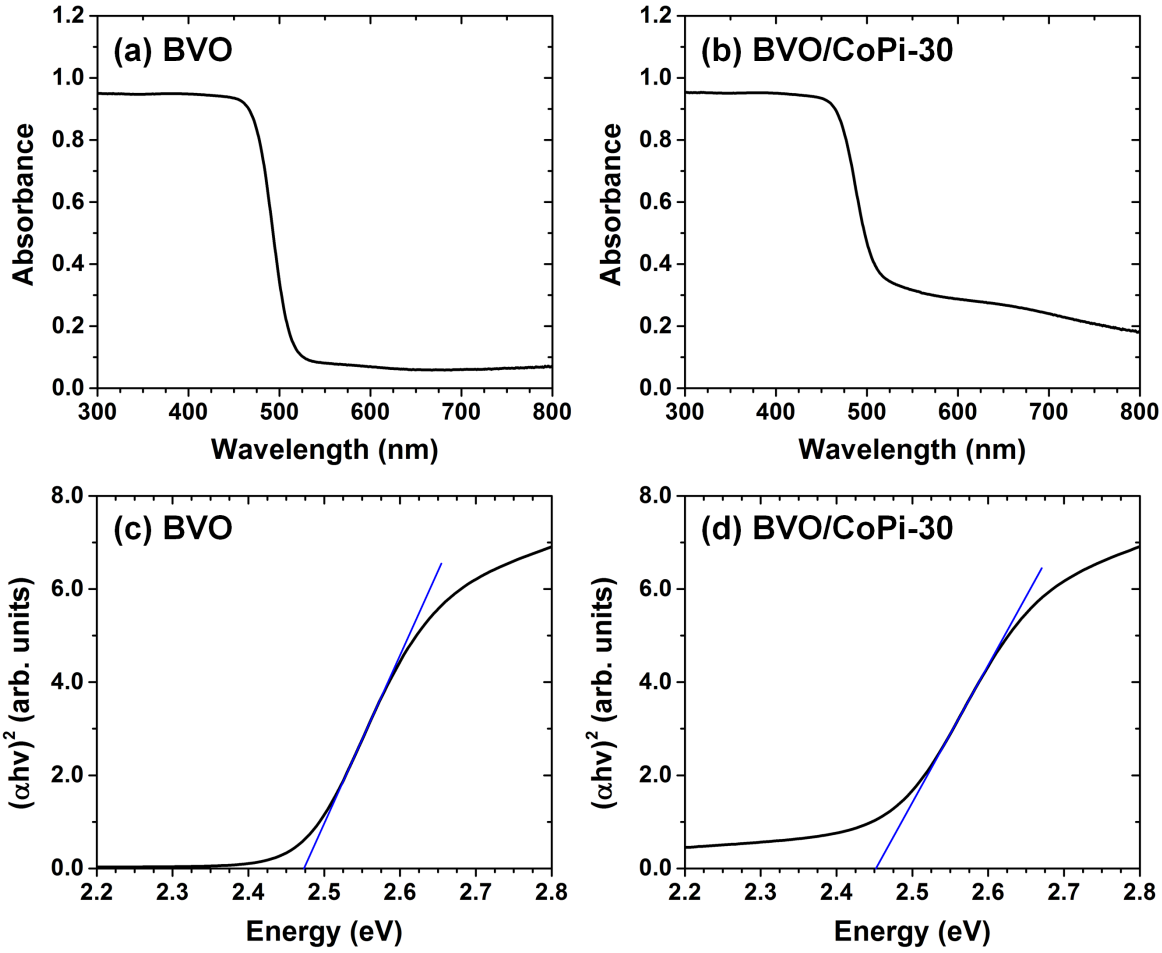

Figure S4.2. UV-vis diffuse absorbance spectra for (a) BVO and (b) BVO/CoPi along with (c-d) corresponding Tauc plots.

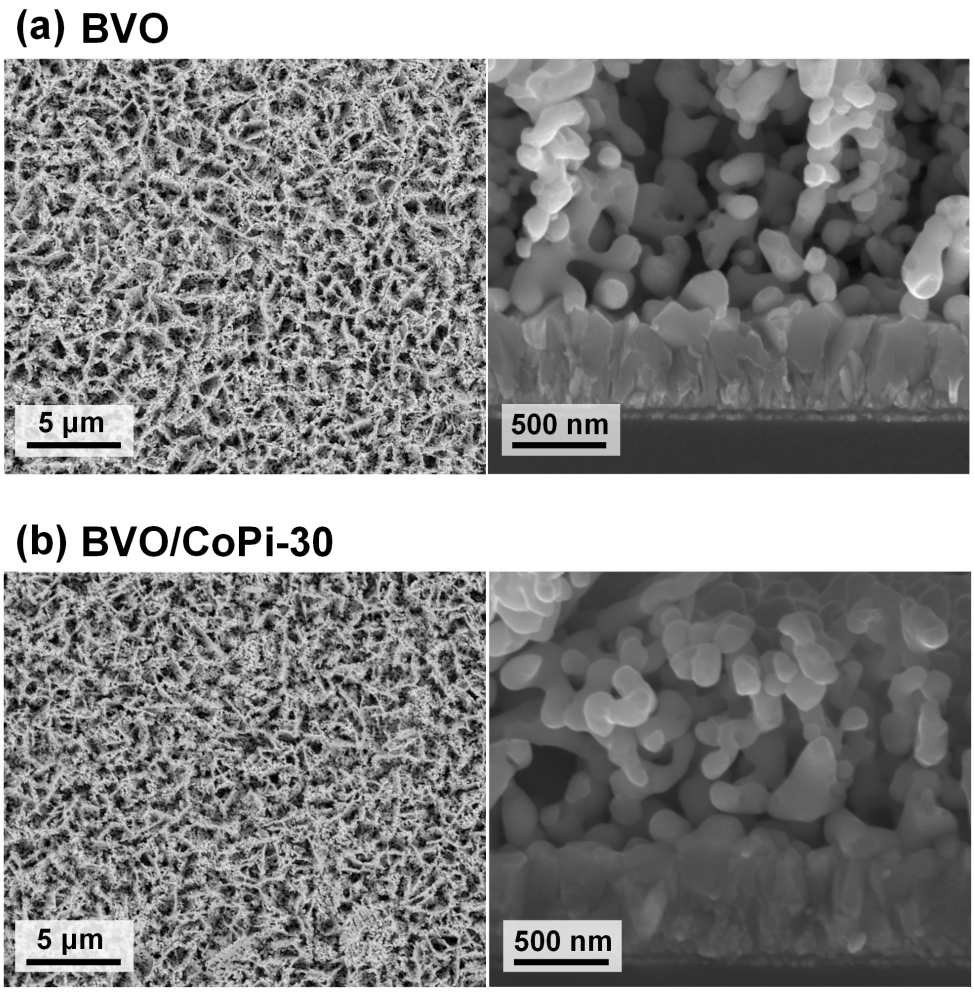

Figure S4.3. Top-view SEM micrographs (left) and cross-sectional SEM micrographs (right) for (a) BVO and (b) BVO/CoPi-30 showing no notable morphological changes after electrochemical CoPi deposition. Top-view micrographs were collected with a backscattered electron detector, whereas cross-sectional micrographs were collected with a secondary electron detector.

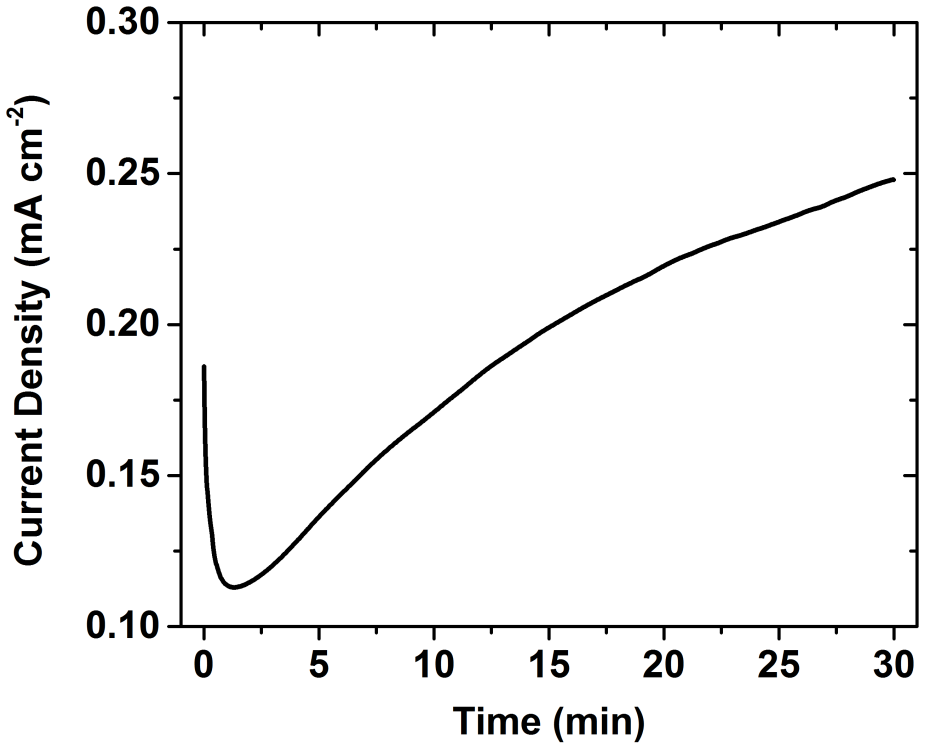

Figure S4.4. Typical electrochemical CoPi deposition on a BVO electrode. Conditions: 1.1 V versus Ag/AgCl in 0.1 M KPi buffer (pH 7.0) containing 0.5 mM cobalt(II) nitrate.

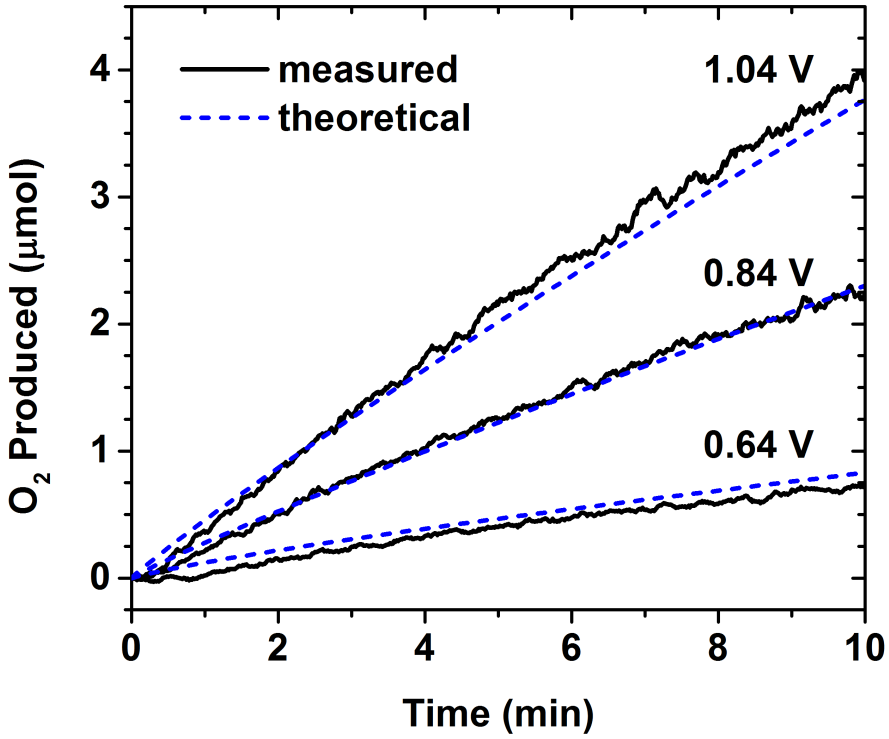

Figure S4.5. Verification of O_2 quantification method for BVO photoanode at three applied potentials (V versus RHE) in electrolytes without TEMPO present. Measured O_2 amounts are in good agreement with theoretical predictions assuming 100% faradaic efficiency to OER.

CHAPTER 5

GENERAL CONCLUDING REMARKS

This work aimed to address the challenges of using electrocatalysis for selective oxidation of biomass-derived compounds, including polyols and polyfunctional compounds. The oxidation of PDO on Pt/C and Au/C catalysts was studied to gain insight into the influences of catalyst material and electrode potential on the selective oxidation of vicinal primary and secondary alcohols, as well as oxidative C–C bond breaking reactions. It was found for Au/C catalysts that oxidation of the secondary alcohol group of PDO was in competition with non-electrochemical transformations, and was promoted at higher anode potentials. The selective electrocatalytic oxidation of HMF using Pd/C, Au/C, and bimetallic PdAu/C catalysts was explored to gain information about the competitive oxidation of alcohol and aldehyde groups, and to elucidate the relationships between electrode potential, reaction pathway, and product selectivity. It was found that bimetallic catalysts achieved high FDCA yield mainly due to their enhanced ability to oxidize the key intermediate product (i.e. HFCA) compared to their monometallic counterparts. Finally, the use of homogeneous electrocatalysts for selective oxidation of alcohols in photoelectrolytic cells was investigated. Heterostructured photoanodes were developed by modifying bismuth vanadate (BVO) semiconductor films with electrodeposited cobalt phosphate (CoPi). The CoPi modifications simultaneously increased TEMPO oxidation photocurrents and suppressed the undesired oxygen evolution reaction, resulting in enhanced TEMPO-mediated HMF oxidation to FDCA.

A goal throughout this work was to achieve high yield of desired products under the most mild conditions possible. Selective oxidation of PDO in Chapter 2 was conducted in a harsh

alkaline environment (i.e. pH > 14), at elevated temperatures, and with expensive precious metal catalysts. These reaction conditions promoted undesired non-electrochemical transformations of intermediate species. Electrocatalytic HMF oxidation in Chapter 3 achieved high yield to FDCA using slightly more mild electrolytes (i.e. pH 13) and ambient temperatures. The high yield to FDCA was largely facilitated by synergistic benefits derived from bimetallic precious metal catalysts. The photoelectrochemical oxidation of HMF to FDCA reported in Chapter 4 was conducted in mild alkaline conditions (pH 9.2), ambient temperature, and with very low applied potentials. This was made possible through the use of TEMPO as a homogeneous electrocatalyst, together with a heterostructured photoanode to harvest solar energy. Furthermore, the photoanodes were composed of Earth-abundant materials. The work presented here demonstrates that electrocatalysis is a versatile tool, capable of integrating sustainable chemical production with renewable energy conversion. With continued research and technology development, electrocatalytic processes may play key roles in the future chemical and energy landscapes.